"New High-Performance GaSb-Based Thermophtovolatic Devices"

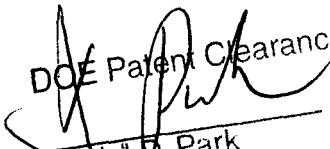## Final Report

Department of Energy Phase II STTR
DE-FG02-97ER86057

AstroPower, Inc.
Solar Park
Newark, Delaware 19716-2000

Principal Investigator:
Michael G. Mauk
221-32-8958
tel: 302-366-0400 ext 3016
e-mail: mauk@astropower.com
fax: 302-283-0162

Project Summary: Thermophotovoltaic (TPV) materials and devices were developed for the direct conversion of heat (infrared thermal radiation) to electricity. State-of-the-art TPV cells in the quaternary alloys of AlGaAsSb and InGaAsSb lattice-matched to GaSb substrates were made by liquid-phase epitaxy (LPE). A 5-element series-interconnected TPV array made by bonding thick epitaxial device structures on insulating substrates was demonstrated. Simple zinc diffusion processes, in combination with anodic oxidation, were developed to form optimized p-n junction profiles. A new class of low-bandgap (0.35 to 0.5 eV) TPV cells made in InAsSbP was developed.

DISCLAIMER

This report was prepared as an account of work sponsored by an agency of the United States Government. Neither the United States Government nor any agency Thereof, nor any of their employees, makes any warranty, express or implied, or assumes any legal liability or responsibility for the accuracy, completeness, or usefulness of any information, apparatus, product, or process disclosed, or represents that its use would not infringe privately owned rights. Reference herein to any specific commercial product, process, or service by trade name, trademark, manufacturer, or otherwise does not necessarily constitute or imply its endorsement, recommendation, or favoring by the United States Government or any agency thereof. The views and opinions of authors expressed herein do not necessarily state or reflect those of the United States Government or any agency thereof.

DISCLAIMER

Portions of this document may be illegible in electronic image products. Images are produced from the best available original document.

Table of Contents

2

Introduction and Overview

This report provides a chronological narrative of AstroPower/JPL progress in developing several new types of low-bandgap (long wavelength) thermophotovoltaic (TPV) devices. The initial focus of the work was to improve the performance of InGaAsSb cells made by liquid-phase epitaxy on GaSb substrates. The baseline device developed in the Phase I effort advanced from simple *p-n* homojunction designs to double heterostructure AlGaAsSb/InGaAsSb with backside mirrors to effect photon recycling. This was followed by development of techniques for series interconnection to make high-voltage InGaAsSb minimodules by bonding thick epitaxial device structures on isulating surrogate substrates. There was also an effort, pursued in the interest of lowering costs, to realize a simplified version of the device using zinc diffusion. Zinc diffusion, in combination with controlled etching and anodic oxidation, could be used to tailor the emitter doping profile and achieve TPV performance comparable to that of more sophisticated double heterostructures. Several theoretical studies by other groups have suggested lower bandgaps to better utilize the thermal radiation of heat sources with relatively low temperatures (< 1200 °C). Top this end, TPV cells were developed in InAsSbP alloys, resulting in devices with spectral responses at wavelengths longer than 3 microns.

TPV cell performance was characterized by the Jet Propulsion Laboratory at their Pasadena facilities. Measurements included spectral response, testing under intense infrared light, and extensive characterization of temperature sensitivity of device operation.

3

Publications from Phase I and Phase II Research Efforts and Related Work

M.G. MAUK and OLEG V. SULIMA, "Low-Bandgap III-V Antimonides for TPV and Tandem Cell Components" *Proc.. International Seminar of Semiconductor Materials for Thermoelectric Devices and Solar Power Engineering*, Institute of Metallurgy and Materials Science, Russian Academy of Science, Moscow, Russia, 2002. 15-16.

O. SULIMA, M.G. MAUK, A.W. BETT, P.S. DUTTA, and R.L. MUELLER, "GaSb-InGaAsSb-InGaSb-InAsSbP-Ge TPV Cells with Diffused Emitters" to be published in Conf. Record 29th IEEE Photovoltaics Specialists Conf. (2002).

O.V. SULIMA, R. BECKERT, A.W. BETT, P.S. DUTTA, M.G. MAUK, and R.L. MUELLER, "GaSb-, InGaAsSb-, InGaSb- and InAsSbP TPV Cells with Zn-Diffused Emitters" *The Fifth Conference on Thermophotovoltaic Generation of Electricity* (2001, accepted for publication).

O.V. SULIMA, R. BECKERT, A.W. BETT, M.G. MAUK, and R.L. MUELLER, "Comparison of Ge, GaSb, and InGaAsSb TPV Cells" *The Fifth Conference on Thermophotovoltaic Generation of Electricity* (2001, accepted for publication).

MICHAEL G. MAUK, JEFFREY A. COX, LOUIS C. DINETTA, and OLEG SULIMA, "Enabling Technologies for Series-Interconnected Thermophotovoltaic Devices" *Monolithic Interconnected Module Research and Development Conf.: Summary of Presentations* P. CAMPBELL and D. RILEY, eds. (Pleasant Hills, PA, October 2000).

MICHAEL G. MAUK, ZANE A. SHELLENBARGER, JEFFREY A. COX, ANTHONY N. TATA, TAMMIE G. WARDEN, LOUIS C. DINETTA, and ROBERT L. MUELLER, "Advances in Low-Bandgap InAsSbP/InAs and GaInAsSb/GaSb Thermophotovoltaics" *Conf. Rec. 28th IEEE Photovoltaics Specialists Conf.* (IEEE Press, 2000) 1028-1031.

O.V. SULIMA, R. BECKERT, A.W. BETT, J.A. COX, and M.G. MAUK, "InGaAsSb Photovoltaic Cells with Enhanced Open Circuit Voltage" *IEE Proc.: Optoelectronics* **147, 3** (June 2000) 199-204

M.G. MAUK, Z.A. SHELLENBARGER, J.A. COX, O.V. SULIMA, A.W. BETT, R.L. MUELLER, P.E. SIMS, J.B. MCNEELY, and L.C. DINETTA, "Liquid-Phase Epitaxy of Low-Bandgap III-V Antimonides for Thermophotovoltaic Devices" *J. Crystal Growth* **211** (2000) 189-193.M.G.

MICHAEL G. MAUK, ZANE A. SHELLENBARGER, PAUL E. SIMS, JEFFREY A. COX, ANTHONY N. TATA, TAMMIE G. WARDEN, JAMES B. MCNEELY, and LOUIS C. DINETTA, "Low Bandgap Thermophotovoltaics Based on InAsSbP Alloys" *Technical Digest of the 11th International Photovoltaic Science and Engineering Conf.* (Hokkaido, Japan, September, 1999) 989.

ANDREAS W. BETT, BORIS Y. BER, MICHAEL G. MAUK, JOSEPH T. SOUTH, AND OLEG V. SULIMA, "Pseudo-Closed Box Diffusion of Zn into InGaAsSb and AlGaSb for TPV Devices" *Thermophotovoltaic Genration of Electricity: Fourth NREL Conf.* T.J. COUTTS, J.P. BENNER, and C.S. ALLMAN, eds., AIP Conf. Proc. **460** (American Inst. Physics, Woodbury, NY, 1999) 237-246.

P.G. SNYDER, T.E. TIWALD, D.W. THOMPSON, N.J. IANNO, J.A. WOOLLAM, M.G. MAUK, and Z.A. SHELLENBARGER, "Infrared Free Carrier Response of $In_{0.15}Ga_{0.85}As_{0.17}Sb_{0.83}$ Epilayers on GaSb" *Thin Solid Films* **313-314** (1998) 667-670.

JOSEPH T. SOUTH, ZANE A. SHELLENBARGER, MICHAEL G. MAUK, JEFFREY A. COX, PAUL E. SIMS, ROBERT A. MUELLER, and JOHN D. MEAKIN, "AlGaSb Window Layers for IngaAsSb / GaSb Thermophotovoltaic Cells" in *Thermophotovoltaic Genration of Electricity: Fourth NREL Conf.* T.J. COUTTS, J.P. BENNER, and C.S. ALLMAN, eds., AIP Conf. Proc. **460** (American Inst. Physics, Woodbury, NY, 1999) 545-553.

Z.A. SHELLENBARGER, M.G. MAUK, J.A. COX, M.I. GOTTFRIED, P.E. SIMS, J.D. LESKO, J.B. MCNEELY, L.C. DINETTA, and R.L. MUELLER, "Improvements in GaSb-Based Thermophotovoltaic Cells" *Third NREL Conference on Thermophotovoltaic Generation of Electricity*, American Inst. Phyics Conf. Proc. **401** T.J. COUTTS. C.S. ALLMAN, and J.P. BENNER, eds., (A.I.P., Woodbury, NY, 1997) 117-128.

M.G. MAUK, Z.A. SHELLENBARGER, M.I. GOTTFRIED, J.A. COX, B.W. FEYOCK, , J.B. MCNEELY, L.C. DINETTA, and R.L. MUELLER, "New Concepts for III-V Antimonide Thermophotovoltaics" *Third NREL Conference on Thermophotovoltaic*

Generation of Electricity, American Inst. Phyics Conf. Proc. **401** T.J. COUTTS. C.S. ALLMAN, and J.P. BENNER, eds., (A.I.P., Woodbury, NY, 1997) 129-137.

Z.A. SHELLENBARGER, M.G. MAUK, and L.C. DINETTA, "Recent Progress in InGaAsSb/GaSb TPV Devices" *Conf. Rec. 25th IEEE Photovoltaics Specialists Conf.* (IEEE Press, Piscataway, NJ, 1996) 81-84.

Z.A. SHELLENBARGER, M.G. MAUK, L.C. DINETTA, and G.W. CHARACHE, "InGaAsSb/GaSb Thermophotovoltaic Cells" *Proc. 14th Space Photovoltaic Research and Technology Conf. 1995 (SPRAT XIV)* NASA Conf. Publication 10180 (1996) 215-222.

J.B. MCNEELY, M.G. MAUK, and L.C. DINETTA, "An InGaAsSb/GaSb Photovoltaic Cell by Liquid-Phase Epitaxy for Thermophotovoltaic (TPV) Applications" *AIP Conf. Proc. 321: 1st NREL Conf. on Thermophotovoltaic Generation of Electricity, 1994* (New York: AIP Press, 1995) 221-225.

Part 1: Progress in InGaAsSb/GaSb TPV Devices

1.1 Summary

AstroPower is currently developing InGaAsSb thermophotovoltaic (TPV) devices. This photovoltaic cell is a two-layer epitaxial InGaAsSb structure formed by liquid-phase epitaxy on a GaSb substrate. The (direct) bandgap of the $In_{1-x}Ga_xAs_{1-y}Sb_y$ alloy is 0.50 to 0.55 eV, depending on its exact alloy composition (x,y), and is closely lattice-matched to the GaSb substrate. Internal quantum efficiencies as high as 95% have been measured at a wavelength of 2 microns. At a wavelength of 1 micron, internal quantum efficiencies of 55% have been observed. At a current density of 1.6 A/cm^2, an open-circuit voltage of 0.250 V and a fill factor of 60% have been measured. Our results to date show that the GaSb-based quaternary compounds provide a viable and high performance energy conversion solution for thermophotovoltaic systems operating with 1000 to 1500 °C source temperatures.

1.2 Introduction

The latest results on AstroPower's InGaAsSb thermophotovoltaic (TPV) cells are reported. TPVs are *p-n* junction semiconductor devices that convert photons emitted by a heated source directly into electrical power. For TPV systems utilizing thermal radiation from an emitter heated at 1000 to 1500 °C, there is a need for low-bandgap cells with a high spectral response in the 1500 to 2500 nm wavelength range. This implies the use of a TPV cell with a bandgap of ~0.5 eV. One important potential application is the radioisotope General Purpose Heat Source (GPHS), where 1100 °C blackbody radiation can be used for thermophotovoltaic energy conversion [1]. In this paper we describe high-efficiency TPV devices based on lattice-matched $In_{0.15}Ga_{0.85}As_{0.17}Sb_{0.83}$ (E_G = 0.55 eV) epitaxial layers on GaSb substrates. To AstroPower's knowledge, this is the first detailed report of the InGaAsSb quaternary alloy applied to TPV devices.

Theoretical studies have indicated that photovoltaic cells based on the InGaAsSb quaternary alloy are good candidates for TPV applications that require high spectral response in the 1500 to 2500 nm wavelength range [2,3]. Depending on its alloy composition (x,y), the direct bandgap of the $In_{1-x}Ga_xAs_{1-y}Sb_y$ alloy varies from 0.18 eV (InSb) to 1.43 eV (GaAs). The quaternary alloy can be closely lattice-matched to the GaSb substrate provided the composition is restrained to values such that $y \approx 0.1 + 0.9\, x$. With this lattice matching condition, the bandgap of the quaternary alloy ranges from approximately 0.3 to 0.7 eV. However, there is a further limitation due to a wide solid-phase miscibility gap in this quaternary at typical growth temperatures. The miscibility gap evidently precludes bandgaps in the range of 0.35 to 0.5 eV [4]. Therefore, for the spectral range of interest, we assume the lowest attainable bandgap is 0.50 to 0.52 eV. This bandgap range corresponds to an optical absorption edge of 2380 to 2480 nm.

It is worth emphasizing that the use of the quaternary alloy, as opposed to a ternary alloy such as InGaAs, provides the required bandgap with near-exact lattice matching to the GaSb substrate. Lattice-matching is important since even a small degree of lattice mismatch degrades device performance and reliability. Although there are epitaxy techniques to partially ameliorate effects associated with lattice mismatch of ternary alloy layers on binary substrates (e.g. defect-filtering superlattices, interrupted growth regimens, etc.), a simpler and more efficient approach is to use the quaternary alloy to avoid lattice mismatch altogether.

This TPV device is a two-layer epitaxial InGaAsSb structure formed by liquid-phase epitaxy on a GaSb substrate at a growth temperature of 515 °C. Liquid-Phase Epitaxy (LPE) is a well-

established technology for III-V compound semiconductor devices. A major advantage of LPE for this application is the high material quality, and more specifically, the long minority carrier diffusion lengths, that can be achieved. This results in devices which are equal or superior in performance to those made by other epitaxy processes such as molecular beam epitaxy (MBE) or metal organic chemical vapor deposition (MOCVD). Another major advantage is that LPE is a simple, inexpensive, and safe method for semiconductor device fabrication. Significantly, the LPE process does not require or produce any highly toxic or dangerous substances—in contrast to MOCVD. Also, the epitaxial growth rate with InGaAsSb LPE is ~2 μm/min., which is 10 to 100 times faster than growth rates for MOCVD or MBE. We have successfully scaled up the LPE process for epitaxial growth in a semi-continuous mode on 3-inch diameter wafers. This, combined with the high growth rates, will dramatically improve the manufacturing throughput compared to traditional and more costly epitaxy processes. The objective is to develop an epitaxial growth technology to produce low-cost, large-area, high efficiency TPV devices.

1.3 Epitaxial Growth and Fabrication of InGaAsSb TPV Cells

InGaAsSb photodiodes, light-emitting diodes, and double heterostructure injection lasers made by liquid-phase epitaxy have been previously reported [5-8]. We have adapted this technology for the production of InGaAsSb TPV cells.

A standard horizontal slideboat technique is used for the liquid-phase epitaxial growth of the InGaAsSb. The graphite slideboat is situated in a sealed quartz tube placed in a microprocessor-controlled, programmable, three-zone tube furnace. The growth ambient is palladium-diffused hydrogen at atmospheric pressure with a flow rate of 300 ml/min.

The substrates are 500-micron thick, chemically polished, (100) oriented, n-type GaSb wafers obtained from MCP Wafer Technology, Ltd. (Milton Keynes, UK) or Firebird Semiconductor, Ltd. (Trail, BC, Canada). Substrates are doped to 3-5 x 10^{17} cm^{-3} with tellurium. The substrate resistivity is 9 x 10^{-3} Ω·cm, and the average etch-pit density is approximately 1000 cm^{-2}.

The growth solutions are indium (x_{In}=0.59), gallium (x_{Ga}=0.19), antimony (x_{Sb}=0.21), and arsenic (x_{As}=0.01). The melts are formulated with 3 to 5 mm shot of high purity (99.9999%) indium, gallium, and antimony metals and arsenic added as undoped polycrystalline InAs material. The total weight of the melt is about 7 g. Prior to growth, the melts are baked out at 700 °C for 15 hours under flowing hydrogen to de-oxidize the metallic melt components and outgas residual impurities. After bake-out, appropriate dopant impurities are added to each melt. The first melt for the growth of the n-type InGaAsSb base layer contains tellurium. The small amount of Te needed to dope the layer (atomic fraction in the melt $\cong$ 10^{-5}) is problematic. For reproducible doping, a weighable amount of Te is added as 100 to 200 mg of Te-doped GaSb (C_{Te}=10^{19} cm^{-3}) or as In-Te alloy (1% Te by weight). The second melt for the growth of the p-type emitter contains 1 to 10 mg germanium. We have begun a more detailed and systematic characterization of impurity segregation and doping in the In-Ga-As-Sb quaternary system with the aim of achieving better control and a greater range of doping concentrations.

The melts are equilibrated for 1 hour at 530 °C and then cooled at a rate of 0.7 °C/min. At 515 °C, the substrate is contacted with the first melt for 2 minutes to grow a 5 micron thick n-type InGaAsSb base layer. Next, the substrate is moved to the second melt for 5 seconds to grow a 0.3 micron thick p-type InGaAsSb emitter layer.

Front and back ohmic contacts are formed on the epitaxial InGaAsSb/GaSb structure by standard processing techniques. The back of the substrate is metallized by plating with a 200 nm thick electron-beam evaporated Sn:Au layer and alloyed at 300 °C. The front contact grid consists of 10 micron wide metallization lines with 100 micron spacing and a single 1-mm wide center

busbar. The grid is formed by a photolithography lift-off process with a 200 nm thick electron-beam evaporated Au:Zn:Au metallization. The front grid is thickened to 5 microns by gold electroplating. The front contact is not sintered. The substrate is masked and patterned to define a 1 cm x 1 cm device and isolation etched with a potassium iodide - iodine etch. Most of our TPV cells are 1 cm x 1 cm in area; although larger cells (2 cm x 2 cm) with comparable performance have also been made. In order to simplify the spectral response analysis, no anti-reflection coating was applied to the cells. Figure 1 is a top-view photograph of a 1 cm x 1 cm InGaAsSb TPV cell.
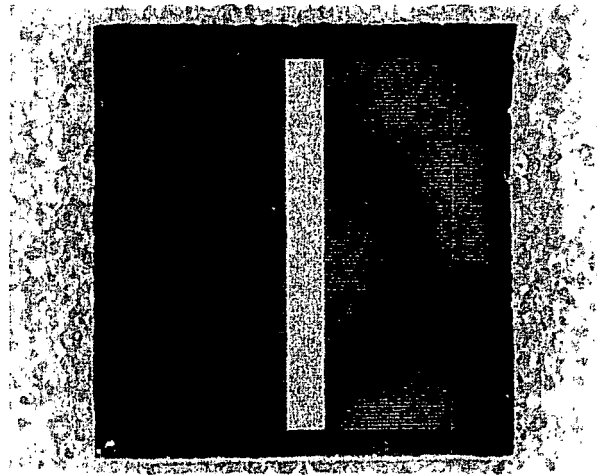

Fig. 1.1. Top-view photograph of a 1 cm x 1 cm InGaAsSb TPV cell.

1.4 TPV Device Design and Optimization TPV

Figure 1.2 shows the TPV device design in cross-section. The fabricated cells have a 0.3 to 0.5 micron thick p-type emitter with a Ge concentration of approximately 10^{19} cm^{-3}, as indicated by Secondary Ion Mass Spectroscopy (SIMS). A thicker, more heavily doped p-layer will reduce the sheet resistance of the emitter and therefore improve the fill-factor, but will tend to reduce spectral response due to higher free-carrier absorption and increased sensitivity to front surface minority carrier recombination.
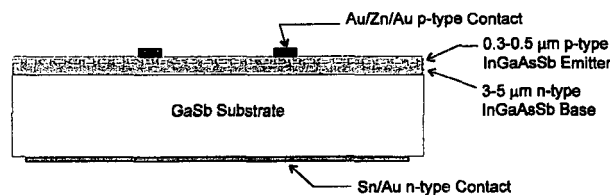

Fig.1.2. InGaAsSb/GaSb p-n junction thermophotovoltaic cell design.

The base thickness ranges from 3 to 5 microns with a Te concentration of about 10^{17} cm^{-3}, as determined from capacitance-voltage measurements and SIMS. Modeling indicates that base dopings in this range will yield the optimum open-circuit voltages and short-wavelength quantum efficiencies. Figure 1.3 shows the SIMS depth profile indicating the abruptness of the p-n junction and the depth uniformity of the doping concentrations. There is apparently very little smearing of the doping profile due to diffusion or segregation of dopants. Discrepancies between the Te dopant concentration measured by SIMS (total impurity concentration) and that implied by capacitance-voltage measurements (net donor concentration) indicate that some of the Te is either not ionized

or is compensated. This is a common problem in Te doping of III-V semiconductors, especially in GaSb-based materials, and is probably due to the formation of electrically inactive telluride complexes or compounds in the material.
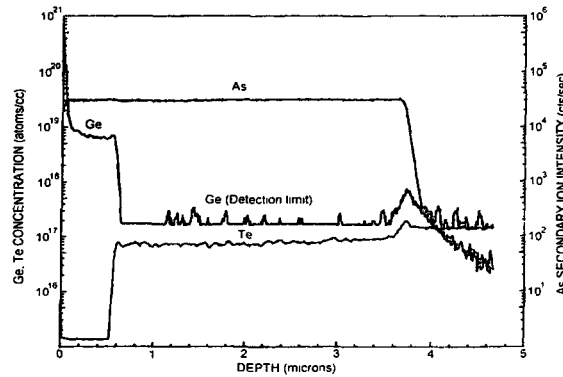

Fig. 1.3. SIMS depth profile of doping.

1.5 TPV Device Evaluation

We present external and internal spectral response curves and current-voltage characteristics for 1 cm x 1 cm p-$In_{0.15}Ga_{0.85}As_{0.17}Sb_{0.83}$:Ge / n-$In_{0.15}Ga_{0.85}As_{0.17}Sb_{0.83}$:Te epitaxial cells on n-GaSb:Te substrates produced as described above. The external spectral response and corresponding internal spectral response of a typical InGaAsSb TPV cell are shown in Figure 1.4. The lower external spectral response is due to grid shading and reflection of incident light from the uncoated InGaAsSb emitter surface. The grid shading is 18.2%. The absorption edge implied by the spectral response measurements of a number of samples ranged from approximately 2250 to 2300 nm. At a wavelength of 2000 nm, internal quantum efficiencies as high as 95% have been measured, and at a wavelength of 1 micron, internal quantum efficiencies of almost 55% have been observed. The internal quantum efficiency averaged over the spectral region from 1 to 2 microns wavelength is 60%. (It should be noted that for the intended TPV applications, the response of the cell for wavelengths less than 1.5 microns is not important.)
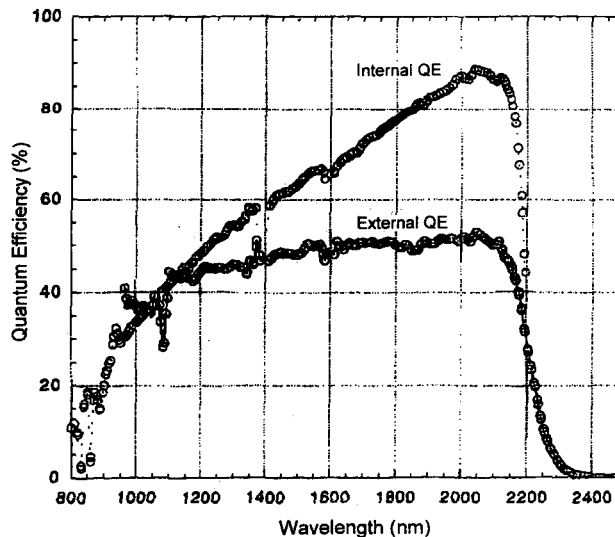

Fig. 1.4. External and internal quantum efficiencies of InGaAsSb/GaSb p-n junction thermophotovoltaic cell.

The 1 cm x 1 cm InGaAsSb TPV cells were tested under simulated infrared light using a ZnSe-filtered tungsten source (Carley Lamps, Inc., Torrance, CA) with a spectral emission in the 800 to 3000 nm wavelength range. Under an illumination intensity corresponding to a short-circuit current density of 2 A/cm^2, open-circuit voltages as high as 0.260 volts have been measured. Cells were also tested by Dr. Bob Mueller at the Jet Propulsion Laboratory using a pulsed solar simulator with an infrared bandpass filter. Figure 5 shows the current-voltage characteristics of a 1 cm x 1 cm InGaAsSb TPV cell tested in this manner which gives an output current density of 0.348 A/cm^2. This intensity yields an open-circuit voltage of 0.235 V and a fill-factor of 0.58. Figure 6 shows short-circuit current vs. open-circuit voltage for varying light intensity. The diode ideality factor changes from m = 1 to m = 2 at an open-circuit voltage of ~0.08 V. This graph implies a reverse saturation current of $J_0 \approx 1.5 \times 10^{-4}$ A/cm^2.
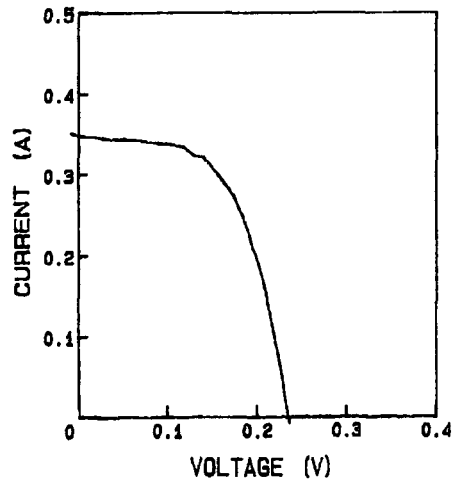

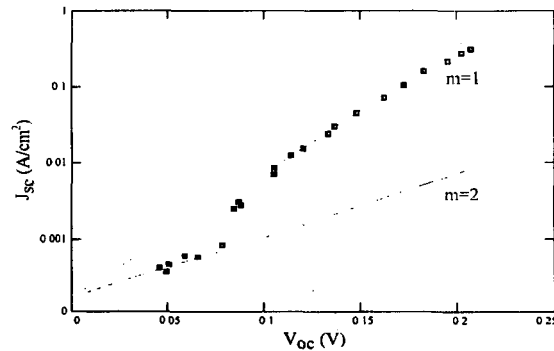Fig. 1. 5. Current-voltage characteristic of 1 cm x 1 cm InGaAsSb TPV cell.

Fig. 1.6. Short-circuit current vs. open-circuit voltage for InGaAsSb TPV cell under varying illumination intensity.

1.6 Conclusion and Discussion

Our results to date have demonstrated the potential of InGaAsSb TPV devices made by liquid-phase epitaxy. There is still room for substantial efficiency enhancements in these devices by optimization of the doping levels and layer thicknesses. Further improvements might include wide bandgap lattice-matched AlGaAsSb window layers for front surface passivation, and AlGaAsSb back-surface field cladding layers to reduce the reverse saturation current and thereby increase the open-circuit voltage. Highly doped contact layers will provide lower series resistance, as will substrate thinning. Lower series resistance will lead to higher fill factors. Thinning the substrate will also improve the heat sinking capability of the device.

The required performance of a TPV device is dependent on its system application. Spectral control of thermal emitters, the use of selective filters and reflectors, heat transfer, and photon recycling effects need to be included in the device design and system optimization. These considerations are not usually relevant for conventional photovoltaic devices and therefore the design and optimization rules for TPVs will be significantly different than those for solar cells. For example, grid obscuration and reflection are not necessarily losses in TPV systems if photons reflected from the front surface are re-absorbed by the emitter. Our next generation of InGaAsSb TPV devices will incorporate design features to fully exploit photon recycling effects.

1.7 References for Part 1

[1] A. Schock, C. Or, and V. Kumar, "Small Radioisotope Thermophotovoltaic (RTPV) Generators", *Proc. 2nd NREL Conf. on Thermophotovoltaic Generation of Electricity,* (New York: American Institute Physics, 1996), pp. 81-97.

[2] E. Kittl, "Unique Correlations Between Blackbody Radiation and Optimum Energy Gap for a Photovoltaic Conversion Device", *Proc. 10th IEEE PV Specialists Conf.,* 1973, pp. 103-106.

[3] L.D. Woolf, "Optimum Efficiency of Single and Multiple Bandgap Cells in Thermophotovoltaic Energy Conversion", *Solar Cells* **19**, 1986, pp. 19-38.

[4] M. Astles, H. Hill, A.J. Williams, P.J. Wright, and M.L. Young, "Studies of the $Ga_{1-x}In_xAs_{1-y}Sb_y$ Quaternary Alloy System I. Liquid-Phase Epitaxial Growth and Assessment", *J. Electronic Materials* **15**, 1986, pp. 41-49.

[5] A. Andaspaeva, A.N. Baranov, A. Guseinov, A.N. Imenkov, L.M. Litvak, G.M. Filaretova, and Y.P. Yakovlev, "Highly Efficient GaInAsSb Light-Emitting Diodes ($\lambda = 2.2$ μm, $\eta=4\%$, $T = 300K$)", *Soviet Technical Physics Letters* **14**, 1988, pp. 377-378.

[6] C. Caneau, A.K. Srivastava, A.G. Dentai, J.L. Zyskind, and M.A. Pollack, "Room-Temperature GaInAsSb/AlGaAsSb DH Injection Lasers at 2.2 μm", *Electronics Letters* **21**, 1985, pp. 815-817.

[7] A.E. Drakin, P.G. Eliseev, B.N. Sverdlov, A.E. Bochkarev, L.M. Dolginov, and L.V. Druzhinina, "InGaSbAs Injection Lasers", *IEEE J. Quantum Electronics* **QE-23**, 1987, pp. 1089-1094.

[8] N. Kobayashi, Y. Horikoshi, and C. Uemura, "Liquid-Phase Epitaxial Growth of InGaAsSb/GaSb and InGaAsSb/AlGaAsSb DH Wafers", *Japanese J. Applied Physics* **18**, 1979, pp. 2169-2170.

Part 2: Liquid Phase Epitaxially Grown $Al_xGa_{1-x}Sb$ Window Layers for $In_{0.15}Ga_{0.85}As_{0.17}Sb_{0.83}$\GaSb Thermophotovoltaic Cells

2.1 Summary

$Al_xGa_{1-x}Sb$ was grown via liquid phase epitaxy as a passivating window layer for $In_{0.15}Ga_{0.85}As_{0.17}Sb_{0.83}$\GaSb thermophotovoltaic cells. The growth of this aluminum ternary alloy allowed for lattice matching to the $In_{0.15}Ga_{0.85}As_{0.17}Sb_{0.83}$ active layer over the aluminum solidus composition range of 5.5 to 78.5 mole%. This corresponded to a bandgap range of approximately 0.81 to 1.96 eV. The $In_{0.15}Ga_{0.85}As_{0.17}Sb_{0.83}$ active layers had a 0.53 eV bandgap with a band edge of 2.33 µm. Fabricated TPV devices with an $Al_xGa_{1-x}Sb$ passivating window layer demonstrated a comparable performance to devices with a 1.2 eV $Al_{0.3}Ga_{0.7}As_{0.02}Sb_{0.98}$ passivating layer. It was determined that the $Al_xGa_{1-x}Sb$ ternary was more favorable to crystal growth by LPE than the $Al_{0.3}Ga_{0.7}As_{0.02}Sb_{0.98}$ quaternary. A V_{oc} of 229 mV and 208 mV was obtained for an aluminum quaternary and ternary window layer respectively. In order to determine the quality of the aluminum ternary layers, mesa photodiodes were fabricated and characterized optically and electrically. The photodiodes yielded a spectral response as high as 0.99 A/W at a wavelength of 770 nm.

2.2 Introduction

Liquid phase epitaxy produces high quality layers and has been utilized in the fabrication of optoelectronic devices such as lasers, light emitting diodes, photocathodes, and solar cells. The interest in LPE has been fostered by the growing interest in III-V materials from simple homojunctions to the lattice matched heterojunctions presented here. These high quality growth layers possess long diffusion lengths, and high minority carrier lifetimes. The dislocation density of the growth layer is generally lower than the substrate material. These benefits are the results of near-equilibrium growth conditions, impurity segregation ratios of less than one and close control of the stoichiometry.

In this project two window layers were grown, $Al_{1-x}Ga_xAs_{1-y}Sb_y$ and $Al_xGa_{1-x}Sb$. The function of the window layer was to reduce the surface recombination velocity of the device by decreasing the number of dangling bonds on the surface. By passivating the front surface of the device with a wide-bandgap layer, the high quantum efficiencies observed in the longer wavelengths can be extended to shorter wavelengths. This type of design is comparable to AlGaAs/GaAs heterojunction solar cells.

2.3 Experimental

One of the first published works investigating the growth of the InGaAsSb quaternary lattice matched to GaSb by liquid phase epitaxy was by Kobayashi et al[1]. Astles et al.[2] described the phase equilibria for this system based upon the regular solution theory approximations of Jordan and Ilegems[3]. Several other researchers have reported growth of InGaAsSb compounds by LPE for optoelectronic devices[4,5-6,7-10].

The liquid phase epitaxy growth technique utilized was the horizontal sliding boat system. The system consisted of a graphite slideboat that was situated inside a sealed quartz tube, which was surrounded by a rolling, cylindrical, microprocessor-controlled, programmable, three-zone furnace. The rolling nature of the furnace allowed rapid heating and cooling of the growth boat. The InGaAsSb quaternary alloy compositional diagram is presented in Figure 2.1. The lines of

interest are the solid lines showing lattice constant and the dashed lines denoting the bandgap. The lattice matching compound for a band edge of 0.53 eV is given by Astles[2] as $In_{0.15}Ga_{0.85}As_{0.17}Sb_{0.83}$. The entire possible range of the quaternary alloy lattice matched to GaSb covers the emission wavelengths of 1.8 to 4.4 μm.
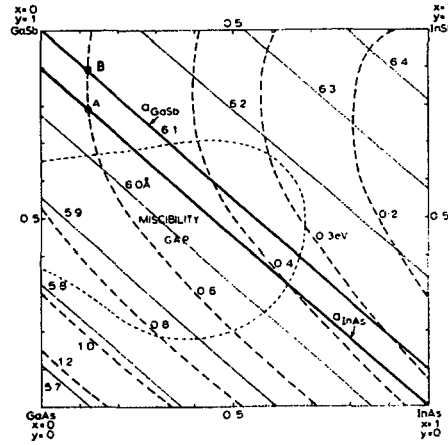
Figure 2.1   **Range of lattice matched compositions to GaSb and InAs that can be grown in the InGaAsSb system. Lines of constant lattice parameter[Å] (——) and energy gap[eV] (---) at 300 K and the immiscible region are shown[2].**

As shown in Figure 2.1, there is a miscibility gap in this system. Tournié et al.[72] have calculated this miscibility region to be due to both binodal and spinodal decomposition. This region of immiscibility limits compound growth from a GaSb rich solution to wavelengths between about 1.8 to 2.4 μm or bandgaps of 0.51 to 0.69 eV at 300 K.

The substrates were chemically polished, 500 μm thick, (100) oriented, n type GaSb wafers. The wafers were Te doped to a carrier concentration of 0.7 - 3×10^{17} cm^{-3} with an average electron mobility of 3000 cm^2/V/sec at 300 K. The wafers were diced into 1.59 cm x 1.59 cm substrates. Prior to a LPE run the substrate and a float wafer underwent a cleaning procedure of five minute immersions in hydrofluoric acid, methanol and isopropanol. The liquid growth solution consisted of $X^L_{In} = 0.59$, $X^L_{Ga} = 0.19$, $X^L_{Sb} = 0.21$ and $X^L_{As} = 0.01$. The metals indium, gallium and antimony were added as high purity (99.9999%) shot pieces. The arsenic was added as an undoped InAs polycrystalline float wafer of size 0.50 cm x 0.50 cm. The total melt weight was approximately 7 g. The three metal components of the melt were baked out at 700 °C for fourteen hours prior to growth under a flow of palladium diffused hydrogen. This was performed in order to outgas any residual impurities and to de-oxidize the melt constituents.

After bakeout, a cleaned InAs float wafer and any dopants were added to the melt. The GaSb substrate was placed within the slider of the growth boat and the run commenced. The melt was held at the liquidus temperature of 534 °C for ninety minutes, under hydrogen flow, in order to equilibrate the melt components. The melt was then supercooled in order to create a driving force for nucleation. A total of 15 °C supercooling was achieved in approximately twenty minutes and from there the system dropped at approximately 1 °C/minute. At the growth temperature of 519 °C

the substrate was brought into contact with the first melt for ninety seconds to grow a 5 μm thick n type base layer. Upon the completion of the growth time the substrate was then brought into contact with the second well of the graphite boat for two seconds to grow a 0.5 μm thick p type emitter layer. The substrate was then pushed clear of the boat and allowed to cool under the flow of hydrogen.

Several researchers have reported LPE growth of AlGaAsSb lattice matched to GaSb layers[1,4,5,8,11]. The compositional diagram for the AlGaAsSb system is presented in Figure 2.2.
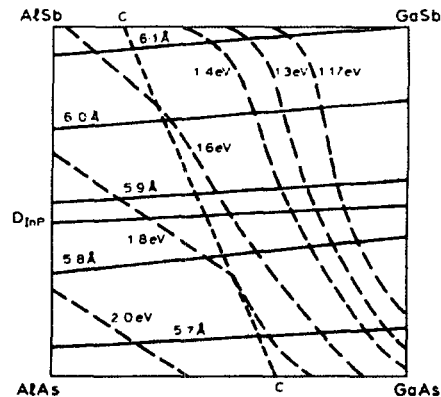
Figure 2.2   **Lines of constant lattice parameter[Å] (—) and energy gap[eV] (---) at 300 K for the AlGaAsSb system. The transition (C-C) from direct to indirect and the lattice constant of InP, D_{InP}, are noted[12].**

The direct bandgap transition absorption edge for the quaternary system varies from 0.75 to 1.7 μm or 1.65 to 0.73 eV. The system goes from a direct to an indirect transition as the composition deviates from a GaSb rich solution. This is due to the increasing contribution of the indirect band transitions from the AlAs and AlSb binaries.

The lattice matched composition of AlGaAsSb to GaSb was $Al_{0.3}Ga_{0.7}As_{0.02}Sb_{0.98}$ [4,15,14] and gave a bandgap of approximately 1.2 eV. This corresponded to a melt solution of $X^L_{Al} = 0.015$, $X^L_{Ga} = 0.957$, $X^L_{Sb} = 0.028$ and $X^L_{As} = 0.001$. The metals indium, gallium and antimony were added as high purity (99.9999%) shot pieces. The arsenic was added as an undoped GaAs polycrystalline float wafer of size 0.5 cm x 0.5 cm. The cleaning and growth procedures were the same as with the InGaAsSb alloy. The AlGaAsSb quaternary was placed in the third well of the growth boat. Upon the completion of the growth of the $In_{0.15}Ga_{0.85}As_{0.17}Sb_{0.83}$ emitter layer, the substrate was pushed into contact with the $Al_{0.3}Ga_{0.7}As_{0.02}Sb_{0.98}$ for two seconds. This grew a 0.5 μm thick window layer. The AlGaAsSb layers were very dependent upon the temperature and small variations yielded a non-planar growth.

As an alternative to the quaternary window layer, growth of the AlGaSb ternary was attempted. The phase diagram of the ternary has been calculated by Cheng et al.[15], Osamura et al.[16], and Joullié et al[17]. The results of Cheng et al. were followed. A saturation technique was employed to ascertain the liquidus data along the 400, 450, 500 and 550 °C isotherms within the Ga rich section of the $Al_xGa_{1-x}Sb$ ternary system. In addition, the liquidus curves were calculated based

on a regular solution thermodynamic model. Figure 2.3 shows the experimentally determined and calculated solidus isotherms of Cheng et al.
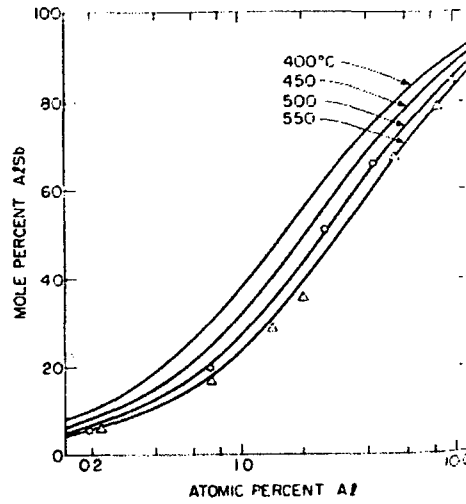
Figure 2. 3   **Solidus isotherms of the $Al_xGa_{1-x}Sb$ ternary system. The data points are the experimental values and the solid lines are calculated[15].**

The solid aluminum composition was set to 67 mole% for the $Al_xGa_{1-x}Sb$ layer . This value was chosen because it allowed for the direct observation of the incorporation of Al into the layer and the ability to view the possible effects of lattice mismatch. The 67 mole% value was enough to shift absorption to lower wavelengths and give the layer a blue appearance. The melt composition was X^L_{Al} = 0.054, X^L_{Ga} = 0.923, X^L_{Sb} = 0.023. The remaining procedure is similar to that for the quaternaries except for the use of a GaSb float and a growth time of 15 seconds for the TPV window layer.

Utilizing the limited linear nature of Figure 2.3, several Al compositions were attempted at different liquidus temperatures. Table 2.1 summarizes the theoretical melt components, temperature and associated aluminum solidus composition.

Table 2.1 Melt composition and aluminum solidus composition at different liquidus temperatures for the AlGaSb ternary alloy[77].

Liquidus Temperature	Melt Composition	Al Solidus Composition
550 °C	$X^L_{Al} = 0.186$, $X^L_{Sb} = 0.080$, $X^L_{Ga} = 0.805$	90.5 mole%
550 °C	$X^L_{Al} = 0.080$, $X^L_{Sb} = 0.016$, $X^L_{Ga} = 0.899$	78.5 mole%
550 °C	$X^L_{Al} = 0.054$, $X^L_{Sb} = 0.023$, $X^L_{Ga} = 0.923$	67.1 mole%
550 °C	$X^L_{Al} = 0.019$, $X^L_{Sb} = 0.042$, $X^L_{Ga} = 0.938$	35.2 mole%
550 °C	$X^L_{Al} = 0.014$, $X^L_{Sb} = 0.048$, $X^L_{Ga} = 0.937$	28.5 mole%
550 °C	$X^L_{Al} = 0.007$, $X^L_{Sb} = 0.055$, $X^L_{Ga} = 0.937$	16.6 mole%
550 °C	$X^L_{Al} = 0.002$, $X^L_{Sb} = 0.063$, $X^L_{Ga} = 0.934$	5.50 mole%
525 °C	$X^L_{Al} = 0.048$, $X^L_{Sb} = 0.017$, $X^L_{Ga} = 0.934$	66.0 mole%
500 °C	$X^L_{Al} = 0.025$, $X^L_{Sb} = 0.017$, $X^L_{Ga} = 0.958$	50.7 mole%

Each of the nine different aluminum solidus compositions were grown successfully via LPE on a (100) GaSb substrate. It was determined that the AlGaSb ternary is favorable to growth by liquid phase epitaxy. In all instances the presence of a GaSb float was necessary in order to achieve saturation. Furthermore, the growth of the 90.5 mole% composition yielded a cross-hatched layer, denoting a substantial lattice mismatch. This was expected given that $a_{GaSb} = 6.09593$ Å and $a_{AlSb} = 6.1355$ Å.

2.4 Results

In order to determine the quality of the AlGaSb ternary layers, mesa photodiodes with 200 µm diameter active areas were fabricated. The liquid phase epitaxy procedure for the AlGaSb ternary was modified to grow an emitter and base layer on a (100) GaSb substrate. The estimated aluminum solidus composition for the layers was 67 mole%. This correlated to an approximate bandgap of 1.79 eV. The emitter was doped p type with Zn and the base n type with Te. The growth time for the base layer was two minutes and the growth time for the emitter was fifteen seconds. The device was then fabricated using standard photolithographic techniques in order to form the mesa structure. The metallization for the back n type contacts was planar Au/Sn, while the front p type contacts were annular Au/Zn. A top view of a completed photodiode is presented in Figure 2.4.

device active area

edge of polyimide layer

←200μm→

mesa isolation trench
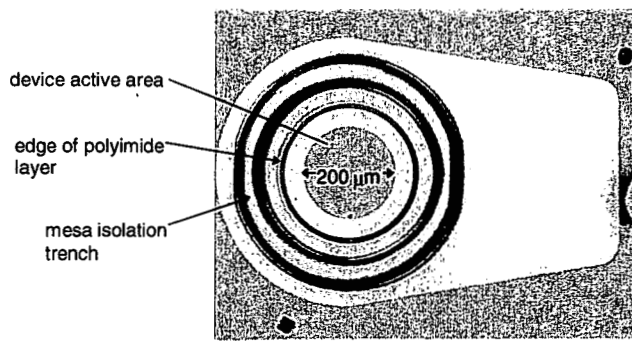
Figure 2. 4   Top view of mesa photodiode.

The purpose of the polyimide layer was to planarize the surface for the deposition of the front contact, insulate the mesa isolation trench and passivate the circumference of the active area. After fabrication, 1 mm x 1 mm die with a single device each were diced and bonded to a TO-18 header with silver conductive epoxy. The devices were wirebonded from the bonding pad of the device to the post of the header. The bonding and configuration is shown in Figure 2.5. In order to protect the photodiode the devices were encapsulated with optically clear Epo-Tek 301 epoxy. This encapsulant served to passivate and reduce reflection from the surface of the device. A view of the encapsulated device is shown in Figure 2.6.

wirebond   p-type contact   isolation trench

collecting area

1 mm
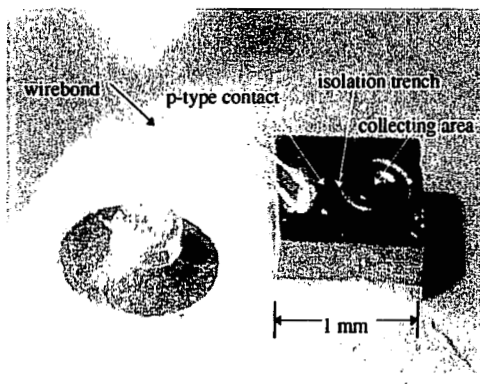
Figure 2.5   Photodiode bonded to header and wirebond.

Encapsulant

Header

1 mm
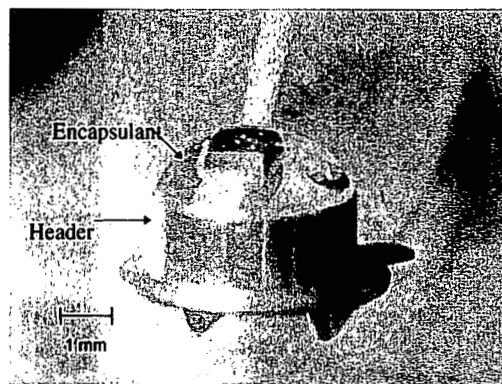
Figure2. 6   Encapsulated photodiode.

A total of eleven AlGaSb photodiodes were mounted onto headers and tested. The initial testing involved the determination of the response of the devices under bias. The I-V curve was obtained using a curve tracer and a probing stage. The potential for photoresponse was evaluated with a microscope stage light. It was found that the devices possessed substantial photoresponse under the microscope light. A characteristic I-V curve for a ternary device is shown in Figure 2.7.
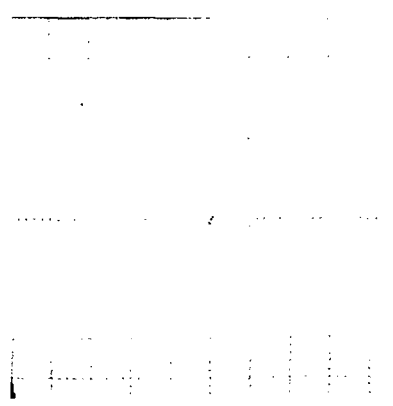
Figure 2. 7   I-V curve for AlGaSb ternary photodiode in the dark. Scale is horizontal 0.1 V/division, vertical 0.5 mA/division.

The mesa photodiodes demonstrated photoresponse under bias characteristic of a diode. The devices were leaky and demonstrated a low breakdown voltage. The breakdown voltage in reverse bias was approximately 0.1 Volts. Due to the leaky nature of the device, capacitance-voltage measurements could not be performed in order to determine the impurity concentration and the built in voltage.

In order to determine the extent of their photoresponse, the photodiodes were tested using an automated spectrometer. Figure 2.8 shows the spectral response for two of the fabricated photodiodes. The total testing range was from 750 to 1000 nm. This testing range was limited by the availability of spectral filters.
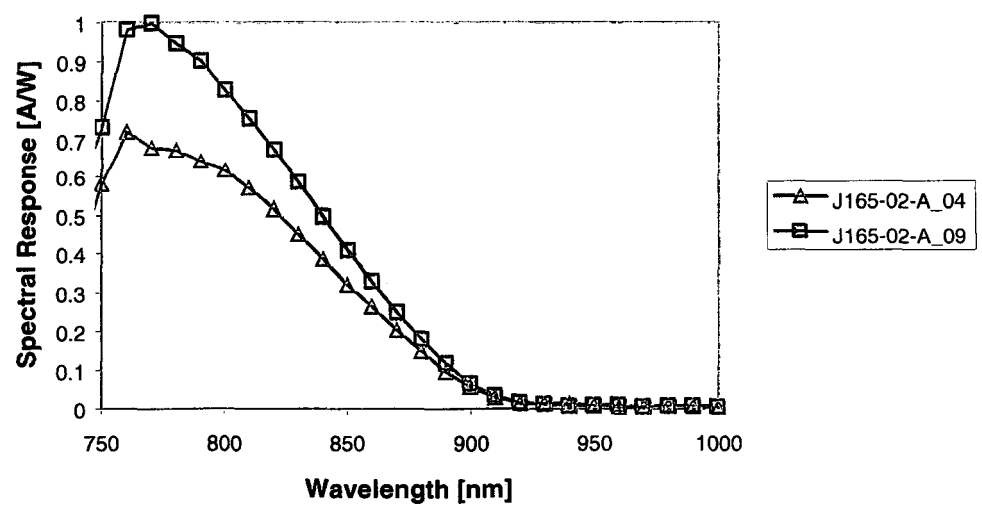
Figure 2. 8   Spectral response for AlGaSb photodiodes.

The band edge of the ternary was 900 nm, corresponding to a bandgap of 1.37 eV. This band edge was lower than the anticipated value of 1.79 eV from the solidus data of Cheng et al[15]. The devices showed a spectral response as high as 0.99 A/W at a wavelength of 770 nm. This experimentally proved the optoelectronic quality of the AlGaSb ternary layers. The soft absorption edge of the spectral response was a result of the indirect nature of the material. The discrepancy between the expected and obtained band edge was not critical, because it was still well below the band edge of the $In_{0.15}Ga_{0.85}As_{0.17}Sb_{0.83}$ quaternary layer and could function properly as a window layer.

Thermophotovoltaic devices were fabricated using standard photolithography techniques. The devices were 1 cm^2 in total area with a front and back contact. The generated current was collected via a top grid contact. The contact grid was a pattern consisting of 10 μm grid lines with 100 μm spacing between. Perpendicular to the grid lines was a 1 mm wide busbar. The front surface of a 1 cm^2 InGaAsSb device is shown in Figure 2.9.
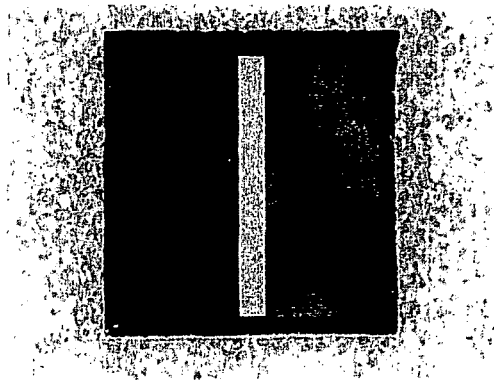
Figure 2.9   **Front surface of TPV device showing the top contact pattern with grid lines and busbar.**

The total shading from the grid pattern and busbar is 18 %. The grid lines and busbar have a total thickness of 5 μm. This metallization was achieved through a series of electron beam depositions and electroplating. Utilizing an electron beam deposition system three individual layers of 300 Å Au, 300 Å Zn and 3000 Å Au were deposited. The deposition of the Zn layer aided in the creation of an ohmic contact with the front surface. This was followed by electroplating to 5 μm thickness.

During the course of this research twelve $In_{0.15}Ga_{0.85}As_{0.17}Sb_{0.83}$ thermophotovoltaic devices were fabricated. The devices were under simulated infrared light using a ZnSe-filtered tungsten source with a spectral emission in the 800 to 3000 nm wavelength range. The estimated radiant flux of the lamp was 1.84x10^{18} photons/sec/cm^2. The results are summarized in Table 2.2.

Table 2.2   Results of fabricated $In_{0.15}Ga_{0.85}As_{0.17}Sb_{0.83}$ TPV devices.

Device	V_{oc}	J_{sc}	Fill Factor	Window Layer
B169-04	163 mV	59 mA/cm^2	19.4 %	None
B169-05	166 mV	69 mA/cm^2	21.0 %	None
B169-06	177 mV	66 mA/cm^2	18.6 %	None
B169-07	224 mV	100 mA/cm^2	18.6 %	AlGaSb
B169-08	200 mV	88 mA/cm^2	18.7 %	AlGaSb
B169-09	208 mV	96 mA/cm^2	19.3 %	AlGaSb
B169-11	26 mV	5 mA/cm^2	22.0 %	AlGaAsSb
B169-12	176 mV	81 mA/cm^2	18.5 %	AlGaAsSb
B169-13	229 mV	84 mA/cm^2	19.4 %	AlGaAsSb
B169-14	228 mV	112 mA/cm^2	20.0 %	AlGaAsSb
B172-03	132 mV	76 mA/cm^2	22.8 %	None
B172-04	2 mV	1 mA/cm^2	10.1 %	None

The fabricated devices all demonstrated low fill factors and short circuit current densities. This low performance was due to a high series resistance of the devices. This resistance was evident from the near linear J-V curves for the devices rather than an exponential for a standard diode curve i.e. Figure 7. The highest V_{oc}, J_{sc} and fill factors were exhibited by those devices that had a window layer. Devices with either the AlGaSb or AlGaAsSb window layers yielded a V_{oc} in the 200 mV range with fill factors near 20 %. A V_{oc} of 229 mV and 208 mV was obtained for an aluminum quaternary and ternary window layer respectively. No quantum efficiency measurements were able to be performed on the TPV devices.

2.5 Conclusions

Thermophotovoltaic devices utilizing an AlGaSb window layer were fabricated and tested. The ternary AlGaSb window layer yielded comparable results to a AlGaAsSb passivating layer. The use of the ternary is more favorable to LPE growth and offers a range of bandgaps while still maintaing the lattice matching condition. Furthermore, the ternary offers more flexibility in the epitaxial layer growth while being less susceptible to variations in temperature and melt composition. Fabricated photodiodes demonstrated the high quality opto-electric properties of the LPE grown AlGaSb ternary semicondutor compound.

2.6 References for Part 2

[1]   Kobayashi N., Horikoshi Y., Uemura C., "Liquid-Phase-Epitaxial Growth of InGaAsSb/GaSb and InGaAsSb/AlGaAsSb DH Wafers," Japanese Journal of Applied Physics, **18**, (1979) pp. 2169-2170.

[2]   Astles M., Hill H., Williams A.J., Wright P.J., Young M.L., "Studies of the $Ga_{1-x}In_xAs_{1-y}Sb_y$ Quaternary Alloy System I. Liquid-Phase Epitaxial Growth and Assessment," Journal of Electronic Materials, **15**, No. 1, (1986) pp. 41-49.

[3]   Jordan A.S., Ilegems M., "Solid-Liquid Equilibria for Quaternary Solid Solutions Involving Compound Semiconductors in the Regular Solution Approximation," Journal of Physical Chemistry of Solids, **36**, (1975) p. 329.

[4]   Shellenbarger Z.A., Mauk M.G., Cox J.A., Gottfried M.I., Sims P.E., Lesko J.D., McNeely J.B.,
        DiNetta L.C., Mueller R.L. "Improvements in GaSb-Based Thermophotovoltaic Cells," <u>Proc. Third
        NREL Conference On Thermophotovoltaic Generation of Electricity</u>, **AIP 401**, (1997).117-128.

[5]   Xiuying G., Bauhua Y., Yindi M., Fensheng G., Ying Y., Wenjian H., Xuefeng L., Jinying X.,
        Zuahguo W., Lanying L., "Liquid Phase Epitaxy Growth and Properties of
        GaInAsSb/AlGaAsSb/GaSb Heterostructures," <u>Japanese Journal of Applied Physics</u>, **30**, No. 7 (1991)
        1343-1347.

[6]   Voronina T.I., Lagunova T.S., Mikhaïlova M.P. Moiseev K.D., Yakovlev Yu.P., "High Carrier
        Mobility in p-type GaInAsSb/p-InAs Heterostructures," <u>Semiconductors</u>, **60** (1996). 523-526.

[7]   DeWinter J.C., Pollack M.A., Srivastava A.K., Zyskind J.L., "Liquid Phase Epitaxial the $Ga_{1-x}In_xAs_{1-y}Sb_y$ Lattice-Matched To (100) GaSb Over the 1.71 to 2.33 µm Wavelength Range," <u>Journal of
        Electronic Materials</u>, **14**, No. 6, (1985) 729-747.

[8]   Joullié A., Jia Hua F., Karouta F., Mani H., Alibert C., "III-V Alloys Based on GaSb for Optical
        Communications at 2.0 –4.5 µm," <u>SPIE Optical Fibers Sources and Detectors</u>, **587**, (1985) 46-57.

[9]   Tournié E., Lazzari J.-L., Mani H., Pitard F., Alibert C., Joullié A., "Growth by Liquid Phase Epitaxy
        and Characterization of GaInAsSb and InAsSbP Alloys for Mid-Infrared Applications (2-3 µm),"
        <u>SPIE Physical Concepts of Materials for Novel Optoelectronic Device Applications</u>, **1361**, (1990).
        641-656.

[10]   Wang J-M., Sun Y-M., Wu M-C., "High-Quality $Ga_{1-x}In_xAs_{1-y}Sb_y$ Quaternary Lasers Grown from
        Antimonide-Rich Solutions by Liquid-Phase Epitaxy," <u>Journal of Crystal Growth</u>, **172**, (1997). 514

[11]   Bhan J., Joullié A., Mani H., Joullié A.M., Alibert C., "III-V Heterostructures for Laser Emission in
        the 2.55 µm Wavelength Region," <u>SPIE: Materials and Technologies for Optical Communications</u>,
        866 (1987). 126-134.

[12]   Astles M.G. 103.

[13]   Baranov A.N., Konnikov S.G., Popova T.B., Umansky V.E., Yakovlev Yu.P., "Liquid Phase Epitaxy
        of $Ga_{1-x}Al_xSb_{1-y}As_y$ /GaSb and The Effect of Strain on Phase Equilibria," <u>Journal of Crystal Growth</u>,
        66, (1984) 547-552.

[14]   Pessetto J.R., Stingfellow G.B., "$Al_xGa_{1-x}As_ySb_{1-y}$ Phase Diagram," <u>Journal of Crystal Growth</u>, **62**,
        (1983) 1-6.

[15]   Cheng K.Y., Pearson G.L., "The Al-Ga-Sb Ternary Phase Diagram and Its Application to Liquid
        Phase Epitaxial Growth," <u>Journal of Electrochemical Society; Solid-State Science and Technology</u>,
        124, No. 5, (1977) 753-757.

[16]   Osamura K., Nakajima K., Murakami Y., "Experiments and Calculation of the Al-Ga-Sb Ternary
        Phase Diagram," <u>Journal of Electrochemical Society; Solid-State Science and Technology</u>, **126**, No.
        11, (1979) 1992-1997.

[17]   Joullié A., Gautier P., "The Al-Ga-Sb Ternary Phase Diagram and Its Application To Solution
        Growth," <u>Journal of Crystal Growth</u>, **47**, (1979)
        pp. 100-108.

Part 3: Improvements in GaSb-Based Thermophotovoltaic Cells Through the Use of Lattice-Matched, Wide-Bandgap AlGaAsSb 'Window' Layers

3.1 Summary

This work seeks to improve the performance of GaSb-based thermophotovoltaic (TPV) devices. Previously, we demonstrated InGaAsSb (~0.53 bandgap) cells with very high internal quantum efficiencies at wavelengths of 2 microns. Enhanced efficiency should be possible using more sophisticated double heterostructures with wide-bandgap, lattice-matched AlGaAsSb front surface passivating "window" layers and Back Surface Field (BSF) cladding layers. The double heterostructure also provides more design flexibility for improved fill factor—by reducing series resistance—and more effective photon recycling—by avoiding high doping and thereby minimizing parasitic optical absorption. We demonstrate a near ten-fold reduction in reverse-saturation current (to as low as 10^{-5} A/cm^2), higher fill factors (over 60%), and much improved short-wavelength spectral response using a wide-bandgap (~1.1 eV) AlGaAsSb window layer to passivate the front surface. The effective use of a BSF layer is less straight-forward, as very non-ideal current voltage characteristics can result from inclusion of a BSF cladding layer. Some preliminary results indicate these problems can possibly be avoided by more detailed optimization of the base and BSF doping.

3.2 Introduction and Background

In the last year we have reported progress in *p-n* homojunction InGaAsSb thermophotovoltaic (TPV) cells [1-2]. This material system has a good spectral match for many practical thermal emitters. These cells have an epitaxial device structure with an absorbing region bandgap of ~0.53 eV and are designed for thermophotovoltaic conversion of ~1200 °C blackbody sources, such as the GPHS (General Purpose Heat Source). TABLE 3.1 summarizes typical performance of 1-cm x 1-cm InGaAsSb homojunction TPV cells with the design of FIGURE **3.1a**. The most significant results from the first stage of effort were the high internal quantum efficiencies achieved at wavelengths between 1800 and 2100 nm. A later version of these cells (FIGURE **3.1b**) was designed to utilize photon recycling by the addition of a "back mirror" contact to reflect sub-bandgap light back to the thermal source. To effect a mirror, silicon dioxide was deposited on the backside of the substrate, patterned with stripe openings, and then overlaid with a gold coating. In this case, a low-doped (10^{16} cm^{-3}) GaSb substrate was used to reduce free-carrier absorption of sub-bandgap energy photons. Sub-bandgap reflection (measured without a front contact grid) was over 90%, but this value is significantly reduced when the device layers and/or substrate are more heavily doped. Although this design achieved the desired optical performance when the doping of the substrate and epilayers was kept low, the cell suffered from reduced fill factors (FF = 40 to 50%) due to high series resistance and possibly non-linear behavior of the InGaAsSb base / GaSb substrate junction.

Table 3.1

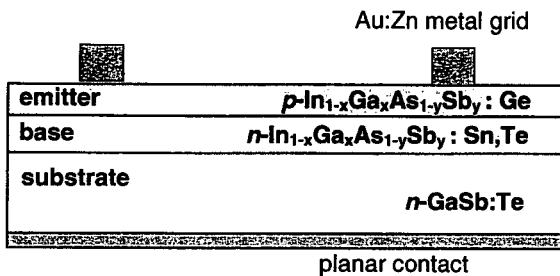|	
open-circuit voltage (V)	0.260
short-circuit current (A/cm^2)	2.0
fill factor	0.58
internal QE at $\lambda = 2$ μm	95%
internal QE at $\lambda = 1$ μm	55%

To help reduce series resistance and free-carrier optical absorption, we thin the GaSb substrate to less than 100 microns thickness in a post-growth etching using a KI-I$_2$ aqueous solution or a Br-methanol "polishing" etch. Substrate thicknesses as low as 60 microns on 1-cm x 1-cm devices have been achieved.

InGaAsSb quaternary alloy are good candidates for TPV applications that require high spectral response in the 1500 to 2500 nm wavelength range [3-5]. Depending on its alloy composition (x, y), the direct bandgap of the In$_{1-x}$Ga$_x$As$_{1-y}$Sb$_y$ alloy varies from 0.18 eV (InSb) to 1.43 eV (GaAs). The quaternary alloy can be closely lattice-matched to the GaSb substrate provided the composition is restrained to values such that $y \approx 0.1 + 0.9$ x. With this lattice matching condition, the bandgap of the quaternary alloy ranges from approximately 0.3 to 0.7 eV. However, there is a further limitation due to a wide solid-phase miscibility gap in this quaternary at typical growth temperatures. The miscibility gap evidently precludes bandgaps in the range of 0.35 to 0.5 eV [6]. Therefore, for the spectral range of interest, we assume the lowest attainable bandgap is 0.50 to 0.52 eV. This bandgap range corresponds to an optical absorption edge of 2380 to 2480 nm.
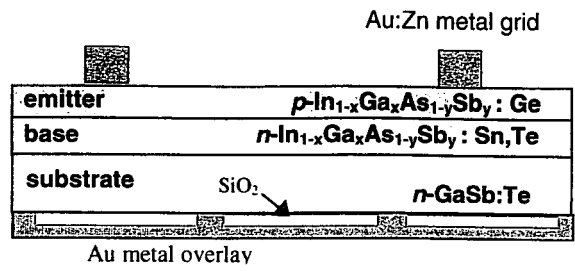
It is worth emphasizing that the use of the quaternary alloy, as opposed to a ternary alloy such as InGaAs, provides the required bandgap with near-exact lattice matching to the GaSb substrate. Lattice-matching is important since even a small degree of lattice mismatch degrades device performance and reliability. Although there are epitaxy techniques to partially ameliorate effects associated with lattice mismatch of ternary alloy layers on binary substrates (e.g. defect-filtering superlattices, interrupted growth regimens, etc.), a simpler and more efficient approach is to use the quaternary alloy to avoid lattice mismatch altogether.

High-quality, lattice-matched heterostructures using alloys of AlGaAsSb and InGaAsSb are also feasible. We believe lattice-matched structures are important in avoiding degradation at the high current densities (1 to 10 A/cm^2) typical in TPV applications. One objective is to extend the high quantum efficiencies to shorter wavelengths by passivating the front surface with a wide-bandgap, lattice-matched AlGaAsSb "window" layer, similar to the designs common in AlGaAs/GaAs heteroface solar cells used for space power. Another objective is to reduce the reverse saturation current for higher open-circuit voltages. This entails the use of a BSF (Back Surface Field) cladding layer. This is the well-established and very effective design approach used in high-efficiency GaAs solar cells. The multilayer structure should also provide more flexibility in achieving reducing series resistance and realizing high fill factors, while still maintaining low parasitic absorption of sub-bandgap photons. For instance, a wide bandgap window layer can help reduce the sheet resistance of the emitter.

We are undertaking a systematic comparison and optimization of the designs shown in FIGURE **3.1** to determine the best structure for GaSb-based TPV cells, specifically with respect to the utility and optimum implementation of front surface window layers, and back surface field (BSF) cladding layers, as well as comparisons between p-n InGaAsSb homojunctions vs. p-n AlGaAsSb/InGaAsSb heterojunctions, and n-on-p vs. p-on-n cell configurations. The experimental cells are characterized on the basis of internal and external quantum efficiency, sub-bandgap reflection, current-voltage characteristics under pulsed solar simulator illumination, and variation of operating characteristics with cell temperature. This study will be useful in exploiting the full potential of GaSb-based alloys for thermophotovoltaic applications.

Au:Zn metal grid

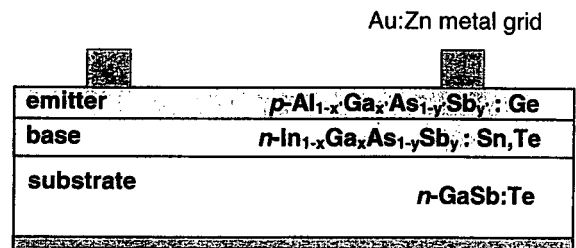| emitter	$p\text{-}In_{1-x}Ga_xAs_{1-y}Sb_y$: Ge
base	$n\text{-}In_{1-x}Ga_xAs_{1-y}Sb_y$: Sn,Te
substrate	$n\text{-}GaSb$:Te

planar contact

a. *p-on-n* homojunction {$x = 0.85$; $y = 0.83$}

Au:Zn metal grid

emitter	$p\text{-}In_{1-x}Ga_xAs_{1-y}Sb_y$: Ge
base	$n\text{-}In_{1-x}Ga_xAs_{1-y}Sb_y$: Sn,Te
substrate	SiO_2 $n\text{-}GaSb$:Te

Au metal overlay

b. *p-on-n* homojunction (with back oxide / gold reflector and thinned substrate)
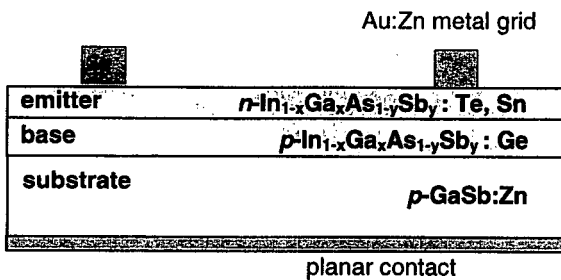
Au:Zn metal grid

emitter	$n\text{-}In_{1-x}Ga_xAs_{1-y}Sb_y$: Te, Sn
base	$p\text{-}In_{1-x}Ga_xAs_{1-y}Sb_y$: Ge
substrate	$p\text{-}GaSb$:Zn

planar contact

c. *n-on-p* homojunction {$x = 0.85$; $y = 0.83$}

Au:Zn metal grid

emitter	$p\text{-}Al_{1-x}Ga_xAs_{1-y}Sb_y$: Ge
base	$n\text{-}In_{1-x}Ga_xAs_{1-y}Sb_y$: Sn,Te
substrate	$n\text{-}GaSb$:Te

d. *p-on-n* AlGaAsSb/InGaAsSb heterojunction

Au:Zn metal grid

emitter	$p\text{-}In_{1-x}Ga_xAs_{1-y}Sb_y$: Ge
base	$n\text{-}In_{1-x}Ga_xAs_{1-y}Sb_y$: Sn,Te
BSF/ cladding	$n\text{-}Al_{1-x}Ga_xAs_{1-y}Sb_y$: Sn,Te
substrate	$n\text{-}GaSb$:Te

e. *p-on-n* homojunction with wide bandgap cladding (BSF) layer.

emitter	$p\text{-}Al_{1-x}Ga_xAs_{1-y}Sb_y$: Ge
base	$n\text{-}In_{1-x}Ga_xAs_{1-y}Sb_y$: Sn,Te
BSF / cladding	$n\text{-}Al_{1-x}Ga_xAs_{1-y}Sb_y$: Sn,Te
substrate	$n\text{-}GaSb$:Te
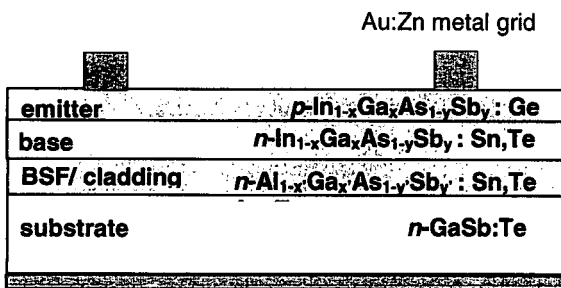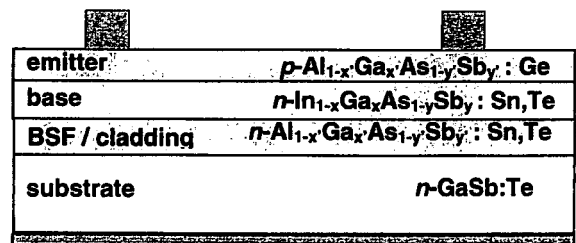
f. *p-on-n* heterojunction with wide bandgap cladding (BSF) layer.
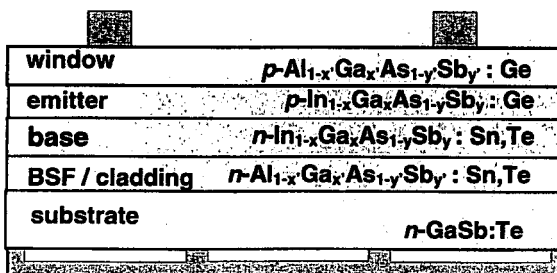
window	$p\text{-}Al_{1-x}Ga_xAs_{1-y}Sb_y$: Ge
emitter	$p\text{-}In_{1-x}Ga_xAs_{1-y}Sb_y$: Ge
base	$n\text{-}In_{1-x}Ga_xAs_{1-y}Sb_y$: Sn,Te
BSF / cladding	$n\text{-}Al_{1-x}Ga_xAs_{1-y}Sb_y$: Sn,Te
substrate	$n\text{-}GaSb$:Te

g. *p-on-n* homojunction (with BSF / cladding layer, window layer, back oxide/Au reflector, and thinned substrate)

window	$n\text{-}Al_{1-x}Ga_xAs_{1-y}Sb_y$: Sn,Te
emitter	$n\text{-}In_{1-x}Ga_xAs_{1-y}Sb_y$: Sn,Te
base	$p\text{-}In_{1-x}Ga_xAs_{1-y}Sb_y$: Ge
BSF / cladding	$p\text{-}Al_{1-x}Ga_xAs_{1-y}Sb_y$: Ge
substrate	$p\text{-}GaSb$:Zn
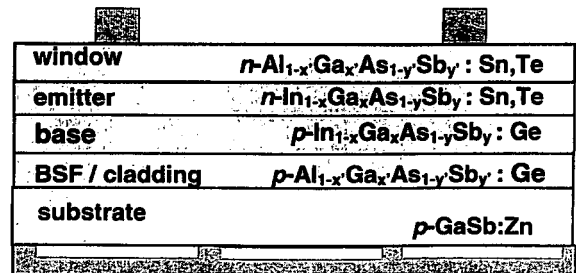
h. *n-on-p* homojunction (with BSF / cladding layer, window layer, back oxide/Au reflector, and thinned substrate)

The 'baseline' homojunction device (FIGURE **1a**) is a two-layer epitaxial InGaAsSb structure formed by liquid-phase epitaxy on a GaSb substrate. The (direct) bandgap of the $In_{1-x}Ga_xAs_{1-y}Sb_y$ alloy is 0.50 to 0.55 eV, depending on its exact alloy composition (x,y), and is closely lattice-matched to the GaSb substrate. Internal quantum efficiencies as high as 95% have been measured at a wavelength of 2 microns. At a wavelength of 1 micron, internal quantum efficiencies of 55% have been observed. At a current density of 1.6 A/cm^2, an open-circuit voltage of 0.250 V and a fill factor of 60% have been measured. Our results to date show that the GaSb-based quaternary compounds provide a viable and high performance energy conversion solution for thermophotovoltaic systems operating with 1000 to 1500 °C source temperatures.

3.3 Epitaxy and Device Fabrication

The TPV devices are epitaxial AlGaAsSb / InGaAsSb structures formed by liquid-phase epitaxy on a GaSb substrates at a growth temperature of 515 °C. Liquid-Phase Epitaxy (LPE) is a well-established technology for III-V compound semiconductor devices. A major advantage of LPE for this application is the high material quality, and more specifically, the long minority carrier diffusion lengths, that can be achieved. This results in devices which are equal or superior in performance to those made by other epitaxy processes such as molecular beam epitaxy (MBE) or metal organic chemical vapor deposition (MOCVD). Another important advantage is that LPE is a simple, inexpensive, and safe method for semiconductor device fabrication. Significantly, the LPE process does not require or produce any highly toxic or dangerous substances—in contrast to MOCVD. Also, the epitaxial growth rate with InGaAsSb LPE is ~2 μm/min., which is 10 to 100 times faster than growth rates for MOCVD or MBE. We have successfully scaled up the LPE process for epitaxial growth in a semi-continuous mode on 3-inch diameter wafers. This, combined with the high growth rates, will dramatically improve the manufacturing throughput compared to traditional and more costly epitaxy processes. The objective is to develop an epitaxial growth technology to produce low-cost, large-area, high efficiency TPV devices.

InGaAsSb photodiodes, light-emitting diodes, and double heterostructure injection lasers made by liquid-phase epitaxy have been previously reported [6-10]. We have adapted this technology for the production of InGaAsSb TPV cells.

A standard horizontal slideboat technique is used for the liquid-phase epitaxial growth of the InGaAsSb. The graphite slideboat is situated in a sealed quartz tube placed in a microprocessor-controlled, programmable, three-zone tube furnace. The growth ambient is palladium-diffused hydrogen at atmospheric pressure with a flow rate of 300 ml/min.

The substrates are 500-micron thick, chemically polished, (100) oriented, n-type GaSb wafers obtained from MCP Wafer Technology, Ltd. (Milton Keynes, UK) or Firebird Semiconductor, Ltd. (Trail, BC, Canada). Substrates are doped to 3-5 x 10^{17} cm^{-3} with tellurium. The substrate resistivity is 9 x 10^{-3} Ω·cm, and the average etch-pit density is approximately 1000 cm^{-2}.

The growth solutions are indium (X_{In}=0.59), gallium (X_{Ga}=0.19), antimony (X_{Sb}=0.21), and arsenic (X_{As}=0.01). The melts are formulated with 3 to 5 mm shot of high purity (99.9999%) indium, gallium, and antimony metals and arsenic added as undoped polycrystalline InAs material. The total weight of the melt is about 7 g. Prior to growth, the melts are baked out at 700 °C for 15 hours under flowing hydrogen to de-oxidize the metallic melt components and

outgas residual impurities. After bake-out, appropriate dopant impurities are added to each melt. The first melt for the growth of the n-type InGaAsSb base layer contains tellurium. The small amount of Te needed to dope the layer (atomic fraction in the melt $\cong 10^{-5}$) is problematic. For reproducible doping, a weighable amount of Te is added as 100 to 200 mg of Te-doped GaSb ($C_{Te}=10^{19}$ cm^{-3}) or as In-Te alloy (1% Te by weight). The second melt for the growth of the p-type emitter contains 1 to 10 mg germanium. We have begun a more detailed and systematic characterization of impurity segregation and doping in the In-Ga-As-Sb quaternary system with the aim of achieving better control and a greater range of doping concentrations.

The melts are equilibrated for 1 hour at 530 °C and then cooled at a rate of 0.7 °C/min. At 515 °C, the substrate is contacted with the first melt for 2 minutes to grow a 5 micron thick n-type InGaAsSb base layer. Next, the substrate is moved to the second melt for 5 seconds to grow a 0.3 micron thick p-type InGaAsSb emitter layer.

For the $Al_{0.3}Ga_{0.7}As_{0.02}Sb_{0.98}$ window and BSF layers, the LPE procedure was similar to that described above except that the melt solution consisted of aluminum (X_{Al} = 0.015), gallium (X_{Ga} = 0.957), antimony (X_{Sb} = 0.028) and arsenic (X_{As} = 0.001). The As is added as undoped polycrystalline GaAs. The bandgap of AlGaAsSb corresponding to this quaternary composition is about 1.2 eV. The layer compositions were verified by electron microprobe analysis.

Front and back ohmic contacts are formed on the epitaxial InGaAsSb/GaSb structure by standard processing techniques. The back of the substrate is metallized by plating with a 200 nm thick electron-beam evaporated Sn:Au layer and alloyed at 300 °C. The front contact grid consists of 10 micron wide metallization lines with 100 micron spacing and a single 1-mm wide center busbar. The grid is formed by a photolithography lift-off process with a 200 nm thick electron-beam evaporated Au:Zn:Au metallization. The front grid is thickened to 5 microns by gold electroplating. The front contact is not sintered. The substrate is masked and patterned to define a 1 cm x 1 cm device and isolation etched with a potassium iodide - iodine etch. Most of our TPV cells are 1 cm x 1 cm in area; although larger cells (2 cm x 2 cm) with comparable performance have also been made. In order to simplify the spectral response analysis, no anti-reflection coating was applied to the cells. FIGURE 3.2 is a top-view photograph of a 1 cm x 1 cm InGaAsSb TPV cell.
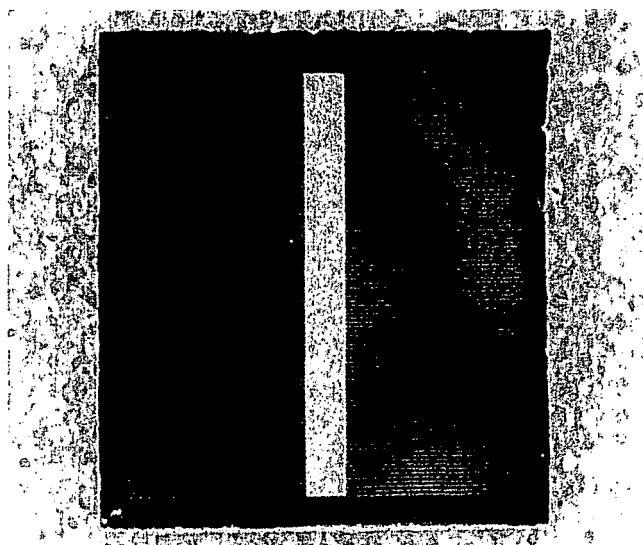

FIGURE 3. 2. Top-view photograph of a 1 cm x 1 cm InGaAsSb TPV cell.

3.4 TPV Device Design and Optimization

FIGURE 3.1 shows various TPV device designs in cross-section. The fabricated cells have a 0.3 to 0.5 micron thick p-type emitter with a Ge concentration of approximately 10^{19} cm^{-3}, as indicated by Secondary Ion Mass Spectroscopy (SIMS). A thicker, more heavily doped p-layer will reduce the sheet resistance of the emitter and therefore improve the fill-factor, but will tend to reduce spectral response due to higher free-carrier absorption and increased sensitivity to front surface minority carrier recombination.

The base thickness ranges from 3 to 5 microns with a Te concentration of about 10^{17} cm^{-3}, as determined from capacitance-voltage measurements and SIMS. Modeling indicates that base dopings in this range will yield the optimum open-circuit voltages and short-wavelength quantum efficiencies. FIGURE 3.3 shows the SIMS depth profile indicating the abruptness of the p-n junction and the depth uniformity of the doping concentrations. There is apparently very little smearing of the doping profile due to diffusion or segregation of dopants. Discrepancies between the Te dopant concentration measured by SIMS (total impurity concentration) and that implied by capacitance-voltage measurements (net donor concentration) indicate that some of the Te is either not ionized or is compensated. This is a common problem in Te doping of III-V semiconductors, especially in GaSb-based materials, and is probably due to the formation of electrically inactive telluride complexes or compounds in the material. We have also employed tin as an n-type dopant. The optimization of target doping levels for high efficiency, and realization of specified doping in the epitaxy process, are areas where much additional effort is needed.
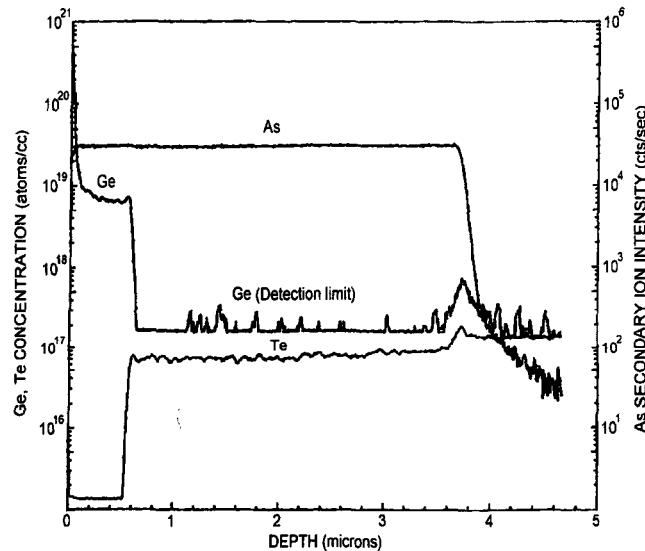

FIGURE 3.3 SIMS depth profile of doping.

3.5 TPV Device Evaluation

We present external and internal spectral response curves and current-voltage characteristics for 1 cm x 1 cm p-In$_{0.15}$Ga$_{0.85}$As$_{0.17}$Sb$_{0.83}$:Ge / n-In$_{0.15}$Ga$_{0.85}$As$_{0.17}$Sb$_{0.83}$:Te epitaxial cells on n-GaSb:Te substrates produced as described above. The *external* spectral response and *internal* spectral response of typical InGaAsSb TPV cells are shown in FIGURE 3.4. The lower external spectral response is due to grid shading and reflection of incident light from the uncoated InGaAsSb emitter surface. The grid shading is 18.2%. The absorption edge implied by the spectral response measurements of a number of samples ranged from approximately 2250 to 2300 nm. At a wavelength of 2000 nm, internal quantum efficiencies as high as 95% have been measured, and at a wavelength of 1 micron, internal quantum efficiencies of almost 55% have been observed. The internal quantum efficiency averaged over the spectral region from 1 to 2 microns wavelength is 60%. (It should be noted that for the intended TPV applications, the response of the cell for wavelengths less than 1.5 microns is not important.) Sub-bandgap external reflection was measured for cells with the back mirror structures shown in FIGURE 1b, but before formation of the front surface contact grid, the presence of which complicates interpretation of reflection measurements. With a thinned substrate (< 100 microns) we can achieve sub-bandgap external reflectivities over 90% over a bandwidth from 2 to 6 microns wavelength.
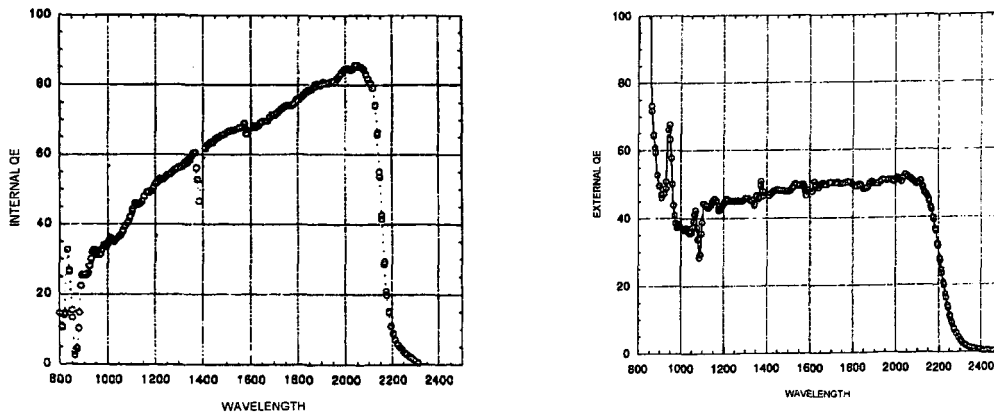
Figure 3.4. Internal and external quantum efficiencies of InGaAsSb/GaSb p-n junction thermophotovoltaic cells.

The 1 cm x 1 cm InGaAsSb TPV cells were tested under simulated infrared light using a ZnSe-filtered tungsten source (Carley Lamps, Inc., Torrance, CA) with a spectral emission in the 800 to 3000 nm wavelength range. Under an illumination intensity corresponding to a short-circuit current density of 2 A/cm^2, open-circuit voltages as high as 0.260 volts have been measured. Cells were also tested at the Jet Propulsion Laboratory using a pulsed solar simulator with an infrared bandpass filter. FIGURE 3.5 shows the current-voltage characteristics of a 1 cm x 1 cm InGaAsSb TPV cell tested in this manner which gives an output current density of 0.348 A/cm^2. This intensity yields an open-circuit voltage of 0.235 V and a fill-factor of 0.58. FIGURE 3.6 shows short-circuit current vs. open-circuit voltage for varying light intensity. The diode ideality factor changes from m = 1 to m = 2 at an open-circuit voltage of ~0.08 V. This graph implies a reverse saturation current of $J_0 \approx 1.5 \times 10^{-4}$ A/cm^2.

The addition of a 1.3-eV bandgap AlGaAsSb window layer (as indicated in FIGURE 3.1g) significantly improves cell performance. The reverse-saturation current is lowered by more than a factor of ten to $J_0 \approx 1.4 \times 10^{-5}$ A/cm^2. Also, the quantum efficiency between 1200 and

1600 nm is improved 30 to 40%. Also, a fill factor of 0.61 has been measured at a current density of 0.7 A/cm². The improvements in open-circuit voltage are seen for cells with a high base doping ($>10^{17}$ cm^{-3}). Cells with low base dopings (10^{16} cm^{-3}) do not benefit as much from the presence of a front surface passivation layer. This is consistent with the reasonable assumption that cells with high base dopings have significant emitter components of reverse saturation current that are relatively sensitive to front surface recombination. We have yet to demonstrate any significant advantage of heterojunction cells (FIGURE 3.1f). To date, such heterojunctions have resulted in cells with very non ideal I-V characteristics.
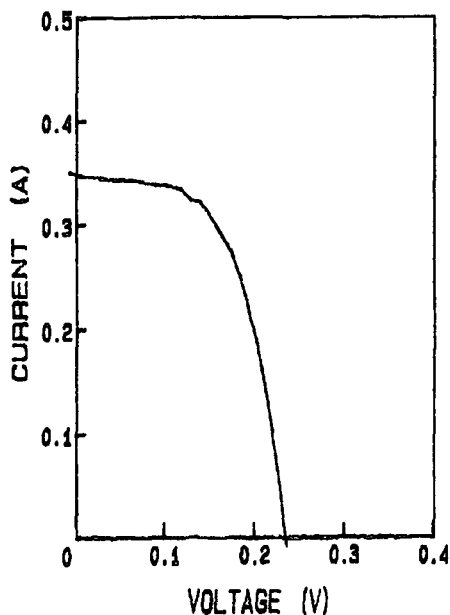

Figure. 3.5. Current-voltage characteristic of 1 cm x 1 cm InGaAsSb TPV cell.

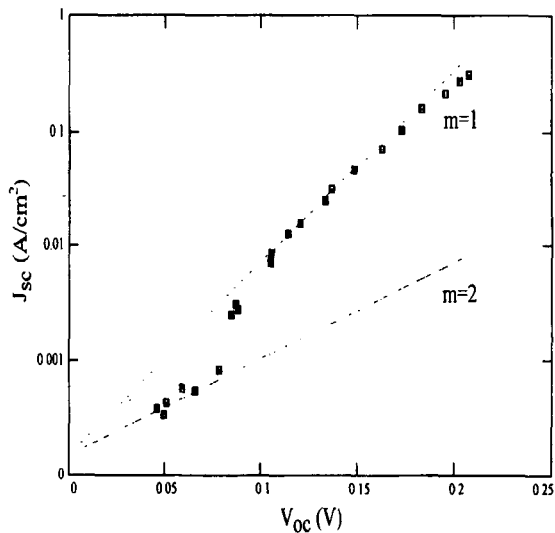Figure 3.6. Short-circuit current vs. open-circuit voltage for InGaAsSb TPV cell under varying illumination intensity.

3.6 Conclusion and Discussion

Our results to date have demonstrated the potential of InGaAsSb TPV devices made by liquid-phase epitaxy. There is still room for substantial efficiency enhancements in these devices by optimization of the doping levels and layer thicknesses. The effectiveness of a wide-bandgap lattice-matched AlGaAsSb window layers for front surface passivation is clearly demonstrated. The use of AlGaAsSb back-surface field cladding layers to reduce the reverse saturation current and thereby increase the open-circuit voltage is still tentative. As yet, we see no advantage to heterojunctions. Highly doped contact layers will provide lower series resistance, as will substrate thinning. Lower series resistance will lead to higher fill factors. Thinning the substrate will also improve the heat sinking capability of the device. Based on the results reported here, we believe a 0.5-eV bandgap GaSb-based TPV cell with an open-circuit voltage well over 300 mV at current densities of 2 A/cm^2, and with a fill factor of 70%, is a realistic near-term goal.

The required performance of a TPV device is dependent on its system application. Spectral control of thermal emitters, the use of selective filters and reflectors, heat transfer, and photon recycling effects need to be included in the device design and system optimization. These considerations are not usually relevant for conventional photovoltaic devices and therefore the design and optimization rules for TPVs will be significantly different than those for solar cells. For example, grid obscuration and reflection are not necessarily losses in TPV systems if photons reflected from the front surface are re-absorbed by the emitter. At this stage, a better computer-based theoretical model to simulate AlGaAsSb/InGaAsSb TPV cells is needed to guide the optimization and interpret experimental results.

3.7 References for Part 3

1. Z.A.Shellenbarger, M.G. Mauk, and L.C. DiNetta, "Recent Progress in InGaAsSb/GaSb TPV Devices" *Conf. Rec. 25th IEEE Photovoltaics Specialists Conf.* (IEEE Press, Piscataway, NJ, 1996) 81-84.

2. Z.A. Shellenbarger, M.G. Mauk, L.C. DiNetta, and G.W. Charache, "InGaAsSb/GaSb Thermophotovoltaic Cells" *Proc. 14th Space Photovoltaic Research and Technology Conf. 1995 (SPRAT XIV)* NASA Conf. Publication 10180 (1996) 215-222.

3. A. Schock, C. Or, and V. Kumar, "Small Radioisotope Thermophotovoltaic (RTPV) Generators", *Proc. 2nd NREL Conf. on Thermophotovoltaic Generation of Electricity*, (New York: American Institute Physics, 1996), pp. 81-97.

4. E. Kittl, "Unique Correlations Between Blackbody Radiation and Optimum Energy Gap for a Photovoltaic Conversion Device", *Proc. 10th IEEE PV Specialists Conf.*, 1973, pp. 103-106.

5. L.D.Woolf, "Optimum Efficiency of Single and Multiple Bandgap Cells in Thermophotovoltaic Energy Conversion", *Solar Cells* **19**, 1986, pp. 19-38.

6. M. Astles, H. Hill, A.J. Williams, P.J. Wright, and M.L. Young, "Studies of the $Ga_{1-x}In_xAs_{1-y}Sb_y$ Quaternary Alloy System I. Liquid-Phase Epitaxial Growth and Assessment", *J. Electronic Materials* **15**, 1986, pp. 41-49.

7. A. Andaspaeva, A.N. Baranov, A. Guseinov, A.N. Imenkov, L.M. Litvak, G.M. Filaretova, and Y.P. Yakovlev, "Highly Efficient GaInAsSb Light-Emitting Diodes (λ = 2.2 μm, η=4%, T = 300K)", *Soviet Technical Physics Letters* **14**, 1988, pp. 377-378.

8. C. Caneau, A.K. Srivastava, A.G. Dentai, J.L. Zyskind, and M.A. Pollack, "Room-Temperature GaInAsSb/AlGaAsSb DH Injection Lasers at 2.2 μm", *Electronics Letters* **21**, 1985, pp. 815-817.

9. A.E. Drakin, P.G. Eliseev, B.N. Sverdlov, A.E. Bochkarev, L.M. Dolginov, and L.V. Druzhinina, "InGaSbAs Injection Lasers", *IEEE J. Quantum Electronics* **QE-23**, 1987, pp. 1089-1094.

10. N. Kobayashi, Y. Horikoshi, and C. Uemura, "Liquid-Phase Epitaxial Growth of InGaAsSb/GaSb and InGaAsSb/AlGaAsSb DH Wafers", *Japanese J. Applied Physics* **18**, 1979, pp. 2169-2 170.

Part 4: Paths to Higher Performance GaSb-Based Thermophotovoltaics

4.1 Summary

Several new device concepts are introduced and assessed for high performance GaSb-based TPV devices. These features are designed for photon recycling, monolithic interconnection for high-voltage TPV arrays, and low-cost surrogate substrates. The new designs are based on 1. epitaxial lateral overgrowth, 2. semi-insulating semiconductors lattice-matched to 0.5-eV GaSb alloys, 3. selective oxidation of Al-containing antimonides, 4. epitaxial film transfer and wafer fusion / bonding to surrogate substrates, and 5. ins- and gabs-on-silicon heteroepitaxy.

4.2 Approaches

New device concepts are introduced, described, and evaluated for a "next-generation" of III-V antimonide (e.g., InGaAsSb, InAsSbP, AlGaAsSb) thermophotovoltaic (TPV) cells. Our broad objectives are:

- to develop novel device designs and fabrication technologies to better exploit optical effects such as photon recycling,

- to circumvent the disadvantages of the presently-used GaSb and InAs substrates (high cost, limited size, lack of semi-insulating substrates), and

- to explore approaches for monolithic, series-interconnection of TPV devices for high-voltage arrays or mini-modules on a single large-area substrate.

In pursuit of these objectives, we are developing several epitaxy and device fabrication technologies for their application to GaSb and/or InAs-based TPV devices:

- epitaxial lateral overgrowth on patterned, masked substrates,

- *epitaxial film transfer* or *wafer fusion* wherein an epitaxial device structure is bonded to a surrogate superstrate and the original substrate is removed by selective etching or separated by "lift-off",

- selective oxidation of Al-containing antimonides,

- heteroepitaxy of GaSb and InAs on silicon, and

- realization of high resistivity or semi-insulating III-V antimonides.

These techniques, alone or in combination, show reasonable prospects for realizing the above-listed aims. While all of these technologies are well established for other III-V semiconductors such as GaAs, there is little or no precedent for their application to III-V antimonides or TPV devices. Some of the above processes can be directly adapted to III-V antimonides in a straightforward way, others are more speculative and long-range; their inclusion at this stage of the work is to assess their feasibility and difficulty of implementation for TPV devices.

GaSb- and InAs-based alloys are good choices for thermophotovoltaic cells intended for conversion of blackbody radiation sources operating in the 1000 to 1500 °C temperature range since:

- the requisite epitaxial growth technology is adequately developed,

- lattice-matched, thermal-expansion matched, high-quality double heterostructures can be grown with bandgaps in the range of 0.5 to 0.8 eV,

- there is a substantial technology base for III-V compound antimonides owing to their use in mid-infrared detectors, LEDs, and lasers, and

- previous work in related areas, although not extensive, indicates that Sb-based optoelectronic devices are stable and robust.

In the last year we reported[1] InGaAsSb/GaSb p-n homojunction TPV cells with internal quantum efficiencies as high as 90%. At an illumination level yielding a short-circuit current density of 1.6 A/cm^2, open-circuit voltages of 0.250 V and fill-factors of 60% have been measured. These devices showed no sign of degradation after many hours of operation. These results encouraged us to pursue more sophisticated devices with the features cited above.

In the context of TPV devices, photon recycling refers to the reflection of sub-bandgap energy photons back to the heated source. This can be accomplished by depositing a reflecting layer on the backside of the substrate. For GaSb-based TPVs, the GaSb substrate (with a bandgap of 0.7 eV) is nominally transparent to light not absorbed in the AlGaAsSb/InGaAsSb active layers (~0.5 eV). Nevertheless, free carrier absorption in the substrate can significantly diminish the effectiveness of the backside mirror.

4.3 Epitaxial Lateral Overgrowth

An alternative approach is the "buried" mirror design shown in FIGURE 1. Here, a reflective layer is situated between the substrate and the epitaxial device structure. Openings in the mask (called vias) provide electrical contact between the substrate and the active layers. This design avoids parasitic substrate absorption in effecting photon recycling.

Several types of films have been employed as "buried" mirror layers including refractory metals such as tungsten, dielectrics such as SiO$_2$ and Si$_3$N$_4$, metal nitrides such as WN, multilayer electron-beam deposited Si/SiO$_2$ quarter wavelength Bragg stacks, and various multilayer combinations of metals and dielectrics. The "buried" mirror structure device structure shown in FIGURE 4.1 can be realized by epitaxial lateral overgrowth or a wafer fusion technique.

The epitaxial lateral overgrowth process is shown in FIGURE 4.2. A GaSb substrate is masked with a dielectric, metal, or composite multilayer coating of metals, dielectrics, or amorphous or polycrystal-line semiconductors and patterned with stripe openings (4.2a).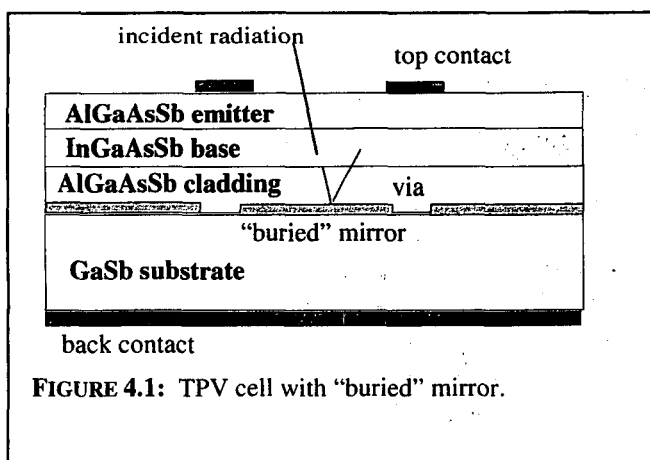 The patterned, masked substrate is used for epitaxial growth of AlGaAsSb and InGaAsSb films. The stripe openings where the underlying GaSb substrate is exposed serve as sites of preferential nucleation and selective epitaxy; there is virtually no nucleation on the mask itself. FIGURES 4.2b to 4.2e show successive stages of epitaxy where the selectively grown epilayer overgrows the mask. Given sufficient time, the overgrowth from adjacent vias impinges to form a continuous epitaxial film (4.2e). By this technique, a single crystal layer of a GaSb-alloy is formed on a masked substrate. FIGURE 4.3 shows a top-view photomicrograph of lateral overgrowth of AlGaAsSb (at a composition lattice matched to GaSb) on a (111)GaSb wafer.

FIGURE 4.1: TPV cell with "buried" mirror.

We are able to achieve impinging lateral overgrowth of AlGaAsSb epilayers on oxide-masked substrates with stripe openings spaced as much as 1000 microns apart. We are presently developing the double heterostructure AlGaAsSb / InGaAsSb / AlGaAsSb TPV device structure using epitaxial lateral overgrowth.

Actually, since the masking layer can be a conductor, insulator, or combination thereof, the lateral overgrowth and underlying mask may have several functions: **1.** as a "buried" mirror, **2.** as a buried contact, or **3.** as an insulating layer to dielectrically isolate the epilayers from the substrate and thus facilitate monolithic series interconnection of TPV device elements. The availability of a semi-insulating GaSb or InAs substrate would greatly simplify approaches for a monolithic, series-interconnected GaSb-based TPV array. For example, in related work WILT *et al.* have described a monolithic, interconnected epitaxial InGaAs TPV module made on a semi-insulating InP substrate. The low bandgap and resulting thermal carrier generation, and the intrinsic electrically active point defects in the III-V antimonides seems to preclude semi-insulating GaSb material.

We will discuss the resistivity requirements for substrate isolation in TPV monolithic interconnected arrays, which specifically entails an estimation of the minimum resistivity necessary for a 5- to 10-element series interconnected array of InGaAsSb TPV cells grown on the same substrate. It is also
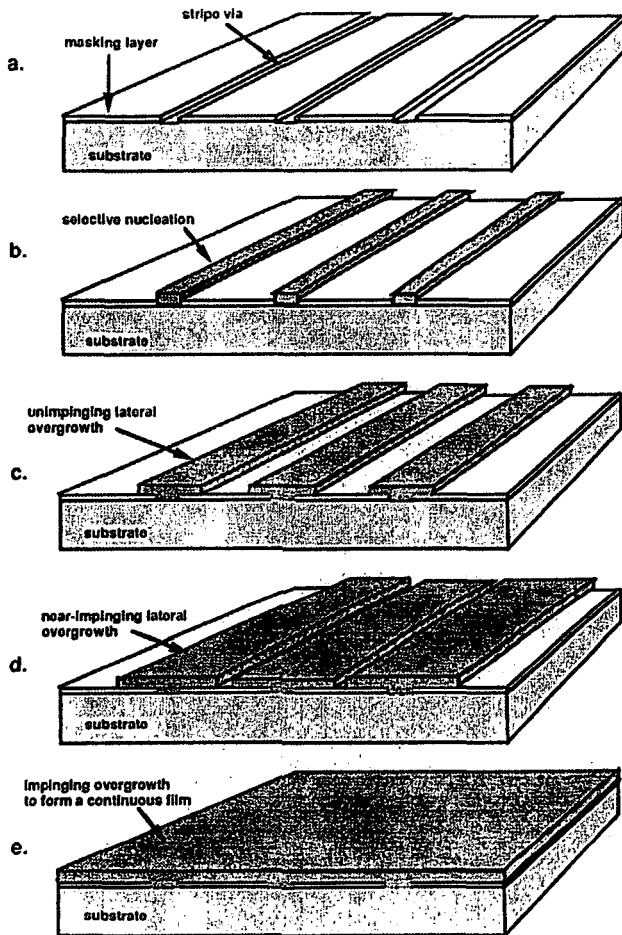
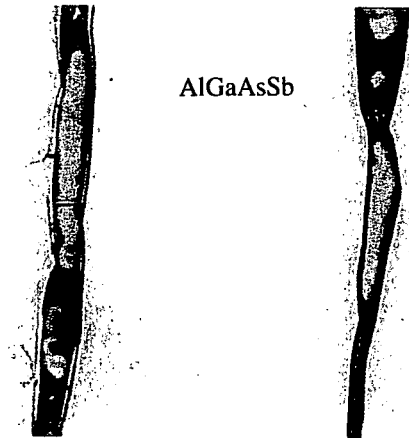

Figure 4.2: Epitaxial lateral overgrowth process.

FIGURE 4.3: Top-view photomicrograph of near-impinging growth of AlGaAsSb epilayer on an SiO_2-masked (111)GaSb substrate patterned with 10-micron wide stripe vias spaced 400 microns apart. (This sample corresponds to epitaxial lateral overgrowth at stage **d** in FIGURE 4.2.)

junction isolation may be sufficient for some designs. Based on an extensive literature review, and a worldwide survey of GaSb and InAs substrate suppliers, we assess the prospects for high resistivity or semi-insulating III-V antimonides. We also discuss the feasibility of lattice-matched, wider bandgap epitaxial layers of AlGaAsSb rendered semi-insulating by doping with transition metals (Cr, Fe, V) and/or rare earths or by using non-stoichiometric compositions to suppress carriers. Such a semi-insulating epitaxial layer sandwiched between the device and substrate wafer could provide a means for electrical isolation of TPV device elements.

4.4 Wafer Bonding and Epilayer Transfer

Another alternative method of forming TPV devices with backside reflectors (or an insulating substrates) uses *wafer bonding* or *wafer fusion* techniques, and related epitaxial film transfer processes. This process is straightforward but to our knowledge has not been previously applied to GaSb-based devices. Selective oxidation refers to steam oxidation processes which convert a buried Al-containing III-V layer to an insulating aluminum oxide. This process could be used to simulate a semiconductor on insulator structure. Finally, work on InAs- and GaSb-on-silicon heteroepitaxy will be discussed for application to low-cost TPV.
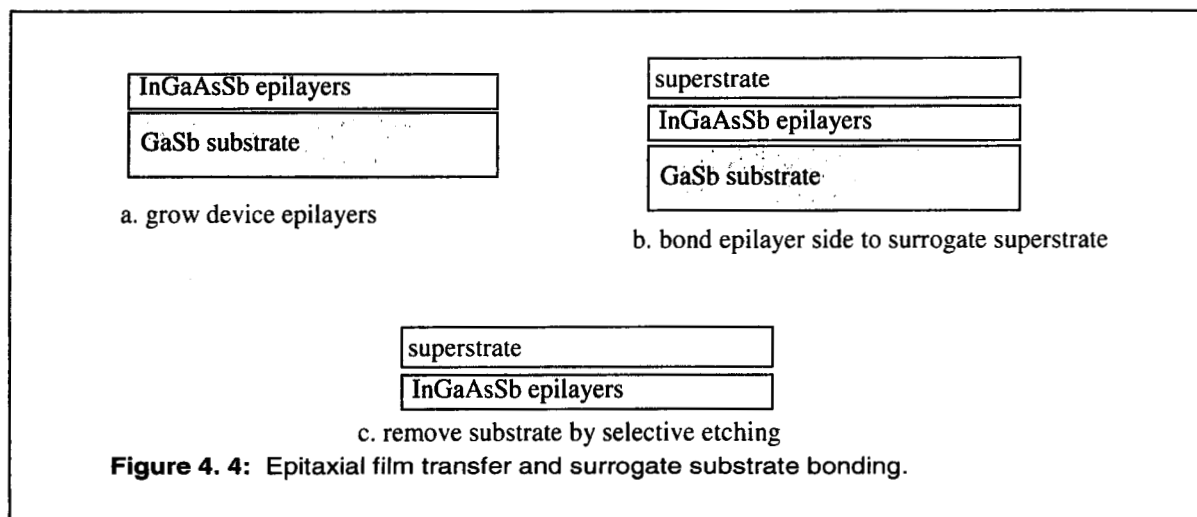

a. grow device epilayers

b. bond epilayer side to surrogate superstrate

c. remove substrate by selective etching

Figure 4. 4: Epitaxial film transfer and surrogate substrate bonding.

FIGURE **4.4** shows a general process sequence for transferring a GaSb-based epitaxial device structure to a surrogate superstrate. We will report our latest results in this area.
There are many issues in developing this type of process, including:

- substrate: ceramic, glass, metal, silicon, thermal expansion matching
- type of bonding: adhesive, van der Waals, electrostatic
- contacts: both base and emitter from one side, application
- substrate removal: selective etchants, "stop etch" layers"
- scribing, dicing
- yield

The lateral overgrowth process using an insulating mask layer can also be adapted for monolithic series-interconnected arrays. FIGURE 4.5 shows a specific implementation for isolating adjacent TPV elements using an isolation etch on an epitaxial TPV device formed over an insulating mask layer which doubles as a dielectric Bragg reflector.
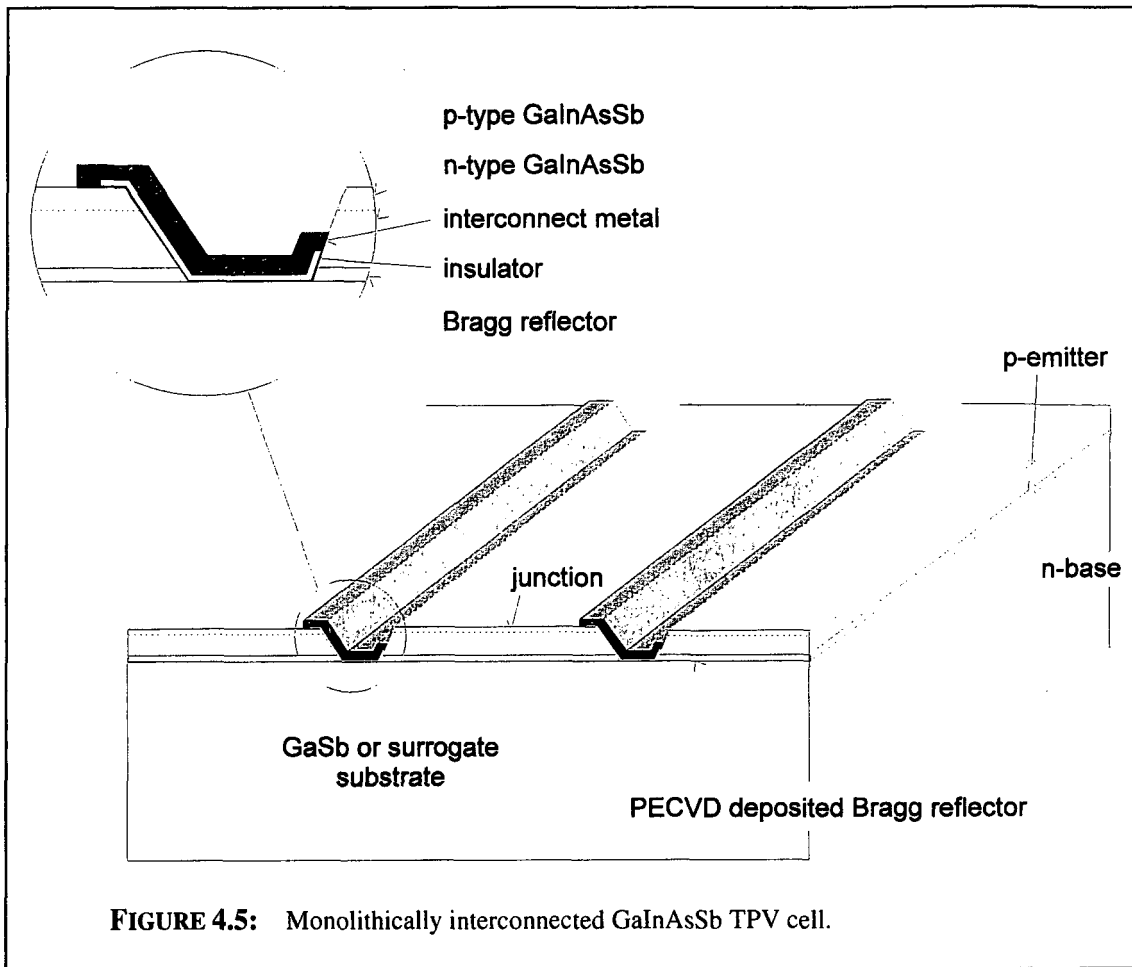

FIGURE 4.5: Monolithically interconnected GaInAsSb TPV cell.

4.5 GaSb and InAs on Silicon

All III-V substrates are at least a factor of ten to twenty times more expensive than silicon. In the interest of reducing costs, we are developing simple heteroepitaxy techniques for growing single-crystal films of InAs and GaSb on silicon substrates. FIGURE 4.6 is a top-view photomicrograph of InAs on silicon grown by a simple atmospheric pressure close-spaced vapor transport process. This InAs-on-silicon structure can be used as a surrogate substrate in place of an InAs bulk wafer. A similar approach is possible with GaSb on silicon.

Although the large lattice mismatch in these systems looks tractable, other important factors in this type of heteroepitaxy include thermal expansion mismatch, cross-doping, anti-phase domain formation, and various defect generation phenomena. We realize the major problems of III-V heteroepitaxy on silicon (e.g., GaAs-on-silicon and InAs-on-silicon) remain unsolved. However, with regard to thermal stress and cross doping, one advantage InAs-on-silicon and GaSb-on-silicon have over GaAs-on-silicon heteroepitaxy is the relatively low growth temperatures. Epitaxy of InAs and

GaSb-related alloys is normally at temperatures of 500 to 550 °C, whereas GaAs epitaxy is typically in the range of 800 °C. This ~300 °C lower temperature is an important advantage for heteroepitaxy of these TPV materials on silicon. Also, epitaxial lateral overgrowth has demonstrated good potential for defect reduction. Therefore, a GaSb-on-silicon or InAs-on-silicon heteroepitaxial lateral overgrowth process could yield very low defect, low stress surrogate substrates for III-V antimonide TPV applications.
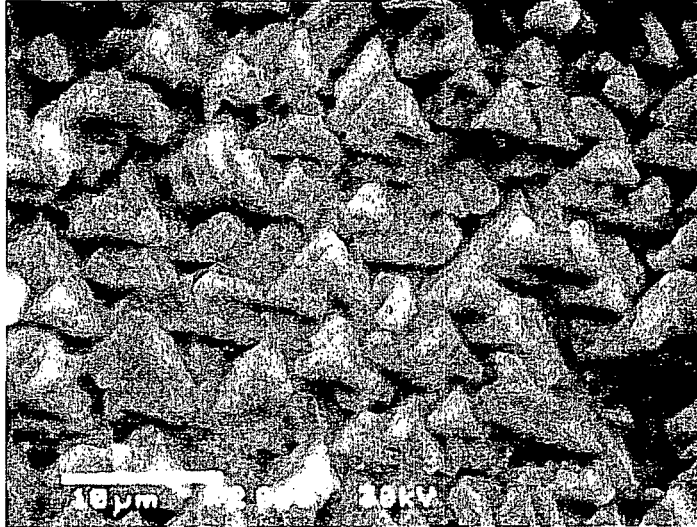
FIGURE 4.6: InAs on silicon heteoepitaxial layer grown by Close-Spaced Vapor Transport (CSVT).

4.3 References for Part 4

1. Z.A. SHELLENBARGER, M.G. MAUK, L.C. DINETTA, and C.W. CHARACHE, "Recent Progress in InGaAsSb/GaSb TPV Devices" *Conf. Rec. 25th IEEE Photovoltaic Spec. Conf.* (1996) 81-84.
2. Z.A. Shellenbarger, submitted to this conference.

3. D.M. WILT *et al.*, "Monolithically Interconnected InGaAs TPV Module Development" *Conf. Rec. 25th IEEE Photovoltaic Specialists Conference* (1996) 43-48.

Part 5: Diffusion of Zn in TPV materials: GaSb, InGaSb, InGaAsSb and InAsSbP

5.1 Summary

This paper reviews recent results of the study of Zn diffusion from the vapor phase in important thermophotovoltaic (TPV) materials such as GaSb-, InGaAsSb-, InGaSb- and InAsSbP. Peculiarities of Zn diffusion in each of these materials and different ways of diffusion profile tailoring for fabrication of optimized Zn-diffused emitters in TPV cells are discussed.

5.2 Introduction

Diffusion of Zn from vapor phase is a simple and productive method of pn-junction fabrication in III-V materials. Especially advantageous is the pseudo-closed box diffusion method that avoids the inconvenience of sealed ampoules [1,2]. First papers about Zn diffusion from vapor phase into GaSb were published at the end of 60-s - begin of 70-s [3]. Different approaches in the pseudo-closed box diffusion of Zn into GaSb are described in [4,5]. L. Fraas et al was the first to apply Zn diffusion into GaSb for solar cells [6]. High-efficiency GaSb solar cells with Zn-diffused emitters developed at Boeing showed a potential of this material for infrared applications and arouse a new wave of interest to thermophotovoltaics. Also, they gave a strong impetus to the study of different antimonides for PV and TPV in many institutions worldwide.

At the present stage of development of TPV systems, TPV cells do not seem to be a bottleneck. Though their efficiency and operation parameters can be certainly increased, much larger improvement potential lies in other parts of a TPV system. Thus, the TPV cell design can be very simple. Actually, in the case of a high-quality substrate material and optimized diffused emitter, TPV cells, contrary to lasers or multi-junction space solar cells, do not require complicated epitaxially grown structures. Moreover, if epitaxial growth on good substrates is not perfect, that is often the case with antimonides; it can even worsen TPV cell parameters. Obviously, one cannot avoid growing of an epitaxial layer, if no substrate is currently available for a certain wavelength range / radiator temperature. However even in this case, a simple one-layer epitaxial structure can be sufficient for a high-efficiency TPV cell with a diffused emitter.

In this work we studied Zn diffusion from the vapor phase in important TPV materials such as GaSb-, InGaAsSb-, InGaSb- and InAsSbP. As it was shown in several papers, optimization of as-diffused Zn profiles in the emitters can lead to an essential improvement of device parameters [7-10]. At the same time, there are some speculations in literature that the surface recombination in GaSb is relatively low and that just this fact allows obtaining good device parameters. However, comparison of experimental and modeled data of GaSb TPV cells with diffused emitters shows that the surface recombination in GaSb is high: ~10^6 cm/sec [11]. Recent data on MOCVD-grown AlGaAsSb/GaSb TPV cells without the diffused emitter also showed the same value [12]. Surface recombination between 10^5-10^7 cm/sec was determined on InGaSb surfaces in MOCVD-grown InGaSb structures [13]. However, despite a high surface recombination in GaSb, optimizing of the diffusion profiles can essentially decrease its influence. We studied the following methods of the diffused Zn profile tailoring:

- Precise thinning of the as-diffused emitter that removes a dead layer with high Zn concentration (GaSb, InGaSb and InGaAsSb)
- Additional shallow Zn diffusion after the emitter thinning (GaSb, InGaAsSb)
- Shallow diffusion followed by a high-temperature annealing under SiN_x (GaSb).

Additionally, we studied the effect of anodic oxidation of a GaSb surface on Zn diffusion.

5.3 Experimental

Diffusion of Zn is performed into n-type materials. In the case of GaSb and InGaSb, single crystal or polycrystalline n-type substrates are used. Single crystal n-InGaAsSb and n-InAsSbP layers are grown by liquid phase epitaxy on n-GaSb and InAs-substrates, respectively.

A standard horizontal slide boat technique is used for the liquid-phase epitaxial growth of the InGaAsSb and InAsSbP. The graphite slide boat is situated in a sealed quartz tube placed in a microprocessor-controlled, programmable, three-zone tube furnace. The growth ambient is palladium-diffused hydrogen at atmospheric pressure. The details of InGaAsSb and InAsSbP growth are published in [14]. Bulk crystal growth of InGaSb is described in [15].

Pseudo-closed box diffusion of Zn from the vapor phase is performed into n-type substrates or layers in a H_2 atmosphere purified by a Pd cell. A specially designed multi-wafer graphite boat described in [5] was applied. Separated pure Zn and Sb vapour sources were used in more than sufficient quantities to provide the saturation of vapour pressures. In experiments with InGaAsSb and InAsSbP, an InAs- or InAs- and InP- powder was used to decrease the loss of As and P from the samples during diffusion.

It was determined for GaSb, InGaSb and InGaAsSb that the maximum (surface) Zn concentration in these materials does not depend on the diffusion temperature or Zn vapor pressure over a broad range of values. This means that the maximum Zn solubility in these materials is achieved at low temperatures/pressures. Therefore, even though it is almost certain that a Zn vapor gradient exists in a pseudo-closed diffusion boat, the same emitter profiles are obtained in different parts of the boat.

1.1 Results and Discussion

GaSb

Zn-diffusion from the vapor phase was performed into polished 2.5 x 2.5 cm^2 n-GaSb:Te (n≈2-3x10^{17} cm^{-3}) (100) substrates. Prior to diffusion the substrates were degreased in acetone. Afterwards, they were treated in diluted HF or HCl to remove native oxides on the surface and dried with nitrogen.

Figure 1 shows the dependence of the Zn surface concentration on the diffusion temperature for different diffusion times. It was found that Zn-diffusion profiles in GaSb generally consist of 5 parts: (i) a part with a steep Zn concentration gradient near the surface, (ii) a first plateau with a relatively slow decrease of Zn concentration, (iii) a kink part (the exact position of the kink is defined as the point where the second derivative of the Zn concentration profile is at maximum), (iv) a second plateau with a relatively slow change of Zn concentration and (v) a steep diffusion front. The first part was usually thinner than 50 nm and it is not shown in Figure 5.1. We consider that this part of the SIMS measurements is not reliable enough. Therefore, we did not take this part into further consideration. Hereafter we define as the surface concentration the maximum concentration at the first plateau region. Our experiments have shown that Zn concentration at part (ii) - close to 1x10^{20} cm^{-3} - is too high for TPV cells. Obviously, one can expect small diffusion lengths and a strong bandgap narrowing in this part of the diffused layer and consider it to be a dead layer. Therefore, the relation of the dead layer depth to a total pn-junction depth is of interest. Figures 5.2 and 5.3 show the dependencies of this ratio on diffusion temperature (T) and time (t), respectively. One can see that the kink depth is close to the half of the p-n junction depth and slightly increases both with T and t.
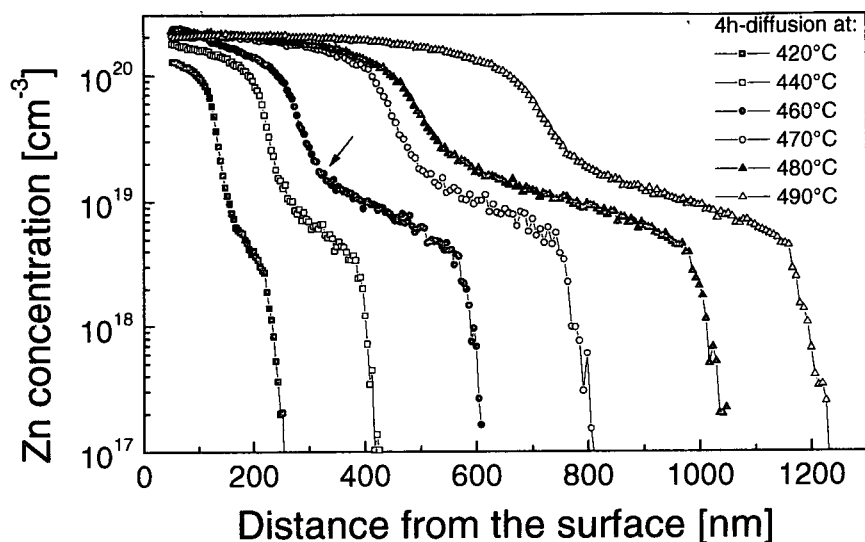
Figure 5.1. Typical SIMS profiles of Zn concentration in GaSb in dependence on temperature after a 4-hour diffusion. The arrow shows the position of the kink in the Zn concentration profile for a 460°C – diffusion.
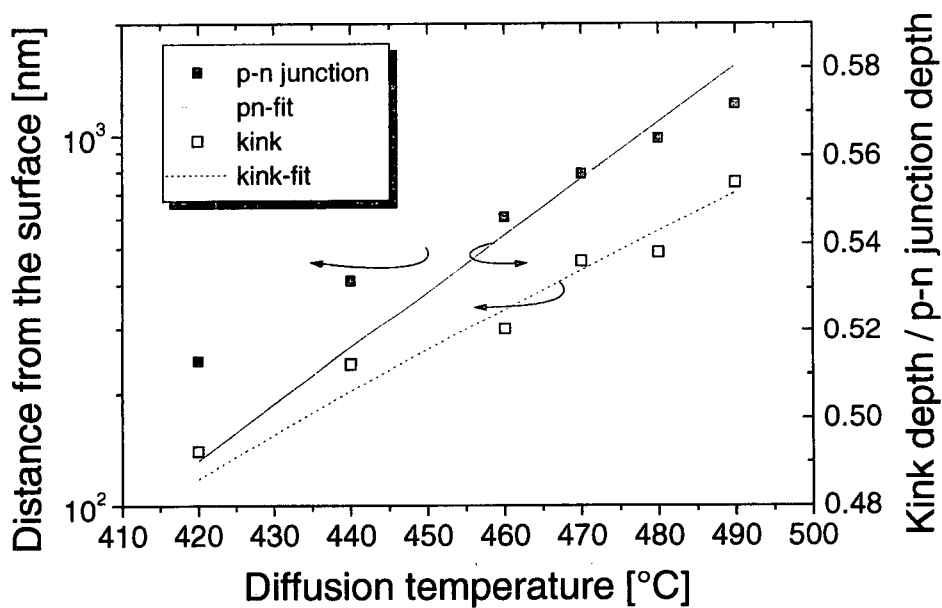
Figure 5.2. pn-junction depth (n = 3×10^{17} cm^{-3}), kink depth and their ratio for 4-h diffusions of Zn into GaSb in dependence on diffusion temperature.
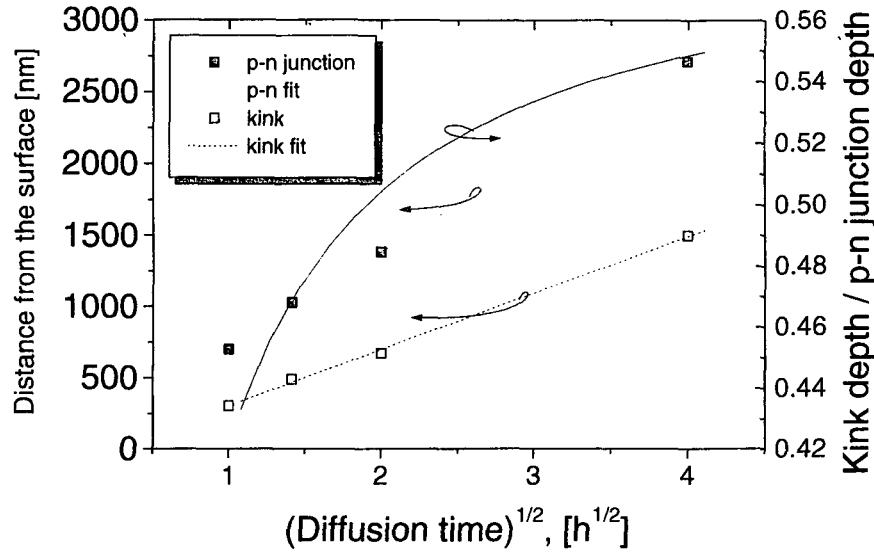
Figure 5.3. pn-junction depth (n = 3×10^{17} cm^{-3}), kink depth and their ratio for 480°C -diffusions of Zn into GaSb in dependence on diffusion time.

As a post-diffusion tailoring of diffused Zn emitter layers in GaSb, precise thinning through anodic oxidation and the following selective etching of anodic oxide is usually performed. The anodic oxidation regime with a GaSb consumption rate about 2.3 nm/V is used. The detailed description of the anodic oxidation process of GaSb is published elsewhere [16]. Through thinning of the diffused emitter in a TPV cell, a highly doped (dead) part of the diffused layer can be removed with a high accuracy. Moreover, a second (shallow) diffusion of Zn can be performed resulting in an optimised Zn profile shown in Figure 5.4.

Figure 5.4 also shows the calculated profile of the net built-in electric field comprised of the (i) electric field E_1, caused by the doping gradient, and (ii) the electric field E_2 due to the band gap gradient caused by the effect of band gap narrowing.

The field E_1 moves photogenerated electrons to the p-n junction, while the field E_2 moves them to the surface. Obviously, the resulting field has a large impact on the TPV cell parameters.

The electric field E_1 caused by the doping gradient between two neighbour points i and $i+1$ of the SIMS-measured Zn profile can be calculated with the following expression:

$$E_1 = \frac{kT}{qd}\ln\frac{N_i}{N_{i+1}},\qquad\qquad (1)$$

where d is the distance between points i and $i+1$; N_i and N_{i+1} are doping densities at the corresponding points.

The electric field E_2 caused by the band gap gradient between two neighbour points i and $i+1$ of the Zn profile measured by SIMS can be calculated with the following expression:

$$E_2 = \frac{A(N_i^{1/3} - N_{i+1}^{1/3})}{qd},\qquad\qquad (2)$$

where the coefficient $A = 10^{-8}$ eV·cm is taken from [17].

One can see from Fig.5.4, that if minority electrons are considered, the sweeping field is especially strong near the surface (up to 8 kV) thus decreasing the influence of surface recombination on separation of photogenerated carriers.
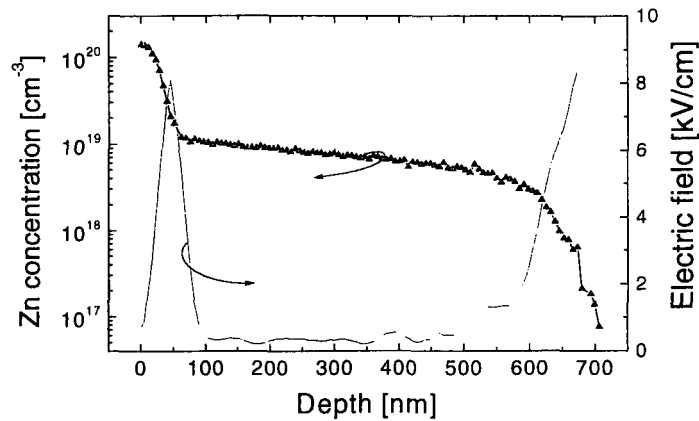
Figure 5.4. SIMS-measured Zn profile of the optimised p-GaSb emitter obtained as a result of three successive operations: (a) deep diffusion, (b) controlled thinning, and (c) shallow diffusion. Also shown is a calculated profile of the net built-in electric field.

Also, we performed a post-diffusion annealing to determine its influence on Zn profiles. After diffusion at low temperature (for example, 420°C), the surface of the diffused layer is covered with 20-50 nm thick SiN_x. Afterwards, annealing in a no-Zn atmosphere at higher temperature (480-520°C) is performed. Figure 5 illustrates changes of Zn profile in an as-diffused sample after annealing. With an increase of annealing temperature and time, the maximum concentration of Zn near the surface drops, while the depth of Zn penetration increases. Such a post-diffusion treatment can be very useful for materials containing volatile components such as P and As (InAsSbP or InGaAsSb). To avoid non-congruent evaporation of P or As from unprotected semiconductor surface, one can use low-temperature initial diffusion followed by applying of a protective SiN_x layer and high-temperature annealing.
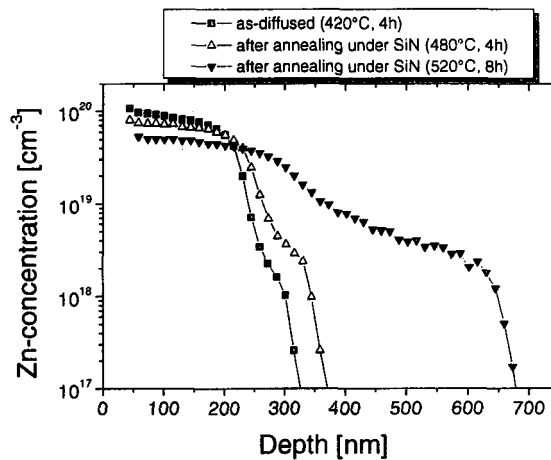
Figure 5.4 SIMS profiles of Zn concentration in a GaSb sample diffused at 420°C (4 h) measured just after the diffusion and after a post-diffusion annealing at 480°C (4 h) and 520°C (8 h). SiN_x layer was deposited on the sample before annealing.

As we have found in this work, another method to accelerate Zn diffusion and thus to avoid high diffusion temperatures and long times, is to perform Zn diffusion through the preliminary formed surface oxide. To form the oxide, we used anodic oxidation providing an oxide layer with precisely controlled parameters [16].

Figure 5.6 shows SIMS profiles of Zn concentration in a GaSb sample diffused through anodic oxide of different thickness. All the samples were diffused in one process, thus all other diffusion parameters were the same. One can see that the diffusion depth rapidly increases with the thickness of anodic oxide.
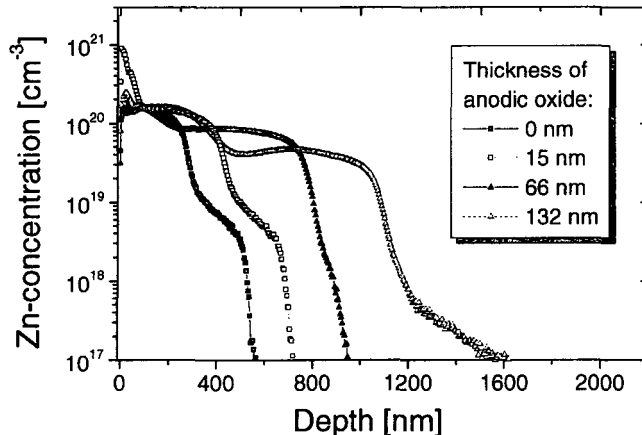
FIGURE 5.6. SIMS profiles of Zn concentration in a GaSb sample diffused through anodic oxide of different thickness.

In a qualitative sense, the dependence of diffusion on the anodic oxide thickness might be also true for a native oxide. Thus, when can speculate that for reproducible results the thickness of the native oxide on the GaSb surface should be minimized and/or kept constant.

InGaSb

InGaSb with band gap 0.5-0.7 eV is of special interest for TPV applications. The availability of ternary bulk substrates would simplify the fabrication of TPV cells with band gaps lower than that of GaSb. The TPV cells could be fabricated using diffusion without expensive epitaxial steps. The antimonide based system (InGaSb) is preferred over the arsenic (InGaAs) and phosphorus (InAsP) counterparts due to technical simplicity during growth [15].

Zn-diffusion from the vapor phase is performed into polished 2 cm^2 n-InGaSb:Te (n $\approx$ 2-3x10^{17} cm^{-3}) (100) and (111)B substrates. These InGaSb substrates are cut from a polycrystalline boule material grown in the Rensselaer Polytechnic Institute. Prior to diffusion the substrates are degreased in acetone. Afterwards, they were treated in diluted HF or HCl to remove native oxides on the surface and dried with nitrogen.

The form of diffusion profiles of Zn into $In_xGa_{1-x}Sb$ (Fig. 5.7) is similar to that in GaSb. All the major parts described above for the Zn profile in GaSb can be also found in the ternary material. However, except diffusion time and temperature, a new parameter – InSb content in $In_xGa_{1-x}Sb$ – affects the Zn diffusion. As it is shown in Figure 5.7, an increase of InSb content in $In_xGa_{1-x}Sb$ strongly enlarges the diffusion depth of Zn in this material. Thus, for fabrication of $In_xGa_{1-x}Sb$ TPV cells diffusion temperatures should be essentially lower than in GaSb. Polycrystalline $In_xGa_{1-x}Sb$ samples with x = 0.12 - 0.19 (E_g = 0.61-0.55 eV) and x = 0.26 (E_g = 0.5 eV) grown as a bulk material at the Rensselaer Polytechnic Institute were studied in this work. Temperatures in the range of 430-

450°C for $In_xGa_{1-x}Sb$ samples with x = 0.12 - 0.19 were used for fabrication of InGaSb TPV cells. No TPV cells have been fabricated of $In_xGa_{1-x}Sb$ with x = 0.26 (E_g = 0.5 eV) yet. However, it is obvious that Zn diffusion temperatures lower than 350°C should be applied for the diffused emitter in this material.

For the tailoring of the diffused profiles anodic oxidation of InGaSb was studied. The anodic oxidation of $In_xGa_{1-x}Sb$ was performed in an electrolyte with the similar basic components as in the process developed for GaSb [16]:

(i) A component providing a suitable ionic conduction in the electrolyte. In this work we used a 5 % tartaric acid aqueous solution (AAS) with a pH value ≈ 6.0

(ii) A component decreasing the dissolution of the anodic oxide. In this work ethylene glycol (EG) with a volume ratio to the component (i) of 20 was used.
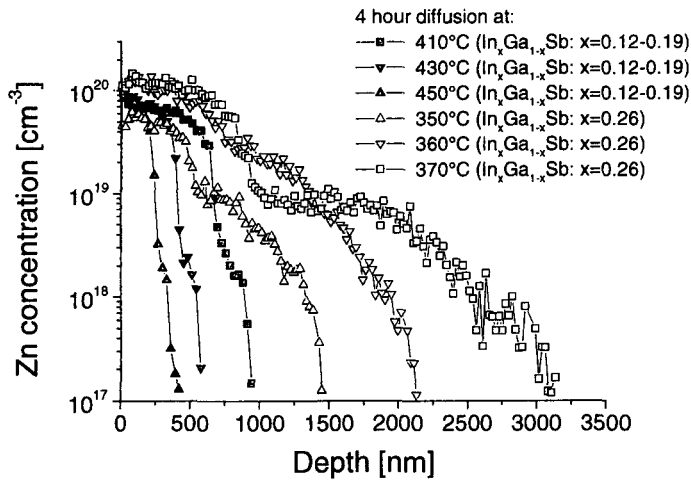

4 hour diffusion at:
—■— 410°C ($In_xGa_{1-x}Sb$: x=0.12-0.19)
—▼— 430°C ($In_xGa_{1-x}Sb$: x=0.12-0.19)
—▲— 450°C ($In_xGa_{1-x}Sb$: x=0.12-0.19)
—△— 350°C ($In_xGa_{1-x}Sb$: x=0.26)
—▽— 360°C ($In_xGa_{1-x}Sb$: x=0.26)
—□— 370°C ($In_xGa_{1-x}Sb$: x=0.26)

FIGURE 5.7. SIMS profiles of Zn concentration in $In_xGa_{1-x}Sb$ with different x in dependence on temperature after a 4-hour diffusion.

A high ratio of EG/AAS = 20 in comparison to that used for GaSb EG/AAS = 5 [16] is caused by a relatively high value of the minimum current that was measured for InGaSb in electrolytes with EG/AAS = 5. Thus, it was not possible to have current densities lower than 0.3 mA/cm² for $In_{0.12}Ga_{0.88}Sb$ and lower than 0.7 mA/cm² for $In_{0.26}Ga_{0.74}Sb$ at an applied voltage of 90V. For comparison, minimum current densities as low as 0.01 mA/cm² were measured for GaSb at the same oxidation conditions. It is not quite clear what causes the relatively high minimum currents by the oxidation of InGaSb: higher dissolution rates of these materials, the presence of surface defects or both of them. High-quality single crystal InGaSb wafers are necessary to determine that. Anyhow, as the low final current densities are important for the homogeneity of anodic oxides [16], electrolytes with the lower dissolution of anodic oxides (EG/AAS = 20) were chosen.

Ellipsometry measurements of the anodic oxide thickness and refractive index were performed within an area of 5 x 5 mm² in 100 points. Figure 5.8 shows thickness of the anodic oxide of the $In_{0.12}Ga_{0.88}Sb$ sample versus applied voltage for an electrolyte EG:AAS=20:1 and final current density J_f = 0.1 mA/cm². The mean values are shown together with the standard deviation. One can see that the dependence of the oxide thickness is linear. The linear fit of the measured data gives the value of the oxidation ratio equal to 2.53 nm/V. Noteworthy, that practically the same dependence of the oxide thickness on the applied voltage was observed for the $In_{0.26}Ga_{0.74}Sb$ sample.
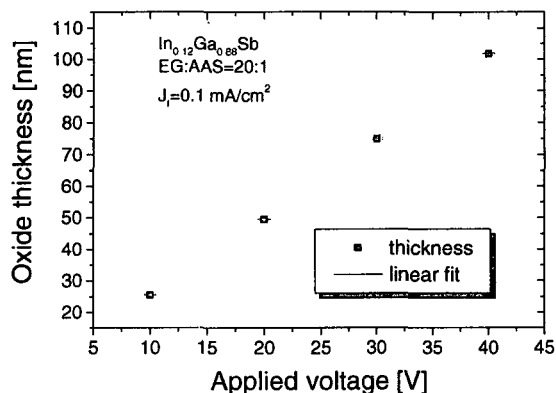
FIGURE 5.8. Thickness of the anodic oxide of the $In_{0.1}Ga_{0.9}Sb$ sample versus applied voltage. Ellipsometry measurements of the anodic oxide thickness and n were performed within an area of 5 x 5 mm^2 in 100 points. The mean values are shown together with the standard deviation. The dependence of the thickness of the anodic oxide of the $In_{0.26}Ga_{0.74}Sb$ sample on applied voltage was practically the same.
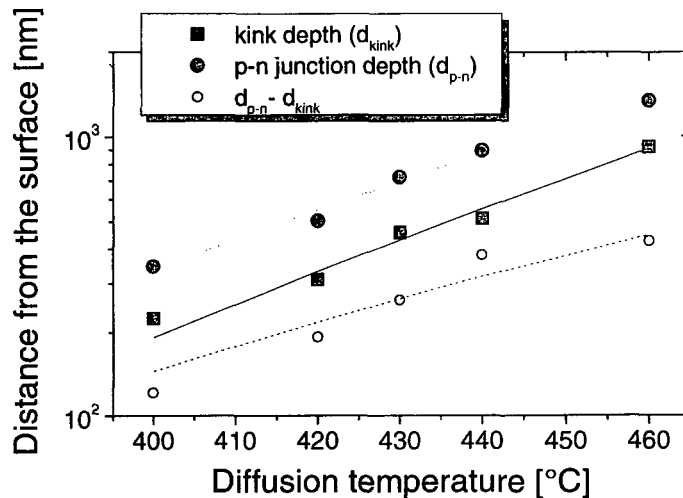
For the practical use of anodic oxidation, it is important to know how much semiconductor is consumed by the oxidation. The consumption ratio can be determined by performing a local oxidation, selective anodic oxide etching and measuring the step height between oxidized and not oxidized parts. It was determined for an electrolyte with pH = 6 and EG:AAS = 20:1 that the consumption rate is 60 ± 3 % of the oxidation rate for the $In_{0.1}Ga_{0.9}Sb$ sample and 58 ± 3 % for the $In_{0.26}Ga_{0.74}Sb$ sample.

InGaAsSb

InGaAsSb as a quaternary system provides a broad variation of bandgaps. For the TPV application only InGaAsSb compositions lattice matched to a GaSb substrate, for example $In_{0.15}Ga_{0.85}As_{0.17}Sb_{0.83}$ that corresponds to a bandgap $E_g \approx 0.55$ eV, are considered. The first InGaAsSb cell was fabricated at AstroPower [18]. Fully epitaxial approach was used for the fabrication of that cell. Later, in a joint work of Fraunhofer ISE and AstroPower the epitaxial emitter was substituted by the diffused one [7,8]. Essentially higher Voc was achieved as a result.

Zn-diffusion from the vapor phase is performed into epitaxial InGaAsSb:Te ($n \approx 2\text{-}3\times10^{17}$ cm^{-3}) layers grown on polished 1.5 x 1.5 cm^2 n-GaSb:Te (100) substrates. Prior to diffusion the wafers are treated in diluted HF or HCl to remove native oxides on the surface and dried with nitrogen.

As Zn profiles in this material have a form with a kink described for GaSb, Figure 5.9 shows pn-junction depth, kink depth and their difference for 4-h diffusions of Zn into GaSb in dependence on diffusion temperature. As in the case of InGaSb, lower than for GaSb diffusion temperatures are necessary for InGaAsSb TPV cell fabrication.

Distance from the surface [nm]

■ kink depth (d_{kink})
● p-n junction depth (d_{p-n})
○ d_{p-n} - d_{kink}

10^3

10^2

400 410 420 430 440 450 460

Diffusion temperature [°C]

FIGURE 5.9. pn-junction depth (n = 3×10^{17} cm^{-3}), kink depth and their difference for 4-h diffusions of Zn into InGaAsSb in dependence on diffusion temperature.

For the tailoring of the diffused layers, precise thinning through anodic oxidation and selective oxide etching, as well as additional shallow Zn diffusion after the emitter thinning is used. As it was determined in [8], the oxidation and consumption rates of $In_{0.15}Ga_{0.85}As_{0.17}Sb_{0.83}$ are 2.26 nm/V and 2.51 nm/V, respectively.
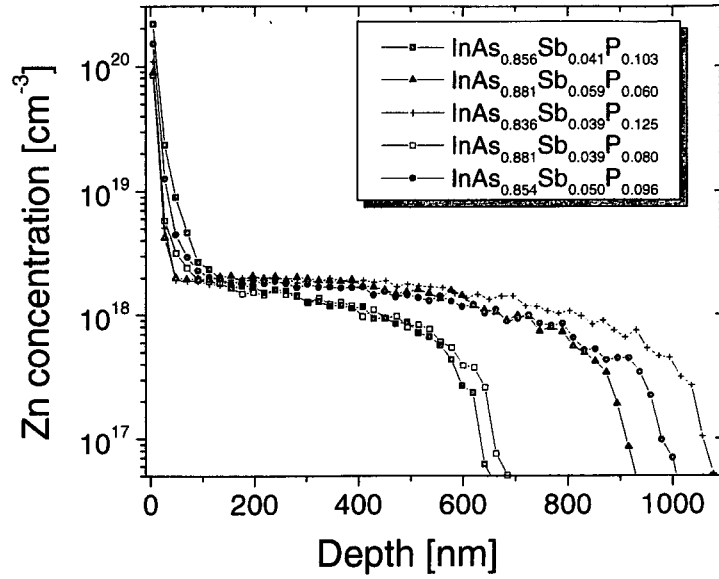
InAsSbP

InAsSbP materials lattice matched to InAs or GaSb are of special interest for the TPV application. Materials with a bandgap down 0.35 eV are available in this system. There is only one publication of AstroPower reporting of an LPE-grown p-InAsSbP/n-InAsSbP/n-InAs TPV cell [19]. In [20] we fabricated a similar TPV cell with a diffused p-InAsSbP instead of an epitaxial one.

Zn-diffusion from the vapor phase is performed into epitaxial InAsSbP doped with Sn or Te (n ≈ 2-3×10^{17} cm^{-3}) layers grown on polished 1.5 x 1.5 cm^2 n-InAs (100) substrates.

Fig. 10 shows an essential difference between Zn profiles in InAsSbP and those in GaSb, InGaAsSb or InGaSb described above. First, Zn profiles in InAsSbP exhibit no kink and relatively low Zn concentration of 2×10^{18} cm^{-3}. The near-surface part with a high Zn concentration can be caused by SIMS measurements like it happens with GaSb, InGaAsSb and InGaSb. In any way, this layer with a high Zn concentration is thin and can be easily removed. In other words, there is no dead layer in Zn diffused InAsSbP and thus the design of an optimal Zn-diffused emitter might be easier.

Also, Fig. 5.10 shows a relatively strong dependence of Zn on variation of As, Sb and P. More experiments are necessary to determine which element plays the main role in the observed dependence.

FIGURE 5.10. SIMS profiles of Zn concentration in $In_xGa_{1-x}Sb$ with different x after 4-hour 340°C diffusion.

For the tailoring of the diffused profiles, anodic oxidation of InAsSbP was studied. The anodic oxidation of InAsSbP is performed in the same electrolyte that was developed for the oxidation of InGaSb (see above). A consumption rate of 1.5 nm/V was determined.

5.3 Conclusions

Diffusion of Zn from vapor into as GaSb-, InGaAsSb-, InGaSb- and InAsSbP using pseudo-closed system is studied.

Diffusion profiles in GaSb, InGaSb and InGaAsSb generally consist of 5 parts: (i) a part with a steep Zn concentration gradient near the surface, (ii) a first plateau with a high Zn concentration and its relatively slow decrease, (iii) a kink part, (iv) a second plateau with a relatively slow change of Zn concentration and (v) a steep diffusion front.

A tailoring of the diffused profiles in GaSb, InGaSb and InGaAsSb is necessary to use the diffused emitter in high-efficiency TPV cell. Precise thinning of the as-diffused emitter that removes a dead layer with high Zn concentration (GaSb, InGaSb and InGaAsSb) and additional shallow Zn diffusion after the emitter thinning (GaSb, InGaAsSb) are studied and found to be advantageous. Additionally, a shallow diffusion followed by a high-temperature annealing under SiN_x and the influence of anodically oxidized surface on Zn profiles are studied in GaSb.

Contrary to GaSb, InGaSb and InGaAsSb, practically no dead layer is found in Zn diffused InAsSbP. Thus the fabrication of an optimal Zn-diffused emitter InAsSbP might be simpler.

The description and comparison of GaSb-, InGaSb-, InGaAsSb- and InAsSbP-based TPV cells with Zn diffused emitters is published elsewhere [20].

5.4 References for Part 5

1. Andreev, V. M., and Sulima, O.V., Sov. Tech. Phys. Lett., 8 , 187- 188 (1982).
2. Spring Thorpe, A. J., and Svilans, M. L., "Low-temperature zinc-diffusion in GaAs, InP and InGaAs using the box-diffusion technique" in Inst. Phys. Conf. Ser., No. 65, 1982, pp.589-596.
3. Blashku, A. I., Boltaks B. I., Burdiyan, I. I., Dzhafarov,T. D, and Rzaev, M. A., Sov. Phys.-Semiconductors, 6, 402-406 (1972).
4. Sundaram, V. S., and Gruenbaum P. E., J. Appl. Phys., 73, 3787-3789 (1993).
5. Bett, A.W., Keser, S., and Sulima, O.V., J. of Cryst. Growth, 181, 9-16 (1997).
6. Fraas, L. M., Avery, J. E., Martin, J., Sundaram, V. S., Girard, G., Dinh, V.T., Davenport, T. M., Yerkes, J. W., and O'Neil, M. J., IEEE Transactions on Electron Devices 37, 443-449, (1990).
7. Sulima, O.V., Beckert, R, Bett, A.W., Cox J.A, and Mauk, M.G., IEE Proc.-Optoelectron., 147, 199-204 (2000).
8. Bett, .W., Ber, B.Ya., Mauk, M.G., South, J.T., and Sulima, O.V., " Pseudo-closed box diffusion of Zn into InGaAsSb and AlGaSb for TPV devices", ", in Thermophotovoltaic Generation of Electricity –1998, edited by T.J. Coutts et al., AIP Conference Proceedings 460, American Institute of Physics, New York, pp. 237-246.
9. Bett, A.W., Keser, S., Stollwerck, G., and Sulima, O.V., "Large-Area GaSb Photovoltaic Cells", in Thermophotovoltaic Generation of Electricity –1997, edited by T.J. Coutts et al., AIP Conference Proceedings 401, American Institute of Physics, New York, pp. 41-53.
10. Sulima, O.V., Faleev, N.N., Kazantsev, A.B., Mintairov, A.M., and Namazov A., "Low-temperature Zn diffusion for GaSb solar cell structures fabrication" in Proceedings of the 4th European Space Power Conference, Poitiers, France, 1995, v.2, pp. 641-644.
11. Sulima, O.V., and Bett, A.W, Solar Energy Materials & Solar Cells, 66, 533-540, 2001.
12. V. Hinkov, personal communication.
13. Hitchcock, C.W., Gutmann, R.J., Borrego, J.M., Bhat, I.B., and Charache, G.W., IEEE Transactions on Electron Devices, 46, 2154-2161 (1999).
14. Mauk, M. G., Shellenbarger, Z. A., Cox, J. A., Sulima, O.V., Bett, A.W., Mueller, R. L., Sims, P. E., McNeely, J. B., DiNetta, L. C., J. of Cryst, Growth, 211, 189-193 (2000).
15. Dutta, P.S., Ostrogorsky, A.G., and Gutmann, R.J., "Bulk crystal growth of antimonide based III-V compounds for TPV applications", in Thermophotovoltaic Generation of Electricity –1998, edited by T.J. Coutts et al., AIP Conference Proceedings 460, American Institute of Physics, New York, pp. 227-236.
16. Sulima O.V., Bett A.W., and Wagner J., Journal of The Electrochemical Society, 147, 1910-1914 (2000).
17. Stollwerck, G., Sulima, O.V., and Bett, A.W., IEEE Transactions on Electron Devices, 47, 448-457 (2000).
18. Shellenbarger, Z.A., Mauk, M.G., and DiNetta, L.C, " Recent Progress in InGaAsSb/GaSb TPV Devices" in Proceedings of the 25th IEEE Photovoltaic Specialists Conf., 1996, pp. 81-84.
19. Mauk, M.G., Shellenbarger, Z.A., Cox, J.A., Tata, A.N., Warden, T.G., and DiNetta, L.C., "Advances in low-bandgap InAsSbP/InAs and GaInAsSb/GaSb thermophotovoltaics", " in Proceedings of the 28th IEEE Photovoltaic Specialists Conf., 2000, pp. 1028-1031.
20. Sulima O.V., Bett, A.W., Mauk, M.G., Dimroth F., Dutta P.S., and Mueller R.L. "GaSb-, InGaAsSb-, InGaSb-, InAsSbP- and Ge-TPV cells for low-temperature TPV applications", this conference.

Part 6: Liquid-Phase Epitaxy of Low-Bandgap III-V Antimonides for Thermophotovoltaic Devices

6.1 Summary

Liquid-phase epitaxial (LPE) growth of low-bandgap III-V antimonides is developed for thermophotovoltaic and other optoelectronic device applications. Epitaxial layers of AlGaAsSb, InGaAsSb, and InAsSbP, with thicknesses up to 200 microns, can be grown in a single LPE step. TPV devices based on InAsSbP extend the spectral response to a wavelength of 3500 nm. These single-epilayer structures are compatible with post-growth zinc diffusion processes that produce high-performance TPV devices. Thick epitaxial layers are also conducive for epilayer film transfer to surrogate substrates and subsequent removal of the GaSb and InAs seeding substrate. An insulating surrogate substrate facilitates isolation schemes for monolithic series-interconnected TPV arrays, and a reflective substrate acting as a backside mirror is used to effect photon recycling.

6.2 Introduction and Background

We describe adaptations, modifications, and improvements of liquid-phase epitaxy (LPE) techniques for the realization of new thermophotovoltaic device structures. The liquid-phase epitaxial growth of device-quality quaternary alloys; specifically lattice-matched or near-lattice-matched compositions of InGaAsSb, InAsSbP, and AlGaAsSb on GaSb and InAs substrates; is well-established [1-7]. Many optoelectronic devices (lasers, solar cells, LEDs, detectors) are based on double heterostructures or similar designs where the luminescent or absorbing layer (e.g., InGaAsSb or InAsSbP) is sandwiched between two wider bandgap cladding layers (e.g., AlAsSb or AlGaAsSb). With respect to TPV devices, some recent work has shown that a post-growth Zn diffusion process can produce p-n homojunction TPV cells with performance comparable to epitaxial double heterostructures [8,9]. Such a simple structure with a single epitaxial layer facilitates some of the new approaches discussed here.

Most previous work on thermophotovoltaic (TPV) devices has concentrated on semiconductors such as silicon ($E_g = 1.1$ eV), InGaAs on InP (typically $E_g = 0.5$ to 0.73 eV, but limited by lattice mismatch to the higher bandgap ranges), or InGaAsSb on GaSb (constrained to $E_g > 0.5$ eV by a miscibility gap). The optimum TPV cell bandgap depends on the radiation spectrum, i.e., the emitter blackbody temperature and its possible modification by spectral control using, for example, rare-earth emitters; and also on the details of device and system features incorporating photon recycling effects implemented by selective filters and/or backside reflectors. Although III-V ternary and quaternary semiconductors have widely tunable spectral responses, miscibility gaps and lattice matching constraints limit the practical range of bandgaps in most of these systems. A recent theoretical study [10] suggests that for 1200 to 2500 K blackbody sources, optimum TPV cell bandgaps are in the range of 0.2 to 0.5 eV, which is considerably lower than virtually all conventional TPV cells. Therefore, we are developing InAsSbP epitaxial structures as lower bandgap alternatives to InGaAsSb-based TPV cells.

Several new enabling technologies that represent variations of conventional LPE, or which are used in combination with LPE, are reported. These techniques are intended to be generic in their compatibility with all three material systems and their applicability to a wide variety of optoelectronic devices, although we focus on TPV devices as a near-term application. They address several technical and cost issues that limit the performance or commercial viability of GaSb- or InAs-based devices made by conventional epitaxial growth methods and standard device fabrication processes. One serious drawback of these materials systems is the unavailability of a

semi-insulating substrate due to intrinsic defect doping and the high thermal carrier generation associated with narrow bandgaps. This complicates approaches to monolithic integration in applications such as series-interconnected monolithic thermophotovoltaic modules [11-14]. Another problem is performance losses due to high substrate optical absorption. Even in cases where the substrate has a wider bandgap than the epitaxial device layers, parasitic free carrier absorption is significant. This limits photon recycling schemes which could otherwise significantly enhance the performance of TPV cells and LEDs.

6.2. Liquid-Phase Epitaxial Growth

The LPE specifications used in this work are summarized in Table **6.1**. We use a conventional horizontal graphite slideboat technique for LPE [5]. The ambient is flowing Pd-membrane purified hydrogen at atmospheric pressure. For InGaAsSb and AlGaAsSb, the p-type dopants are Zn or Ge; the n-type dopants are Te or Sn. For InAsSbP, Cd or Mg are p-type dopants. Under the growth conditions used here, the InAsSbP appears to be intrinsically n-type, and it was not necessary to intentionally dope it. We have previously reported epitaxial growth of relatively thin (< 5 micron) epitaxial layers of InGaAsSb, InAsSbP, and AlGaAsSb for TPV [6,7]. Here, we present results for the growth of thick (5 to 200 microns) epitaxial layers which can be more easily separated from their substrate than thin epitaxial layers. Figure **6.1** is a photomicrograph of a cross-sectioned 200-micron thick AlGaAsSb layer grown on a GaSb substrate. This thickness required a growth time of 180 minutes. This sample demonstrates the high practical growth rates achieved uniquely with liquid-phase epitaxy.

A top view and a cross-section photomicrograph of a 60-micron thick InAsSbP epilayer on a sulfur-doped, n-type (100)± 0.5° InAs substrate is shown in Figure **6.2**. We are using thick epitaxial InAsSbP layers with the aim of transferring the epilayer to an electrical insulating, highly reflective, surrogate substrate, and with the objective of taking advantage of intrinsic compositional-grading effects to tune the bandgap of the cell [4].

6.3 TPV Devices

Technology and characterization of LPE-grown heterostructure p-AlGaAsSb / p-InGaAsSb:Ge / n-InGaAsSb:Te / n-GaSb:Te TPV cells has been reported [7]. The front surface passivating AlGaAsSb layer has a bandgap of 1.3 eV and the bandgap of the InGaAsSb layers is approximately 0.55 eV. Open-circuit voltages of 285 mV were measured for illumination intensities corresponding to a short-circuit current density of 2 A/cm^2. As a simpler, alternative TPV structure, single epitaxial layers of n-InGaAsSb:Te / GaSb:Te were diffused with zinc to form p-n homojunction [8]. At illumination intensities corresponding to short-circuit current densities of 2 A/cm^2, the open-circuit voltages were approximately 350 mV. Consistent with the improved open-circuit voltage, a near 5-fold decrease in diode dark current was observed compared to the heterostructure cell. Thus, high-performance InGaAsSb TPV cells based on a single epitaxial layer are feasible.

With the aim of extending the spectral response of TPV cells to wavelengths of 3500 nm, InGaAsSb based devices were developed. The spectral response of a TPV cell fabricated in an epitaxial p-InAsSbP:Cd/n-InAsSbP/n-InAs heterostructures is shown in Figure **6.4**.

6.4. Surrogate Superstrates and Epitaxial Film Transfer

An InGaAsSb epilayer on GaSb substrates is bonded epi-side down to a glass slide using Crystalbond™ adhesive. There are unfortunately few, if any, highly selective etchants for these materials thus precluding the use of "stop etch" layers [15]. Instead, the substrate is substantially removed by a slow, highly uniform etching in a Br (5% by volume) : methanol solution. Figure **6.3** is a top-view photomicrograph of a 15-micron thick free-standing $In_{0.15}Ga_{0.85}As_{0.2}Sb_{0.8}$ that was "floated off" the glass superstrate by acetone dissolution of the Crystalbond™.

6.5 Discussion and Conclusion

Contrary to usual trends in semiconductor device technology where progress is predicated on more complex structures and more sophisticated epitaxy, we make the case that TPV devices based on a single, relatively thick epitaxial layer in combination with simple post-growth processing can achieve high performance. The superstrate-bonded or free standing epilayer(s) have a variety of optoelectronic applications including photon recycling LEDs and resonant-cavity photodiodes [16]. Low-temperature (350 to 460 °C) pseudo-closed box zinc diffusions as described by BETT *et al.* [11] should be compatible with the glass bonded InGaAsSb or InAsSbP structures. This will facilitate simple structures and processes for monolithic, series-interconnected high-voltage TPV arrays in these materials and provide for photon recycling device designs.

6.4 References for Part 6

1. H. KANO, S. MIYAZAWA and K. SUGIYAMI, "Liquid-Phase Epitaxial Gowth of GaInAsSb Quaternary Alloys on GaSb" *Japanese J. Applied Physics* **18, 11** (1979) 2183-2184.

2. G. XIUYING, Y. BAUHUA, M. YINDI, G. FENSHENG, Y. YING, H. WENJIAN, L. XUEFENG, X. JINYING, W. ZUANGUO, and L. LANYING, "Liquid Phase Epitaxy Growth and Properties of GaInAsSb / AlGaAsSb / GaSb Heterostructures" *Japanese J. Applied Physics* **30, 7** (1991) 1343-1347.

3. M-C. WU and C-C. CHEN, "Liquid-Phase Epitaxial Growth of GaInAsSb with Application to GaInAsSb / GaSb Heterostructure Diodes" *J. Applied Physics* **71, 12** (1992) 6116-6120.

4. M.P. MIKHAILOVA, S.V. SLOBODCHIKOV, N.D. STOYANOV, N.M. STUS', AND YU. P. YAKOVLEV, "Noncooled InAsSbP/InAs Photodiodes for the Spectral Range 3-5 μm" *Tech. Phys. Lett.* **22, 8** (1996) 672-673.

5. M.G. ASTLES, *Liquid-Phase Epitaxial Growth of III-V Compound Semiconductor Materials and Their Device Applications* (Hilger, 1990).

6. Z.A. SHELLENBARGER, M.G. MAUK, P.E. SIMS, M.I. GOTTFRIED, J.A. COX, J.D. LESKO, J.R. BOWER, J.D. SOUTH, and L.C. DINETTA, "Progress on GaInAsSb and InAsSbP Photodetectors for Mid-IR Wavelengths" *Infrared Applications of Semiconductors* II MRS Symposium Proc. **484** (1998) 135-140.

7. Z.A. SHELLENBARGER, M.G. MAUK, J.A. COX, M.I. GOTTFRIED, P.E. SIMS, J.D. LESKO, J.B. MCNEELY, L.C. DINETTA, and R.L. MUELLER, "Improvements in GaSb Thermophotovoltaics" *Thermophotovoltaic Generation of Electricity* AIP Conf Proc. **401** (American Inst. Physics, 1997) 117-128.

8. A.W. BETT, B.Y. BER, M.G. MAUK, J.T. SOUTH, and O.V. SULIMA, "Pseudo-closed Box Diffusion of Zn into InGaAsSb and AlGaSb for TPV Devices" " in *Thermophotovoltaic Generation of Electricity: Fourth NREL Conf.* T.J. COUTTS, J.P. BENNER, and C.S. ALLMAN, eds. AIP Conf. Proc. **450** (1998) 237-246.

9. O.V. SULIMA, "InGaAsSb Photovoltaic Cells with Enhanced Open-Circuit Voltage" *Proc. Third International Conf. Mid-Infrared Optoelectronics Materials and Devices (MIOMD II)* (Aachen, Germany, 1999) to be published.

10. G.D. CODY, "Theoretical Maximum Efficiencies for Thermophotovoltaic Devices" in *Thermophotovoltaic Generation of Electricity: Fourth NREL Conf.* T.J. COUTTS, J.P. BENNER, and C.S. ALLMAN, eds. AIP Conf. Proc. **450** (1998) 58-67.

11. J.S. WARD, A. DUDA, M.M. WANLASS, J.P. CARPELLA, X. WU, R.J. MATSON, T.J. COUTTS, T. MORIARTY, C.S, MURRAY, and D.P. RILEY, "A Novel Design for Monolithically Interconnected Thermophotovoltaic Power Conversion" *Thermophotovoltaic Generation of Electricity* AIP Conf Proc. **401** (American Inst. Physics, 1997) 227-236.

12. N.S. FATEMI, D.M. WILT, P.P. JENSKINS, R.W. HOFFMAN, Jr., V.G. WEIZER, C.S. MURRAY, and D.R. RILEY, "Materials and Process Development for Monolithic Interconnected Module (MIM) InGaAs/InP TPV Device" *Thermophotovoltaic Generation of Electricity* AIP Conf Proc. **401** (American Inst. Physics, 1997) 249-262.

13. M.G. MAUK, Z.A. SHELLENBARGER, M.I. GOTTFRIED, J.A. COX, B.W. FEYOCK, J.B. MCNEELY, and L.C. DINETTA, "New Concepts for III-V Antimonide Thermophotoovoltaics" *Thermophotovoltaic Generation of Electricity* AIP Conf Proc. **401** (American Inst. Physics, 1997) 129-137.

14. K. MASU, Y.S. QUAN, M. KONAGI, and K. TAKAHASHI, "A Monolithic GaAs Solar Cell Array" *Conf. Record 15th IEEE Photovoltaics Specialists Conf.* (IEEE, 1981) 1337-1342.

15. C. GATZKE, S.J. WEBB, K. FOBELETS, and R.A. STRANDLING, "In Situ Raman Spectroscopy of the Selective Etching of Antimonides GaSb/AlSb/InAs heterostructures" *Semiconductor Science and Technology* (1998) 399-403.

16. I-H. TAN, E.L. HU, J.E. BOWERS, and B.I. MILLER, "Modeling and Performance of Wafer-Fused Resonant-Cavity Enhanced Photodetectors" *IEEE J. Quantum Electronics* **31, 10** (1995) 1863- 1875.
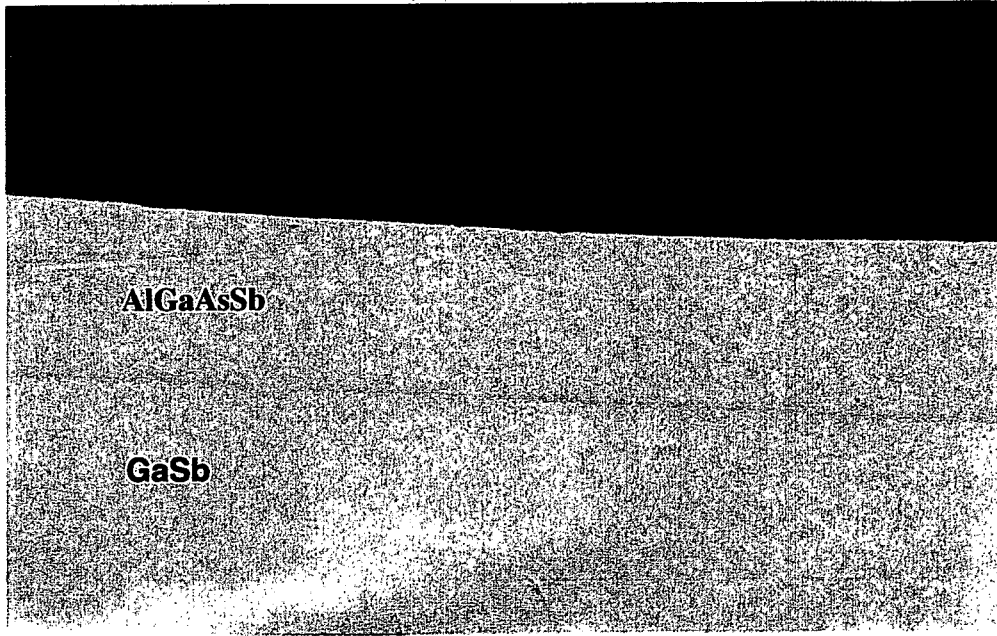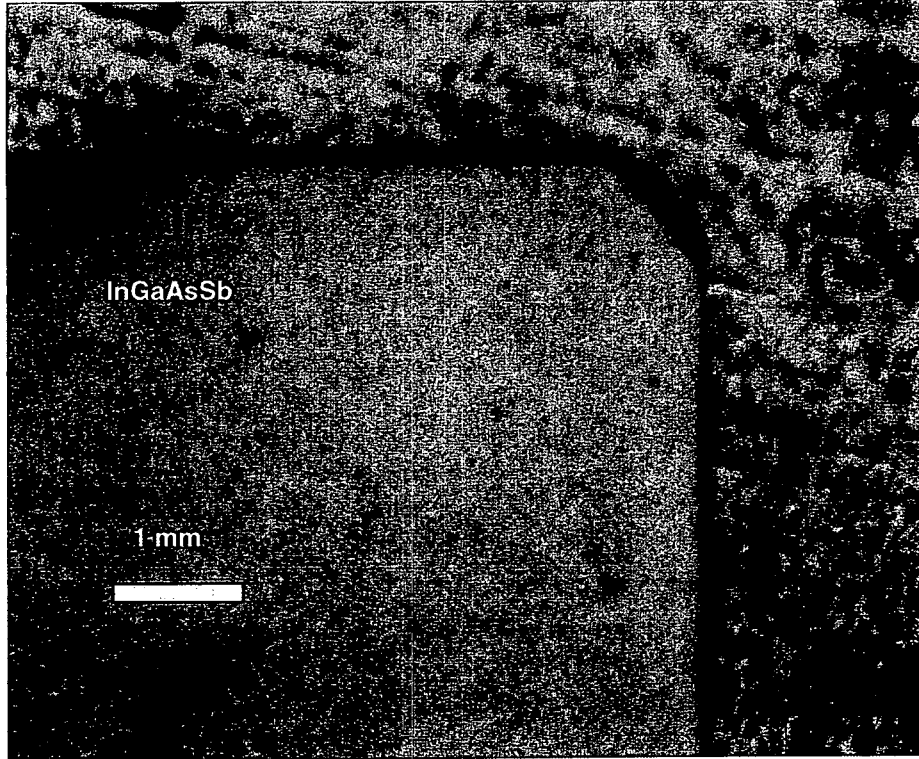
FIGURE **6.1:** Cross-section photomicrograph of a 200-micron thick (0.2 mm)layer of AlGaAsSb on a (100) GaSb substrate.
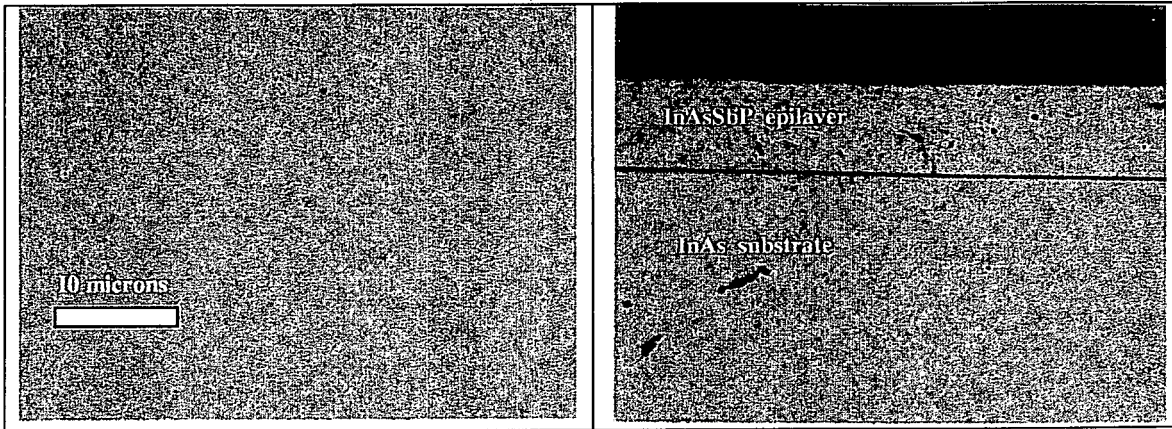
FIGURE 6.2: a. top-view photomicrograph of InAsSbP epitaxial layer grown on (100) InAs substrate; **b.** photomicrograph of cross-section.

FIGURE 6.3: Top-view photomicrograph of 15-micron thick InGaAsSb layer removed from GaSb seeding substrate by controlled etching.
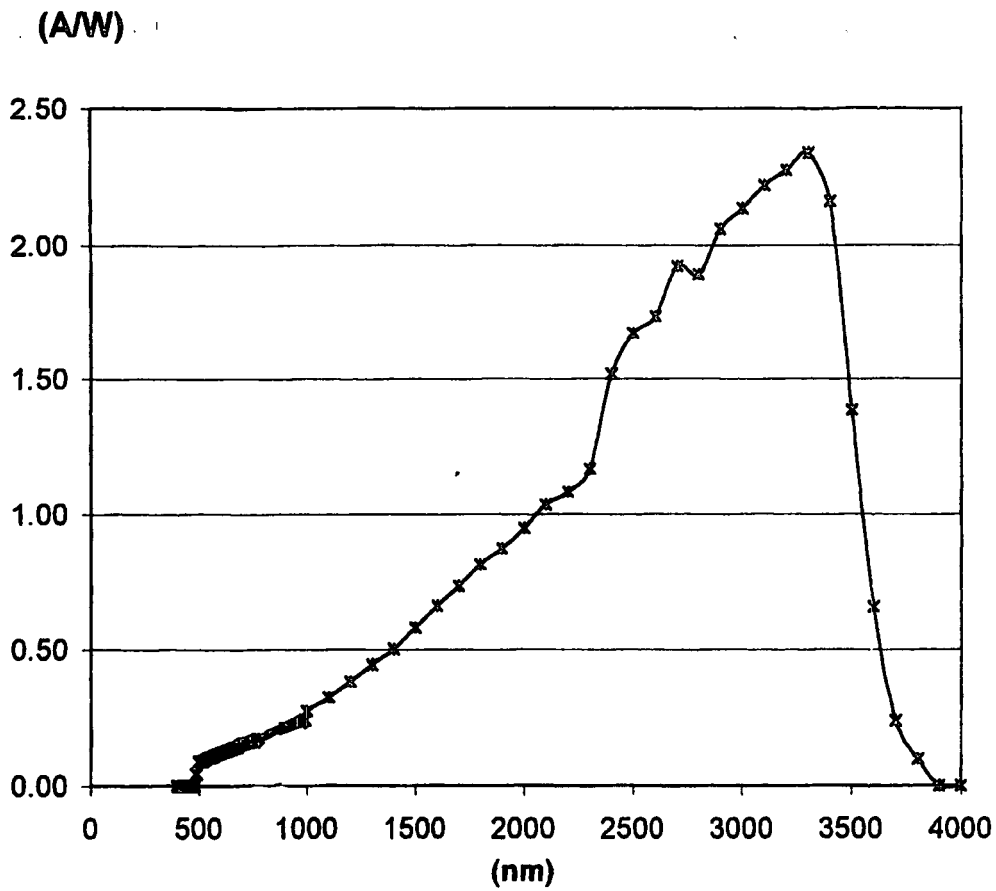
FIGURE 6.4: Spectral response of an epitaxial *p*-InAsSbP:Cd / *n*-InAsSbP / *n*-InAs:Te TPV cell.

Table 6.1: Summary of Liquid-Phase Epitaxy Parameters

	Solid Composition	Sub-strate	Growth Temp. (°C)	Melt Composition (atomic fraction)						Bandgap (eV) / Wavelength (µm)
				X_{Al}	X_{In}	X_{Ga}	X_{As}	X_{Sb}	X_P	
A	$In_{0.15}Ga_{0.85}As_{0.17}Sb_{0.83}$	GaSb	515	0	0.59	0.19	0.01	0.21	0	0.53 / 2.3
B	$In_{0.15}Ga_{0.85}As_{0.17}Sb_{0.83}$	GaSb	519							
C		GaSb	537	0.199		0.032	0.046	0.723		
D	$InAs_{0.61}Sb_{0.18}P_{0.21}$	InAs	565		0.589				0.00088	0.44
E	$InAs_{0.84}Sb_{0.03}P_{0.13}$	InAs	518	0	0.794	0	0.026	0.179		1.10
F	$Al_{0.28}Ga_{0.72}As_{0.015}Sb_{0.985}$	GaSb	515	0.015		0.957	0.001	0.028		1.10 /
G	$Al_{0.67}Ga_{0.33}Sb$	GaSb	518	0.053		0.924	0	0.023		1.30

Part 7: Further Advances in Low-Bandgap InAsSbP/InAs and GaInAsSb/GaSb Thermophotovoltaics

7.1 Summary

Thermophotovoltaic devices based on InGaAsSb and InAsSbP alloys made by liquid-phase epitaxy are described. These alloys can be readily grown as thick (> 50 micron) layers to form "virtual" substrates. We are developing cell fabrication technologies to realize series-interconnected InGaAsSb and InAsSbP TPV cell arrays for high-voltage "minimodules" by transferring epitaxial device structures to insulating surrogate substrates.

7.2 Introduction

The aim of the present work is to widen the design options of thermophotovoltaic (TPV) device technology in two ways. First, we are extending the spectral response of TPV devices to longer wavelengths (> 2.5 microns) by demonstrating TPV cells based on lattice-matched compositions of InAsSbP on InAs substrates. Second, we are developing cell fabrication technologies to realize series-interconnected InGaAsSb and InAsSbP TPV cell arrays for high-voltage "minimodules". Such monolithic integrated modules (MIMs) have been reported in wider bandgap devices such as InGaAs/GaAs but are difficult to implement in InGaAsSb or InAsSbP due to the lack of a semi-insulating substrate wafers with the appropriate lattice constants for epitaxial growth.

The prior work [1-4] on thermophotovoltaics has been concentrated mostly on devices based on silicon, epitaxial InGaAs on InP substrates, or epitaxial InGaAsSb on GaSb substrates. The relatively high bandgap of silicon (E_g = 1.1 eV) is not suitable for many TPV systems applications. InGaAs/InP has a bandgap range of E_g = 0.5 to 0.73 eV, but in practice is limited to the higher end of the bandgap range due to lattice mismatch considerations. InGaAsSb/GaSb TPV devices have a potentially wider range of bandgaps, but a miscibility gap generally limits bandgaps to E_g > 0.5 eV. The optimum TPV cell bandgap depends on the radiation spectrum, i.e., emitter blackbody temperature and/or spectral control using, for example, rare-earth emitters. Bandgap selection also depends on the details of device and system features incorporating photon recycling effects implemented by selective filters and/or backside reflectors. While III-V ternary and quaternary semiconductors generally have widely tunable spectral responses, miscibility gaps and lattice matching constraints limit the practical range of bandgaps in most of these systems. Recent theoretical studies by CODY [5] and COUTTS and WARD [6] suggest that for 1200 to 2500 K blackbody sources, optimum TPV cell bandgaps are in the range of 0.2 to 0.5 eV, which is considerably lower than virtually all conventional TPV cells. Although the optimum TPV cell bandgap can still be debated, and depends on system specifics, the availability of lower bandgap cells should be investigated to provide this option for future TPV applications

7.3 Epitaxy

The InGaAsSb/GaSb heterostructure TPV cell is shown in Figure **7.1a.**). The InAsSbP *p-on-n* homojunction thermophotovoltaic cell structure is shown in FIGURE **7.1b**. The $InAs_xSb_yP_{1-x-y}$ quaternary alloy lattice-matched to an InAs substrate covers a bandgap range of 0.34 to 0.65 eV (1.9 to 3.6 microns wavelength). TABLE **7.1** summarizes the liquid-phase epitaxy parameters for the alloys of interest. Prior LPE work by others [7-13] in these alloys has been directed toward detectors, light-emitting diodes, and lasers. The emitter layer is ≈1 micron thick and the base layer is 5 microns thick. Doping of the emitter and base layers is an important issue since very little

segregation or electrical activity data exist for controlled impurity doping of InAsSbP. Further, there are generally defect-mediated compensation phenomena in the low-bandgap III-V antimonide alloys so doping may be complicated. Rare-earth gettering using Gd or Yb is useful for reducing residual background doping [15].

7.4 Device Characterization

FIGURES **7.2** and **7.3** show the spectral response and current-voltage characteristics for our InAsSbP TPV cells. The *I-V* curves are measured under pulse illumination testing for three different intensities. TPV devices in InAsSbP alloys generally exhibited good spectral response, but there is much variation in current-voltage characteristics. Not surprisingly, such low-bandgap *p-n* junctions are susceptible to excessive leakage currents, the origins and mechanism of which are not completely certain at this stage. In most cases, a soft *I-V* characteristic improved when measured at 77K, implying the cells were not shunted. This was corroborated by impedance measurements on small-area devices (0.5-mm x 0.5-mm) that indicated shunt resistances of 400 to 1500 Ω. A systematic study of emitter thickness, and base and emitter doping is in progress in order to minimize the dark diode current and improve fill-factors.
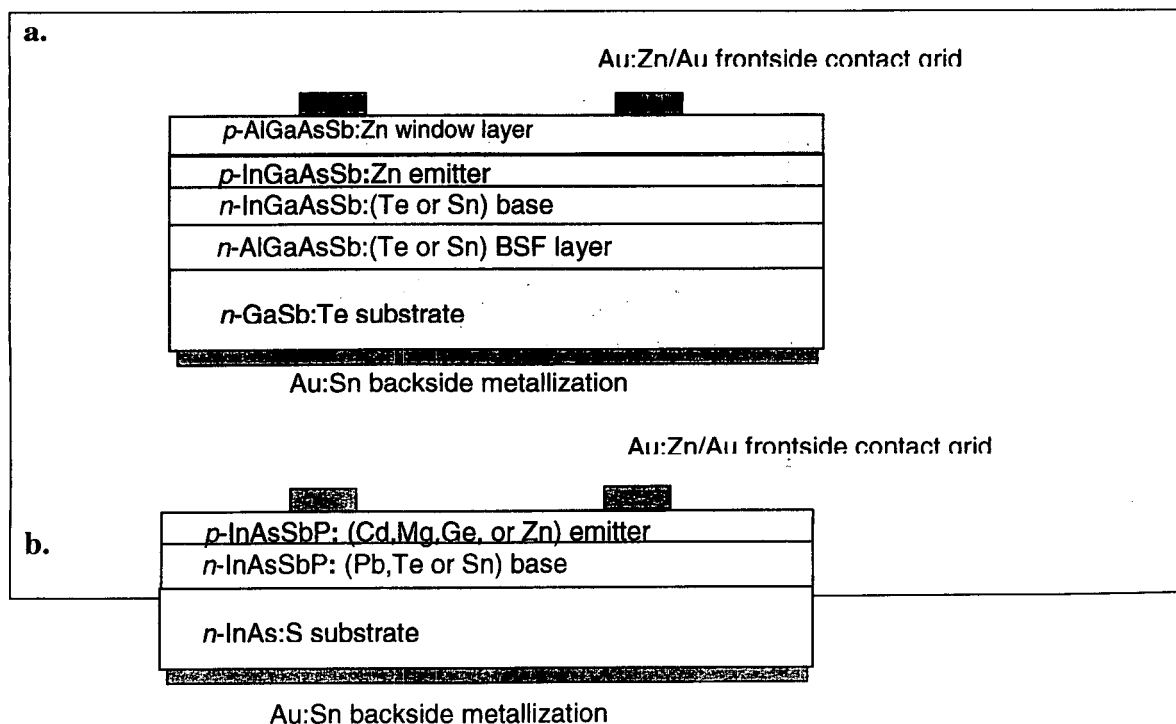
7.5 Series-Interconnected TPV Cells

Conventional schemes for monolithic integration for series interconnection of TPV cells to make MIMs (Monolithic Interconnected Modules) is thwarted in these materials systems due to the inavailability of semi-insulating substrates needed for device isolation. For minimodule arrays, our approach is based on transferring a thick epitaxial layer of InAsSbP or InGaAsSb to an insulating surrogate substrate such as glass, ceramic, oxide-coated silicon, or printed circuit board. Liquid-phase epitaxy permits the growth of thick (> 20 microns) epitaxial layers of InGaAsSb or InAsSbP substrate (FIGURE **7.4**). The epitaxial layer is then bonded to a surrogate substrate and the GaSb or InAs substrate is selectively removed by controlled wet etching (FIGURE **7.5**). We are investigating both epitaxial junctions and Zn-diffused junctions to form the TPV cell. For an epitaxial junction a two-layer structure is grown and transferred to the surrogate substrate. For a diffused junction, we have the option of forming the junction after bonding to the substrate since the Zn diffusion is relatively low temperature ($\approx$ 500 °C) process [SULIMA *et al.*, 1999]. TPV cell elements can then be isolated by dicing (FIGURE **7.6**). A prototype 9-element InGaAsSb minimodule module is shown in FIGURE **7.7**. These modules have achieved over 1-volt output under AM1.5 simulated insolation.
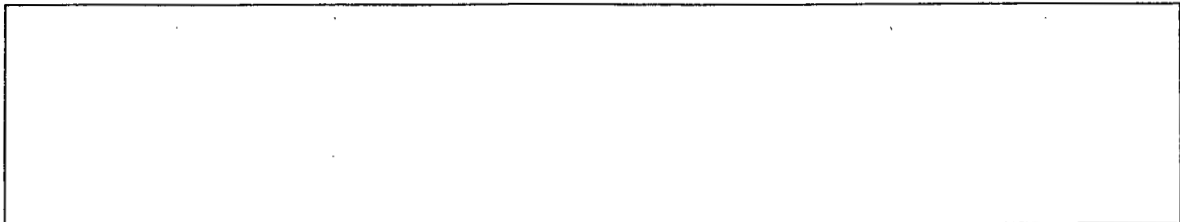
7.6 References for Part 7

1. T.J. COUTTS and J.P. BENNER, *The First NREL Conf. on Thermophotovoltaic Generation of Electricity,* American Inst. Physics Conference Proc. **321** (AIP, Woodbury, New York, 1995).

2. J.P. BENNER, T.J. COUTTS, and D.S. GINLEY, *The Second NREL Conf. on Thermophotovoltaic Generation of Electricity,* American Inst. Physics Conference Proc. **358** (AIP, Woodbury, New York, 1996).

3. T.J. COUTTS, C.S. ALLMAN, and J.P. BENNER, *Thermophotovoltaic Generation of Electricity: Third NREL Conf.* American Inst. Physics Conference Proc. **401** (AIP, Woodbury, New York, 1997).

4. T.J. COUTTS, J.P. BENNER, and C.S. ALLMAN, *Thermophotovoltaic Generation of Electricity: Fourth NREL Conf.* American Inst. Physics Conference Proc. **460** (AIP, Woodbury, New York, 1999).

5. G.D. CODY, "Theoretical Maximum Efficiencies for Thermophotovoltaic Devices" in *Thermophotovoltaic Generation of Electricity: Fourth NREL Conf.* (1999) 58.

6. T.J. COUTTS and J.S. WARD, "Thermophotovoltaic and Photovoltaic Conversion at High-Flux Densities" *IEEE Trans. Electron Devices* **46**, 10 (1999) 2145.

7. A. JOULLIÉ, F. JIA HUA, F. KAROUTA, H. MANI, and C. ALIBERT, "III-V Based Alloys Based on GaSb for Optical Communications at 2 – 4.5 μm)" *Optical Fiber Sources and Detectors* SPIE Proc. **587** (1985) 46-57.

8. E. TOURNIÉ, J.L. LAZZARI, H. MANI, F. PITARD, C. ALIBERT, and A. JOULLIÉ, "Growth by Liquid Phase Epitaxy and Characterization of GaInAsSb and InAsSbP Alloys for Mid-Infrared Applications (2 – 3 μm)" *Physical Concepts of Materials for New Optoelectronic Device Applications* SPIE Proc. **1361** (1990) 641- 656.

9. H. MANI, E. TOURNIÉ , J.L. LAZZARI, C. ALIBERT, A. JOULLIÉ, and B. LAMBERT, "Liquid Phase Epitaxy and Characterization of $InAs_{1-x-y}Sb_xP_y$ on (100) InAs" *J. Crystal Growth* **121** (1992) 463-472.

10. M.G. ASTLES, *Liquid-Phase Epitaxial Growth of III-V Compound Semiconductor Materials and Their Device Applications* (Adam Hilger, New York, 1990).

11. A.M. LITVAK, K.D. MOISEEV, M.V. STEPANOV, V.V. SHERSTNEV, and Y.P. YAKOVLEV, "Preparation of In-As-Sb-P Solid Solutions Isoperiodic to InAs and GaSb Near the Boundary of the Immiscibility Region" *Russian J. Applied Chemistry* **67**, 12 (1994) 1708.

12. R.A. GARNHAM, M.D. LEARMOUTH, J.J. RIMINGTON, A.S.M. ALI, M.J. ROBERTSON, and W.A. STALLARD, "140 Mbit/s Receiver Performance at 2.4 μm Using InAsSbP Detector: *Electronics Letters* **24**, 23 (1988) 1416.

13. D.R. ROWE and A. KRIER, "Liquid Phase Epitaxial Growth and Luminescence of $InAs_{1-x-y}Sb_xP_y$ p-n Junctions" *J. Physics* **D** 26, 7 (1993) 198-204.

14. W. YONGZHEN, J. CHANGCHUN, and L. GUIJIN, "Liquid-Phase Epitaxial Growth of InAsSbP/InAs Heterostructure" *J. Crystal Growth* **187** (1998) 194-196.

15. A. KRIER, H.H. GAO, AND V.V. SHERSTNEV, "Investigation of Rare Earth Gettering for the Fabrication of Improved Mid-Infrared Leds" *IEE Proc. Optoelectronics* **147**, 3 (2000) 217-221.

16. O.V. SULIMA, R. BECKERT, A.W. BETT, J.A. COX, and M.G. MAUK, "InGaAsSb Photovoltaic Cells with Enhanced Open-Circuit Voltage" *IEE Proc. Optoelectronics* **147**, 3 (2000) 199-203.

**a.**

Au:Zn/Au frontside contact grid

p-AlGaAsSb:Zn window layer

p-InGaAsSb:Zn emitter

n-InGaAsSb:(Te or Sn) base

n-AlGaAsSb:(Te or Sn) BSF layer

n-GaSb:Te substrate

Au:Sn backside metallization

Au:Zn/Au frontside contact grid

b.

p-InAsSbP: (Cd,Mg,Ge, or Zn) emitter

n-InAsSbP: (Pb,Te or Sn) base

n-InAs:S substrate

Au:Sn backside metallization

FIGURE 7.1: **a.** AlGaAsSb/InGaAsSb/GaSb double heterostructure TPV cell and **b.** *p-n* junction InAsSbP/InAs thermophotovoltaic device structure. The window and BSF layers are optional in the GaSb-based TPV cell.

Table 7.1: **LPE Parameters for Near-Lattice Matched InAsSbP on InAs and InGaAsSb on GaSb Epitaxy**

| Solid Quaternary Composition	Melt Composition (atomic fractions)					Growth Temp (°C)	Approx. Bandgap (eV)
	X_{Ga}	X_{In}	X_{As}	X_{Sb}	X_{P}		
$InAs_{0.61}Sb_{0.18}P_{0.21}$	0	0.589	0.0100	0.40	0.0012	565	0.44
$InAs_{0.84}Sb_{0.03}P_{0.13}$	0	0.794	0.026	0.179	0.00042	580	0.35
$In_{0.15}Ga_{0.85}As_{0.17}Sb_{0.83}$	0.19	0.59	0.01	0.21	0	515	0.53
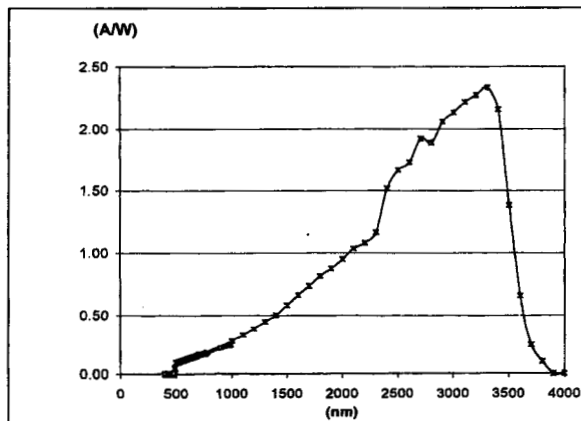
**FIGURE 7.2:** Spectral response of the InAsSbP/InAs TPV cell.
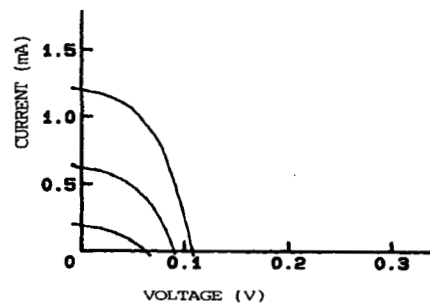
FIGURE 7.3: Current-voltage characteristic of InAsSbP cell under three illumination intensities: 1.0, 3.0 and 5.8 W/cm^2. (Cell testing temperature = 21 °C, TPV cell active area 0.4-mm diameter).
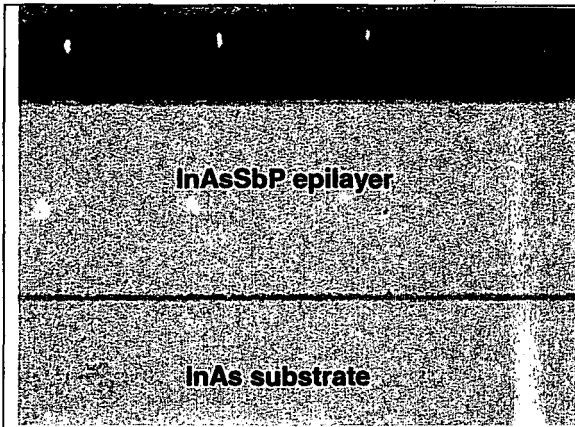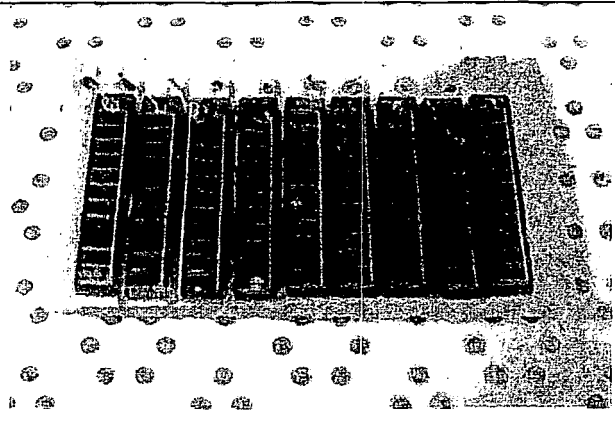
FIGURE 7.4: Cross-section of a 60-micron thick InAsSbP layer grown on a InAs substrate
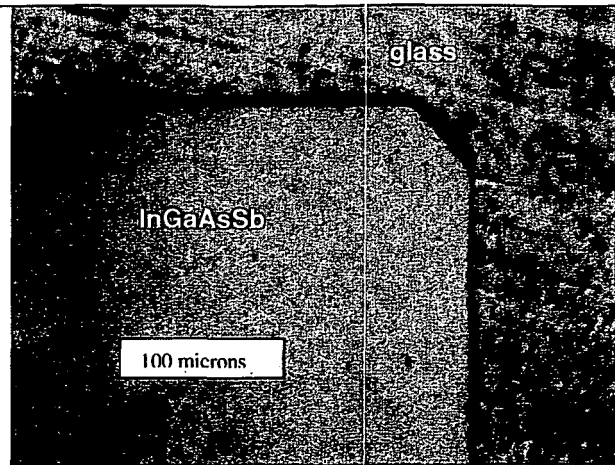
FIGURE 7.5: 20-micron thick InGaAsSb bonded to a glass substrate. GaSb substrate has been removed by controlled etching.
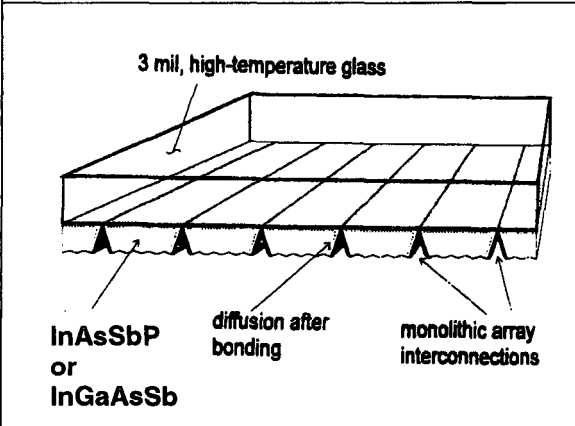
FIGURE 7.6: Monolithic InAsSbP diffused junction array on surrogate substrate.

FIGURE 7.7: Nine-element series-interconnected InGaAsSb TPV cell array.

Part 8: Comparision of GaSb-, InGaAsSb-, InGaSb-, InAsSbP- and Ge-TPV Cells for Low-temperature TPV Applications

8.1 Summary

GaSb thermophotovoltaic (TPV) cells are the most suitable choice for modern TPV generators, both in terms of efficiency and simplicity of the diffusion technology used. Actually, TPV generators based on GaSb solar cells are the only ones available on the market. However, TPV cells with band gaps (E_g) lower than GaSb are expected to be advantageous for low-temperature (< 1000°C) non-wavelength-selective TPV radiators because they provide more effective absorption of the blackbody infrared radiation. In this work, together with GaSb (E_g = 0.72 eV), semiconductors with a lower E_g - Ge (E_g = 0.66 eV), InGaSb (E_g = 0.60 eV), InGaAsSb (E_g = 0.55 eV) and InAsSbP (E_g = 0.39 eV) - were studied for TPV cells. InGaAsSb cells seem to be the most promising candidate to replace GaSb cells in the low-temperature TPV generators.

8.2 Introduction

A simple and economic "no-epitaxy" technology of GaSb TPV cells using Zn diffusion from the vapor phase has proven to be suitable for production. Currently, only TPV generators based on GaSb solar cells are available on the market [1].

Nevertheless, materials with band gaps lower than GaSb are desirable for low-temperature (< 1000°C) non-wavelength-selective TPV radiators. Therefore, in this work, together with GaSb (E_g = 0.72 eV), semiconductors with a lower E_g - Ge (E_g = 0.66 eV), InGaSb (E_g = 0.60 eV), InGaAsSb (E_g = 0.55 eV) and InAsSbP (E_g = 0.39 eV) - are studied for TPV cells.

To form pn-junctions in III-V materials, we used the most simple and productive method – low-temperature (from 340°C for InAsSbP to 480°C for GaSb) pseudo-closed-box Zn diffusion from the vapor phase. One-layer n-type epitaxial structures were grown by liquid phase epitaxy prior to the Zn diffusion only in the case of InGaAsSb and InAsSbP.

Further ways to simplify the technology of III-V TPV cells and reduce their price include using polycrystalline substrates and/or ternary substrates such as InGaSb. In this work, a first attempt to fabricate an InGaSb TPV cell from a polycrystalline boule material was made.

It was determined that a careful optimization of the Zn diffusion profiles in TPV cells leads to a significant improvement of device performance [2,3]. The formation of strong built-in electrical fields near the emitter surface provides a dramatic decrease in the surface recombination losses. Thus high-efficiency TPV cells can be fabricated without any passivating window.

The main obstacle to the large-scale application of III-V TPV cells is the high cost of III-V substrates (including polycrystalline). Ge TPV cells made on substrates that are 6-7 times less expensive than those of GaSb, can be a cost-effective alternative to III-V cells. In this work, Ge cells were fabricated using diffusion of P into p-type substrates.

8.3 Experimental

TPV cells based on single crystal GaSb, InGaAsSb, InAsSbP and Ge, as well as on polycrystalline GaSb and InGaSb structures fabricated at Fraunhofer ISE, AstroPower and RPI were tested at Fraunhofer ISE and JPL. A schematic of a TPV cell with a diffused emitter investigated in this work is presented in Figure 8.1. Description of the cell parts is given in Table 8.1.
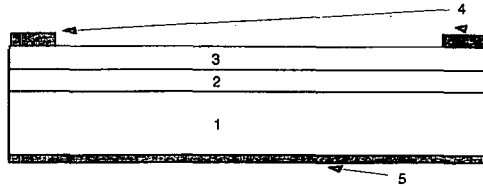
FIGURE 8.1. Scheme of TPV cells with a diffused emitter investigated in this work. Description of the cell parts is given in the Table 1. Numbers refer to column 1 of Table 8. 1. Different contact grid designs used in this work are described in [4].

TABLE 8.1. Materials used for different parts of the studied TPV cells.

Part of the cell	GaSb-cell	InGaSb-cell	InGaAsSb-cell	InAsSbP-cell	Ge-cell
1. Substrate	n-GaSb single and polycrystal.	n-InGaSb polycrystalline	n-GaSb single crystal	n-InAs single crystal	p-Ge single crystal
2. Epitaxial base	none	none	n-InGaAsSb	n-InAsSbP	none
3. Diffused emitter	p-GaSb	p-InGaSb	p-InGaAsSb	p-InAsSbP	n-Ge
4. Front side contact	Ti/Ni/Au				Ni/Au-Ge
5. Backside contact	Au-Ge				Ti/Pd/Ag

Details of the Zn diffusion process applied for III-V cells are published in Ref. [5]. Liquid phase epitaxy is used to grow base n-InGaAsSb or n-InAsSbP layers. Details of the epitaxial growth are described elsewhere [6].

Diffused n-type emitters in p-Ge ($p = 3\text{-}5\times10^{17}$ cm^{-3}) substrates are formed through diffusion of phosphorus. Two different methods of phosphorus diffusion are used: (i) diffusion during the MOCVD growth of InGaP on Ge, and (ii) diffusion from phosphorus spin-on dopants. In the case of method (i) the epitaxial InGaP layer is selectively removed from the Ge substrate after the diffusion. Method (i) in comparison with method (ii) seems to be too complicated. However, InGaP/Ge structures may be available as a sub-product of multi-junction solar cell fabrication.

Carrier concentration in Ge was measured by electrochemical CV profiling. Figure 8.2 shows the carrier concentration profile of a Ge cell that exhibited the best device parameters in this work (see below).
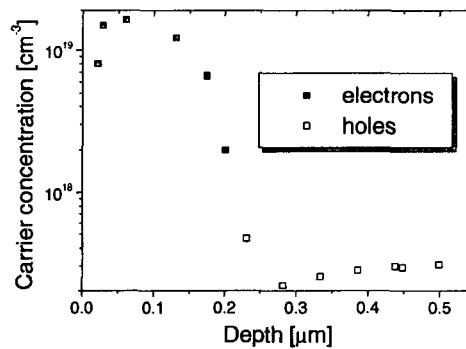

FIGURE 8.2. Carrier concentration profile in the Ge cell considered in this work. The profile is measured by electrochemical CV-profiling.

8.4 Results and Discussion

Figure 8.3 shows the external quantum efficiency (EQE) spectra of a typical GaSb TPV cell together with other single crystal and polycrystalline TPV cells studied in this work. The larger the long wavelength sensitivity of the TPV cell, the lower can be the radiator temperature. Hence if one considers only the photosensitivity range, InAsSbP cells with their sensitivity up to 3500 nm look to be the most promising for the low-temperature TPV generators. However, decrease of the bandgap inevitably causes reduction of the generated voltage. Thus, a trade-off between the increasing current and falling voltage must be found. Regarding the InAsSbP cells, problems with achieving sufficient voltage and FF impede their application. The open-circuit voltage (V_{oc}) achieved in these cells has been limited to about 0.1 V both in the cells with epitaxial [7] and diffusion emitters (this work). Thus, the ratio between V_{oc} and the potential difference at the pn-junction in the used InAsSbP (E_g = 0.39 eV) is only $\approx$ 0.25. It is noteworthy that nearly the same low voltages (0.12 V) were observed in polycrystalline InGaSb cells, where the above mentioned ratio was even lower: $\approx$ 0.20. For comparison, this ratio equals 0.5 - 0.6 in GaSb and InGaAsSb. One can assume that it is the surface leakage that prevents obtaining a V_{oc} of around 0.2 V in InAsSbP. In the case of the polycrystalline InGaSb, both the surface and the bulk can cause the reduced voltage.

Let us now consider the InGaAsSb cell that has the next longest wavelength response up to 2250 nm (Fig. 8.3). In contrast to the InAsSbP cell, relatively high voltages were achieved in such a cell using an optimized diffused emitter [2]. Thus as shown below, InGaAsSb is a very promising candidate to replace GaSb in the low-temperature TPV applications.
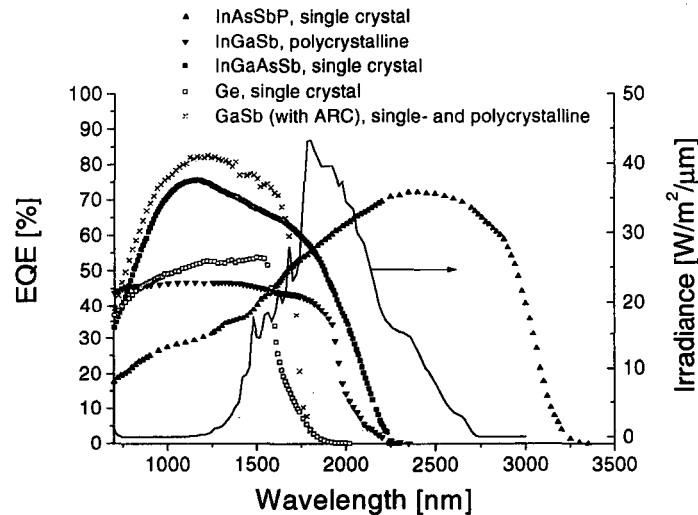

FIGURE 8.3. External quantum efficiency spectrum of the TPV cells (long wavelength part) measured in this work. Antireflection coating (anodic oxide) was applied only to the GaSb cell. Shadowing losses caused by the contact grid were within 15-20%. The spectrum of the JPL IR bandpass filtered large area pulsed solar simulator (LAPSS) irradiance (solid line, right axis) is shown for comparison.

Device parameters of GaSb, InGaAsSb and Ge TPV cells were measured under different illumination conditions including the JPL IR bandpass filtered large area pulsed solar simulator (LAPSS). The spectrum of the filtered LAPSS irradiance is shown in Figures 8.3 and 8.6. Output electric power densities of the measured devices is shown in Figure 8.4. The InGaAsSb cell demonstrated a superior performance under the LAPSS illumination. Ge cells showed the worst

EQE (Fig. 8.3) and thus the lowest current. The voltage of Ge cells was relatively poor as well (Fig. 8.5) - lower than of the InGaAsSb ones despite the higher bandgap of Ge.

Concerning the LAPSS measurements one should note the following. It is clear from Figure 8.6, that even the blackbody spectrum (T = 1610 K, 3206-fold attenuated) that is the closest to the LAPSS spectrum does not match it very closely. That is the reason why additional calculations of the output power were performed for different blackbody spectra.
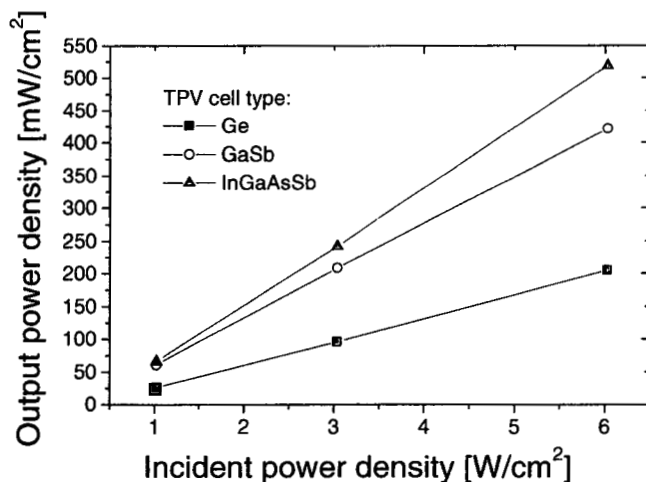
FIGURE 8.4. Output power density of Ge, GaSb and InGaAsSb TPV cells measured with the JPL LAPSS at different incident power densities at a cell temperature of 30°C.
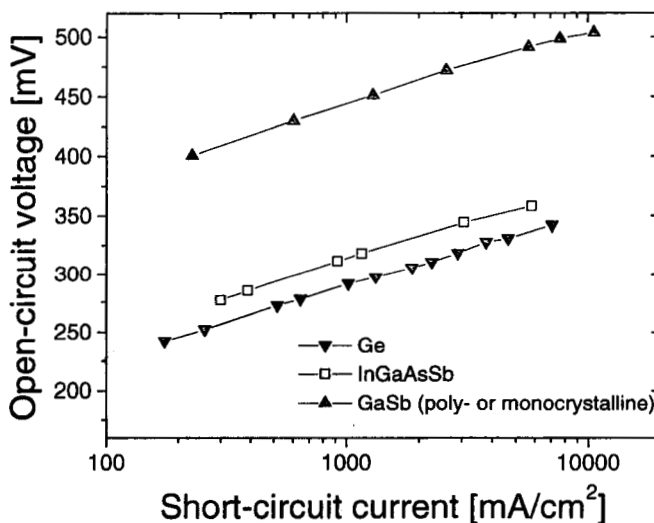
FIGURE 8.5. Open-circuit voltage of Ge, InGaAsSb and GaSb TPV cells vs. short-circuit current at 25°C.

Experimentally determined IV-characteristics and EQE-spectra allow an accurate calculation of TPV cell performance for any blackbody illumination at any temperature. Figure 8.7 shows the calculated output power of GaSb and   InGaAsSb TPV cells as a function of the blackbody temperature. Taking into account optical losses in a TPV system, we assumed that the blackbody illumination of the cell is "scaled" (its intensity at all wavelengths is proportionally reduced). The scaling factor was assumed to be 0.6. Figure 8.7 shows that the low bandgap InGaAsSb TPV

cells are advantageous for low radiator temperatures if no filters or selective emitters are used. For example, at T = 973K the output power of the InGaAsSb cell is 1.6 times higher than that of the GaSb one.
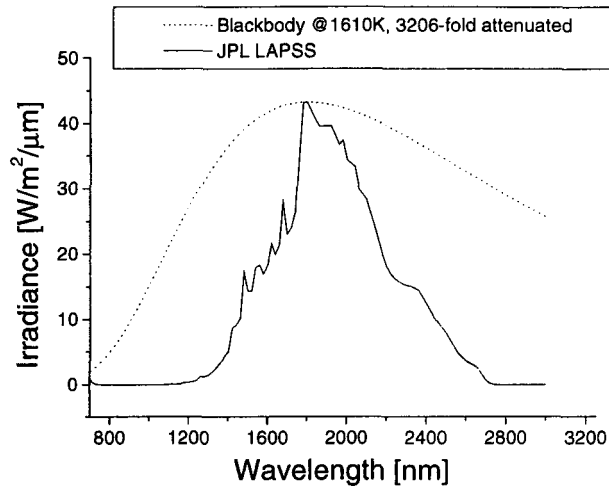

FIGURE 8.6. Comparison of the JPL LAPSS spectrum with the closest fit attenuated blackbody 1610 K spectrum.
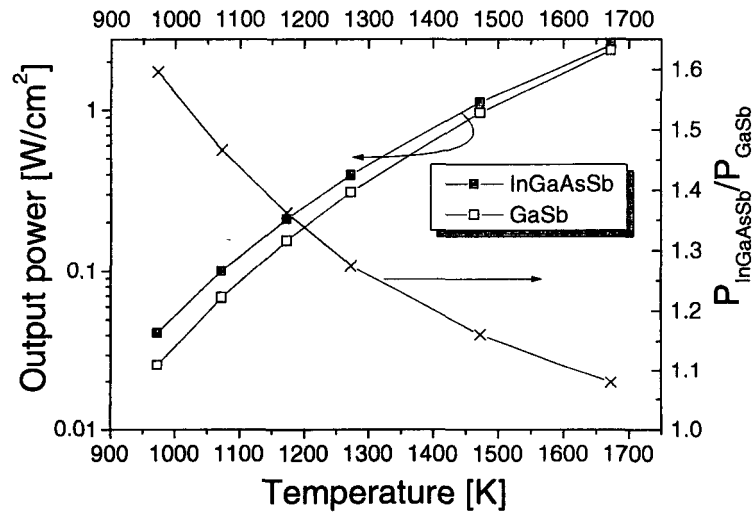

FIGURE 7. Calculated output power density of GaSb and InGaAsSb TPV cells as a function of blackbody temperature for the blackbody spectra with a scaling factor of 0.6. The calculations are performed for a cell temperature of 25°C and are based on measured device parameters (EQE, V_{oc}, FF). The ratio between the output power generated in the InGaAsSb and GaSb cells is shown on the right axis.

It is commonly believed that TPV cells operate at elevated temperatures. In this work, we determined temperature coefficients (TC) of short-circuit current (I_{sc}), V_{oc}, FF of GaSb, InGaAsSb and Ge cells using the JPL LAPSS. As the bandgap of semiconductors decreases with temperature, the spectral range of the photosensitivity widens into the long wavelength part. It is the prime reason why the TC of I_{sc} is usually positive. However, the exact value of the TC of I_{sc} is dependent on illumination spectrum and thus can be used only for the relative and not absolute

cell comparison. TCs of V_{oc} and FF are not spectrum dependent and can be compared with the results of other authors. Table 8.2 shows the absolute and relative temperature coefficients of V_{oc} and FF at different LAPSS illumination. The lowest absolute and relative TCs of V_{oc} were determined at $P_I = 6$ W/cm^2: -1.465 mV/°C (in InGaAsSb-cells) and -0.33 % /°C (in GaSb-cells), respectively. The lowest absolute and relative TCs of FF were measured in InGaAsSb-cells at $P_I = 1$ W/cm^2: -0.00079 /°C and 0.13 %/°C, respectively. TCs of V_{oc} and FF in Ge-cells were essentially worse.

TABLE 8. 2. Absolute and relative temperature coefficients of V_{oc} and FF at different LAPSS illumination.

Incident power density → Cell material ↓	$P_{inc} = 1021$ mW/cm^2	$P_{inc} = 3037$ mW/cm^2	$P_{inc} = 6029$ mW/cm^2
Open-circuit voltage (V_{oc})			
InGaAsSb	- 1.525 mV/°C - 0.49 %/°C	- 1.496 mV/°C - 0.43 %/°C	- 1.465 mV/°C - 0.40 %/°C
GaSb	- 1.687 mV/°C - 0.39 %/°C	- 1.672 mV/°C - 0.36 %/°C	- 1.620 mV/°C - 0.33 %/°C
Ge	- 1.877 mV/°C - 0.67 %/°C	- 1.916 mV/°C - 0.62 %/°C	- 1.913 mV/°C - 0.59 %/°C
Fill factor (FF)			
InGaAsSb	- 0.00079 /°C - 0.13 % /°C	- 0.00108 /°C - 0.17 %/°C	- 0.00128 /°C - 0.19 %/°C
GaSb	- 0.00102 /°C - 0.15 % /°C	- 0.00155 /°C - 0.22 % /°C	- 0.00216 /°C - 0.31 % /°C
Ge	- 0.00268 /°C - 0.39 % /°C	- 0.00280 /°C - 0.41 % /°C	- 0.00254 /°C - 0.41 % /°C

8.5 Conclusions

- Device parameters of GaSb-, InGaAsSb-, InGaSb-, InAsSbP- and Ge- TPV cells were compared. GaSb- and InGaAsSb- based TPV cells showed the best performance.
- Compared to GaSb, InGaAsSb cells demonstrated better parameters when measured under the JPL LAPSS or calculated on the basis of experimental results. The advantage of InGaAsSb cells is especially large if low-temperature blackbody radiators without filters are used.
- Although Ge TPV cells exhibit lower efficiencies and worse temperature characteristics than GaSb and InGaAsSb ones, the relatively low cost of Ge may still make TPV Ge cells attractive.
- Polycrystalline InGaSb- and single crystal InAsSbP-based cells demonstrated high photocurrent. However, their voltage and FF need to be improved.

8.6 References for Part 8

1. www.realgoods.com/renew/shop/product.cfm?dp=1000&sd=1006&ts=3006374
2. Sulima, O.V., Beckert, R, Bett, A.W., Cox J.A, and Mauk, M.G., IEE Proc.-Optoelectron., 147, 199-204 (2000).
3. Sulima, O.V., and Bett, A.W, Solar Energy Materials & Solar Cells, 66, 533-540, 2001.
4. Bett, A.W., Keser, S., Stollwerck, G., and Sulima, O.V., "Large-Area GaSb Photovoltaic Cells", in Thermophotovoltaic Generation of Electricity –1997, edited by T.J. Coutts et al., AIP Conference Proceedings 401, American Institute of Physics, New York, pp. 41-53.
5. Sulima, O.V., Bett, A.W., Mauk, M.G., Ber, B.Ya., and Dutta, P.S., "Diffusion of Zn in TPV materials: GaSb, InGaSb, InGaAsSb and InAsSbP", this conference.
6. Mauk, M. G., Shellenbarger, Z. A., Cox, J. A., Sulima, O.V., Bett, A.W., Mueller, R. L., Sims, P. E., McNeely, J. B., DiNetta, L. C., J. of Cryst. Growth, 211, 189-193 (2000).
7. Mauk, M.G., Shellenbarger, Z.A., Cox, J.A., Tata, A.N., Warden, T.G., and DiNetta, L.C., "Advances in low-bandgap InAsSbP/InAs and GaInAsSb/GaSb thermophotovoltaics", in Proceedings of the 28th IEEE Photovoltaic Specialists Conf., 2000, pp. 1028-1031.